STUDIES OF THE ACCEPTOR COMPLEX OF PHOTOSYSTEM II FROM THE THERMOPHILIC CYANOBACTERIUM *PHORMIDIUM LAMINOSUM*

and

OF THE MANGANESE CLUSTER OF THE WATER-OXIDISING COMPLEX OF PHOTOSYSTEM II

A thesis presented for the degree of

Doctor of Philosophy

in the

University of London

by

Andrew Robert Corrie

Department of Biology,

University College London,

Gower Street

London WC1E 6BT

November, 1990

ABSTRACT

This thesis reports studies of the components of the electron acceptor complex of Photosystem II isolated from the thermophilic cyanobacterium *Phormidium laminosum*. The principal technique used has been electron paramagnetic resonance spectrometry (epr): epr signals are characterised by lineshape and g-value. This thesis reports the first detection of the g = 1.9 signal (assigned to the interaction $Q_a \cdot^- - Fe^{2+}$) by photoreduction at 77K of Q_a in PS II from *P. laminosum*. This signal could be replaced by the g = 1.8 signal by treatment with formate, an inhibitor of electron transfer between the two quinones, which displaces bicarbonate from its ligation site at the non-heme iron. A third signal, with g ≈ 1.6 was detected and assigned as described below.

Using epr signals, the midpoint potential of $Q_a/Qa \cdot^-$ was measured with either bicarbonate or formate bound to the iron. At pH 7.8, both were found to have midpoint potentials of ≈ +25mV. This represented the first direct determination of the redox potential of Q_a in the presence of bicarbonate, and suggested that formate does not inhibit simply by affecting the redox potential of Q_a. Unlike titrations of Q_a in higher plant PS II, there was no indication of further low-potential quinone acceptors. However, the behaviour of a signal due to the interaction of the iron-semiquinone and photoreduced pheophytin indicated some involvement of another electron acceptor, with midpoint potential of -250mV. These results were supported by kinetic optical spectrophotometry.

The assignment of the epr signal with g ≈ 1.6 to an interaction of $Q_a^- - Fe^{2+}$ with Q_b^- was made. Using this signal, a direct estimate of the midpoint potential for the Q_b/Q_b^- couple in PS II (≈ +60mV) was made; evidence was found also for pH-dependence of the signal which indicated the possible second

reduction of Q_b at around this potential. It was found that the g $\approx$ 1.6 can be either 77K or 200K photoinduced following saturating illumination at room temperature, indicating the dark stability of the Q_b^- species. Applying this protocol, an epr signal due to $Q_b^{\cdot -}$ $-Fe^{2+}$ was proposed; and interactions of a Q_b-analogue (phenyl-para-benzoquinone) with the non-heme iron could be monitored. Similar signals are seen following 77K illumination of both cyanobacterial and spinach PS II treated with the Q_b analogue, tribromotoluquinone.

The technique extended X-ray absorption fine-structure (EXAFS) was used to probe of the structure of the manganese complex of PS II from spinach. The results were consistent with an arrangement of the four manganese of the oxygen-evolving complex either as two μ-oxo bridged dimers, or a μ-oxo-bridged trimer with a single monomeric manganese.

ACKNOWLEDGEMENTS

I should like to thank my supervisor Professor Mike Evans, for giving me (and urging me to take) the opportunity to do this work, and for his advice and help throughout the course. I am also very grateful to Dr. Jonathan Nugent for many helpful ideas and enthusiastic discussions. I thank Dr. Julia Hubbard for practical assistance with the kinetic-optical experiments and collecting the EXAFS data; and for useful discussions. I should also like to express thanks to Dr. Richard Strange and Dr. Samar Hasnain at the SRS in Daresbury. I acknowledge all members of the U.C.L. Photosynthesis Group, and in particular Chris Lockett and Simon Bowden. The work was funded by S.E.R.C.

I am deeply conscious of a debt to my parents, for giving me not only material but also unwavering moral support.

TABLE OF CONTENTS

LIST OF FIGURES AND TABLES

ABBREVIATIONS

ADRY	acceleration of the deactivation reactions of OEC
APC	allophycocyanin
ATP	adenosine triphosphate
$\underline{B}$	magnetic field
Bchl	bacteriochlorophyll
Bpheo	bacteriopheophytin
CCCP	carbonyl cyanide *m*-chlorophenylhydrazone
Chl	chlorophyll
CP	chlorophyll-binding polypeptide
Cyt	cytochrome
D	tyrosine residue 160 of the D2 polypeptide
DCMU	3-(3,4-dichlorophenyl)-1,1-dimethylurea
DMBQ	2,6-dimethyl-1,4-benzoquinone
EDTA	ethylenediaminotetraacetic acid
E_{mn}	midpoint potential at pH *n*
EPR	electron paramagnetic resonance
EXAFS	extended X-ray absorption fine structure
Fd	ferredoxin
FT	Fourier transform
HEPES	4-(2-hydroxyethyl)-1-piperazineethanesulphonic acid
kDa	kiloDalton
LDAO	lauryl dimethylamine oxide
LHC	light-harvesting complex
mT	millitesla
MES	2-(N-morpholino)-ethanesulphonic acid
MW	molecular weight
μ_B	Bohr magneton
NADP(H)	nicotinamide adenine dinucleotide phosphate

OEC	oxygen-evolving complex
P	primary electron donor
PC	plastocyanin or phycocyanin
PE	phycoerythrin
PEG	poly(ethylene glycol)
PPBQ	phenyl-1,4-benzoquinone
PQ	plastoquinone
PS I	photosystem I
PS II	photosystem II
Q_a	first stable electron acceptor of PS II
Q_b	second stable electron acceptor of PS II
SB12	N-dodecyl-N,N-dimethylammonio-3-propane sulphonate
TBTQ	2,3,5-tribromo-6-methyl-1,4-benzoquinone, tribromotoluquinone
Tris	tris-(hydroxymethyl)-aminomethane
Triton	octyl phenoxy poly(oxyethanol)
Z	tyrosine 161 of the D1 polypeptide

1. INTRODUCTION

1.1 General

There are many biological systems which are driven by light. Quantitatively the most important is photosynthesis, whereby plants, algae and some prokaryotes are able to convert sufficient radiant energy into forms used by these organisms for their maintenance and growth.

Several ways have evolved by which organisms achieve this: oxygenic photosynthesis is the subject of this thesis, but there are simpler, non-oxygenic forms of photosynthesis used by anaerobic bacteria. Some of these will be mentioned in this introduction because the information gained from these simpler systems has been shown to give important clues to the mechanisms of the more complex.

Oxygenic photosynthesis occurs in both eukaryotes (plants and algae) and in prokaryotes (cyanobacteria and prochlorophytes). In this process light is used to drive the oxidation of water to yield protons, electrons and molecular oxygen:

$$2H_2O + \text{light} \longrightarrow 4H^+ + 4e^- + O_2$$

The protons and electrons are used in a light-independent reaction to reduce carbon dioxide to carbohydrate:

$$CO_2 + 4H^+ + 4e^- \longrightarrow (CH_2O) + H_2O,$$

giving an overall equation:

$$CO_2 + 2H_2O + \text{light} \longrightarrow (CHOH) + H_2O + O_2$$

The transformation of the Earth's early, reducing atmosphere

into an oxidising one has been brought about by this means. Inorganic processes alone could not have done the same, due to the highly unfavourable equilibrium of the water-splitting reaction. From an evolutionary point-of-view this step was critical, since an oxygen-containing atmosphere, and hence aerobic respiration, is necessary to sustain the metabolism of multicellular organisms. It is estimated that global photosynthesis fixes $2x10^{11}$ tons of carbon dioxide per year. A part of this supplies, directly or indirectly, by far the greater part of man's food needs; and the products of ancient photosynthesis meet most of his fuel demands.

Photosynthesis research has among its long-term aims an understanding which may be applied to improve the efficiency of photosynthetic energy transformation in plants and to develop artificial means of utilising solar energy.

1.2 Overview of Oxygenic Photosynthesis

Oxygenic photosynthesis in eukaryotes takes place in a specialised organelle called the chloroplast, shown in Fig 1.1(a). Chloroplasts are approximately 5μm in length and have a double membrane (envelope) enclosing an enzyme-rich matrix called the stroma, and an internal system of membranes called the thylakoids. The thylakoids appear as flattened sacs which enclose an aqueous lumenal phase. In places these sacs stack together to form structures termed grana which are linked by unstacked regions of membrane called lamellae. The thylakoid membrane is selectively permeable and therefore able to maintain differences in the chemical composition of the stromal and lumenal phases.

Oxygenic prokaryotes also contain thylakoids analogous to those in plants and algae. Those found in the prochlorophytes are similar to those described above; while those found in

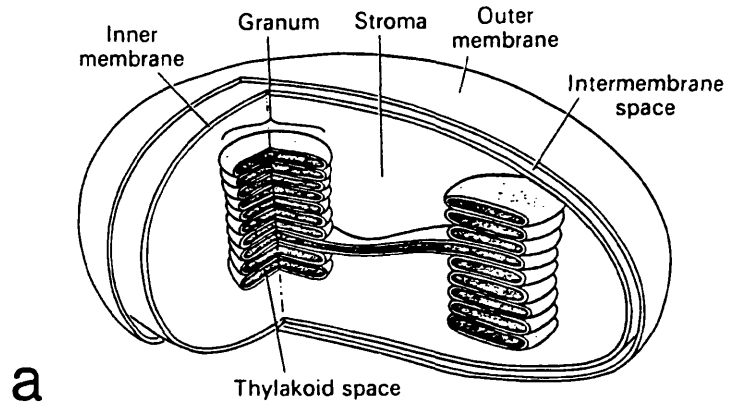

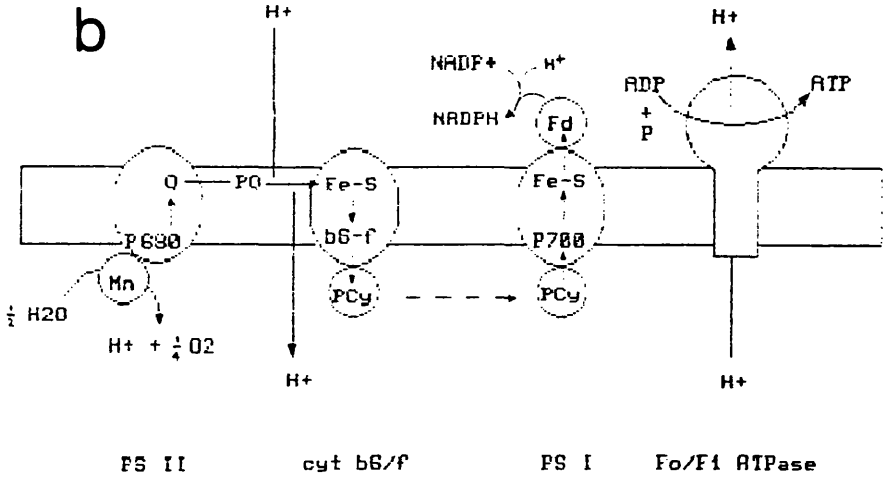

Figure 1.1 Chloroplast and Thylakoid Membrane Structure

(a) represents the arrangement of the membranes in a chloroplast, the photosynthetic organelle of plants and algae. The energy-transducing membrane, the thylakoid membrane, is shown in (b). This houses the protein complexes associated with light-driven electron transfer and associated proton translocation (PS I, cyt b6/f, PS II) as well as the F_0/F_1-ATPase complex, which catalyses ATP synthesis. Abbreviations: PCy, plastocyanin; Fd, ferredoxin; PQ, plastoquinone.

cyanobacteria do not form distinct granal and lamellar regions, but often form closely-packed concentric layers.

The fixing of CO_2 as carbohydrate by chloroplasts is catalysed by enzymes localised in the stroma. This reaction requires NADPH, as well as ATP, to reduce CO_2 to carbohydrate (the formal oxidation state of carbon changes from IV to 0). NADPH and ATP are generated by the 'light' reactions which occur in protein complexes associated with the thylakoid membranes. In these reactions electrons are transferred from water, which is oxidised to molecular oxygen, to $NADP^+$, which is reduced to NADPH.

The membrane-bound complexes associated with photosynthetic electron and proton transfer are shown in Fig 1.1(b). Absorption of light serves to form chemical species with low reducing potentials. However, the difference in reduction potential between the O_2/H_2O (800mV) and the $NADP^+$/NADPH (-300mV) couples is large and, since the energy transfer is not 100% efficient, a single visible photon cannot lower the potential by this amount. The problem is solved by the use of two light reactions occurring in series. The light reactions occur in multi-subunit protein complexes called photosystems I and II (PS I and PS II). In both photosystems, photooxidation of 'special' chlorophyll occurs: in PS I these special chlorophyll molecules form a dimer, called P700 due its bleaching at 700nm on oxidation, while in PS II the special chlorophyll, which probably also functions as a dimer, is called P680.

In PS II water is oxidised and the electrons passed through a sequence of cofactors associated with the protein complex, finally being transferred to plastoquinone in the membrane phase. PS I oxidises plastocyanin, a copper-containing protein, and reduces $NADP^+$. The link between the two photosystems is made by a third membrane-bound complex, the cytochrome b/f complex, containing two

cytochromes and an iron-sulphur centre.

The distribution of the membrane-spanning complexes throughout the thylakoid membrane is not uniform. It is possible, using specific detergents, to separate the granal (stacked) regions from the lamellar regions of the membrane. Analysis of such fractions indicates that the PS I and ATPase complexes are located principally in the lamellar regions, whereas the bulk of PS II complexes are found in the grana [1].

There are several implications of this fact. Transfer of electrons from PS II to PS I requires mobile electron carriers, which are plastoquinone (which moves in the hydrophobic part of the membrane) and plastocyanin. In addition, the regulation of distribution of excitation energy is thought to rely on this lateral heterogeneity. The structure and function of these membrane proteins is reviewed in [2].

1.3 Historical Perspective

This section briefly summarises the contribution of research efforts in the 19th and early 20th centuries, when the light- driven processes in oxygenic photosynthesis were elucidated and distinguished from the 'dark' reactions that follow. For fuller reviews see [3] and [4].

It had been known since the beginning of the 19th century that plants could use light, carbon dioxide and water to synthesise carbohydrate and oxygen. The importance of chlorophyll was guessed at, since it made up the obvious difference between the green and colourless tissues in plants. Early theories held that molecular oxygen was derived from carbon dioxide; for example, H_2CO_3 bound by chlorophyll might undergo molecular rearrangement following absorption of light:

$$H_2CO_3 + \text{light} \longrightarrow H_2CO.O_2 \longrightarrow (CHOH) + O_2$$

However, determination of a quantum requirement of 4 for oxygen evolution in Chlorella, by Warburg in 1922 [5], indicated that this was not a simple, but more likely a multi-step, process.

Van Neil first proposed in the 1930s the modern idea that the molecular oxygen was derived not from CO_2 but from water, having analysed the growth conditions of anaerobic photosynthetic bacteria [6]. For the purple and green sulphur bacteria (Chromatiaceae and Chlorobiaceae respectively) the equation for formation of free sulphur was:

$$CO_2 + 2H_2S \longrightarrow (CHOH) + H_2O + 2S$$

Van Neil stressed the analogy with the reaction in green plant photosynthesis:

$$CO_2 + 2H_2O \longrightarrow (CHOH) + H_2O + O_2$$

and put forward the idea that these two were instances of the general type:

$$CO_2 + 2H_2A \longrightarrow (CHOH) + H_2O + 2A$$

It was later envisaged by van Neil [7] that the 'primary photochemical event' common to these systems was not the splitting of CO_2 but of water, to yield reducing and oxidising equivalents (represented [H] and [OH]). These would be used in two dark processes, reduction of CO_2 and oxidation of the H_2A donor, separate

both from the photochemistry and from each other.

It was shown by Hill and Scarisbrick [8] that isolated chloroplasts evolve oxygen in the presence of artificial oxidants, e.g., ferric oxalate, ferricyanide and benzoquinone, which were simultaneously reduced. The simplest interpretation of the Hill reaction, as it came to be known, was in agreement with van Neil's model of photochemically-induced hydrogen (or electron) transfer involving water, the reduction of CO_2 being a dark process.

This model was further supported by experiments using ^{18}O-labelled water [9], but the occurrence of exchange reactions meant a full proof that water was the sole source of oxygen was lacking. A later repetition of this experiment at controlled pH in chloroplasts free of carbonic anhydrase provided the necessary proof [10].

The observation that illuminated chloroplast suspensions could reduce cytochrome c in solution prompted a search for natural acceptors of reducing equivalents. Two cytochromes, called f and b_6, were characterised by Hill and Scarisbrick [11],[12] as native chloroplast components. Soluble cytochrome f could be photoreduced, but no enzyme could be found analogous to the mitochondrial cytochrome c oxidase, i.e., responsible for the reoxidation of cytochrome f.

A red-brown protein was isolated from a variety of species which showed properties similar to those of the Hill reagent ferric oxalate by catalysing photoreduction of metmyoglobin to myoglobin [13]. Davenport [14] found this to be identical to a protein previously shown to catalyse photoreduction of NADP by chloroplasts [15]; and Tagawa and Arnon [16] noted its similarity with an iron-containing electron-transfer protein isolated from Clostridium pasteurianum. This protein is now called ferredoxin; a flavoprotein, ferredoxin-NADP reductase, is also necessary for electron transfer to

NADP.

The discovery that photosynthetic systems could phosphorylate ADP in the light was also made in the 1950s by Frenkel [17], using a preparation of chromatophores from a photosynthetic bacterium and independently by Arnon, Whatley and Allen [18] using chloroplasts. Arnon's group noted yields of ATP in chloroplast preparations were greater in the presence of catalytic concentrations of flavine mononucleotide (FMN) and vitamin K_3 [19], and coined the term 'cyclic photophosphorylation' to describe the effect. Phosphorylation would also occur when added NADP (in the presence of ferredoxin) or ferricyanide were reduced, together with the stoichiometric evolution of oxygen. This process was termed 'non-cyclic photophosphorylation'. Bassham and Calvin showed in 1957 that ATP, generated by light-driven processes, is necessary for CO_2 fixation [20].

By analogy with mitochondrial oxidative phosphorylation, it was assumed that photophosphorylation in chloroplasts would proceed by means of electron transfer, and that the role of light was therefore to drive redox processes. $NADPH_2$ and ATP, the products of the light reactions, brought about the reduction of CO_2.

Hill and Bendall summarised the conclusions from a number of groups in 1960 [21] when they first put forward the 'Z-scheme', connecting oxidation of water with reduction of NADP by means of electron transfer through two light reactions acting in series, and the cytochromes $\underline{b}_6$ and $\underline{f}$. Hill and Bendall proposed that reduction of NADP should be correlated with oxidation of cytochrome $\underline{f}$, and the production of oxygen with reduction of cytochrome $\underline{b}_6$; re-reduction of cytochrome $\underline{f}$ by cytochrome $\underline{b}_6$ was seen as the connecting redox event between the two light reactions.

Direct evidence for this proposal came from the work of Duysens

et al [22], who followed oxidation of an analogous c-type cytochrome in the red alga Porphyridium, by measuring absorbance changes at 420nm. Light of 680nm was used to excite one photochemical reaction and light of a shorter wavelength, 562nm, to excite a second. Excitation using 680nm light alone was seen to oxidise cytochrome, whilst use of both wavelengths caused its partial rereduction. Repetition of the experiment in the presence of the herbicide DCMU was seen to abolish the effect of the 562nm light, but had no effect on the oxidation of cytochrome by the longer wavelength light.

The involvement of two light reactions explained the results of Emerson et al [23], who had observed an increase in the efficiency of photosynthesis by light of 700nm when supplemented by light of shorter wavelengths. It was also consistent with the observations of Myers and French [24] who had found distinct action spectra for generation of photosynthetic transients. The two light reactions in oxygenic photosynthesis are now believed to take place in physically distinct protein complexes designated Photosystems I and II, corresponding to Duysens' original terms (reactions 1 and 2) for the cytochrome -oxidising and -reducing processes.

The processes of photophosphorylation and light-driven electron transfer are now understood in terms of the chemiosmotic model proposed by Mitchell, reviewed in [25]. This views proton translocation across the thylakoid membrane as a consequence of electron transfer along the chain of redox components; the electrical and chemical potential gradients formed then drive condensation of ADP and inorganic phosphate at a separate site, the F_0F_1-ATP synthase. Evidence that this theory applied to photosynthesis in chloroplasts came first from the 'acid bath' experiments of Jagendorf and Uribe [26]: chloroplasts equilibrated at pH 4 synthesised ATP in the dark when transferred to buffer at pH 8, containing ADP and

phosphate. Coupled with the earlier observation that illuminated thylakoid suspensions took up protons and that the extent of phosporylation was related to that of proton uptake, this result was interpreted as strong evidence for the mediating role of the proton gradient.

1.4 Prokaryotic Photosynthetic Organisms

As indicated in Section 1.1, it has become apparent that there are functional similarities between the simpler photosynthetic processes used by non-oxygenic prokaryotes and the more complex oxygenic systems. In particular, the homology between the reaction centre of the purple non-sulphur bacteria and the photosystem II reaction centre has been established, over the last twenty years, by a range of biophysical and gene- and protein- sequencing methods.

Prokaryotic photosynthetic organisms are classified into three groups, distinguished by the photosynthetic pigments they contain and by whether or not they evolve oxygen. They are all Gram-negative.

A) The phylum *Prochlorophyta* contains oxygen-evolving bacteria having both chlorophyll *a* and *b*, see Fig. 1.2(a), as their light-harvesting pigments. Examples of this phylum include the free-living *Prochlorothrix* and the endosymbiont *Prochloron*, associated with some tropical marine snails, which has cells of ≈30μm diameter enclosing thylakoids which show prominent granal stacks, similar to chloroplasts in higher plants. For this reason, *Prochlorophyta* have been suggested to be the ancestral precursor of chloroplasts.

B) Cyanobacteria are classified into the order *Cyanobacteriales*, which in general perform oxygenic photosynthesis in a way similar to eukaryotes: they possess two photosystems located in thylakoid

a

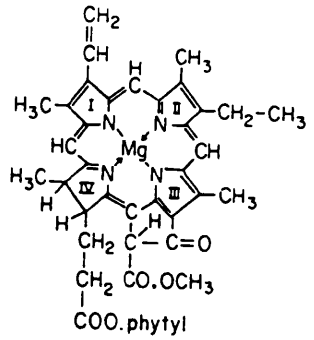

Chlorophyll a

In chlorophyll b the - CH_3 of ring II is oxidized to - CHO

b

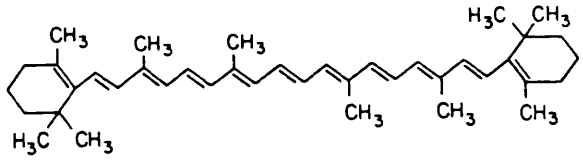

β-carotene

c

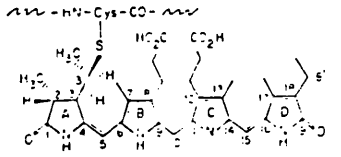

Peptide-linked PHYCOCYANOBILIN

Figure 1.2 Chemical Structures of Photosynthetic Pigments

(a) shows the structure of chlorophyll (Chl) a, the most abundant pigment in higher plants. There are numerous structurally-related molecules: Chl b, also found in plants and algae, has an aldehyde (-CHO) group in place of the methyl (-CH_3) on ring II. The bacteriochlorophylls, found in many prokaryotes, are saturated at rings II and IV. (b) ß-carotene is one of a group of polyunsaturated molecules found in most photosynthetic organisms and have a photoprotective role. (c) shows a phycobilin pigment which have a light-harvesting role in cyanobacteria and red algae. It is a linear tetra-pyrrole, related to the cyclic chlorophylls.

membranes, with reaction centre pigments P700 and P680, and evolve oxygen by oxidation of water. The general morphology of a cyanobacterial cell is shown in Fig. 1.3, and described in the figure legend.

There are a number of variations to this general pattern: some species perform anoxygenic photosynthesis using H_2S as the source of reducing equivalents; some are facultative photo- or chemo-heterotrophs, although growth in the dark is always much slower than under conditions of photoautotrophic growth; some have the capacity to fix nitrogen in specialised cells lacking PS II; and some have extra nutritional requirements, e.g., vitamin B_{12}.

Cyanobacteria can be found in a wide variety of terrestrial, freshwater, marine and hypersaline environments. For example, the species studied in this thesis, Phormidium laminosum, is a moderate thermophile, growing optimally at temperatures of $\approx 50^{o}C$; the wild population grows in warm pools near hot springs, but not in the springs themselves. Unlike most other prokaryotes, i.e., eubacteria and archaebacteria, cyanobacteria are frequently visible as plankton 'blooms', turfs or mats composed of individual species. Different species have different colours, determined by the composition of their light-harvesting pigments, and may be green, blue-green, olive green, red, purple and black. Under conditions of sulphur or nitrogen deficiency, or of high light intensity combined with low CO_2, phycobiliprotein content is decreased and the cells appear yellow-green, due to chlorophyll a.

Whilst the central features of photosynthesis are the same in cyanobacteria and eukaryotic systems, there are several important differences.

i) The light-harvesting complexes differ from those of the prochlorophytes and all eukaryotes (except red algae), having

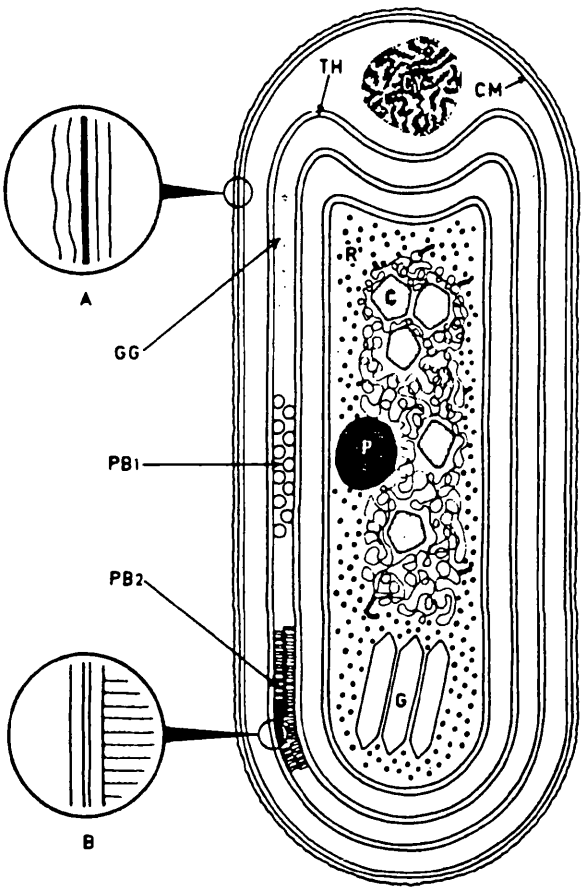

Figure 1.3 Schematic Diagram of a Cyanobacterial Cell

CM, cell membrane; TH, thylakoid; PB1 and PB2, face and side views of phycobilisomes attached to thylakoids; GG, glycogen granules; CY, cyanophycin granule; P, polyphosphate granule; C, carboxysome surrounded by nucleoplasm; R, ribosomes; G, gas vesicles. (A) shows enlarged view of cell envelope showing outer membrane and peptidoglycan layers overlying the cell membrane. (B) Enlarged view of a thylakoid showing paired unit membrane with attached phycobilisomes in side view. [From R.Y. Stanier and G. Cohen-Bazire (1977) Ann.Rev.Microbiol., 31, 225.]

chlorophyll a and phycobilins (a group of related linear tetrapyrroles, Fig. 1.2(b)), but no chlorophyll b. This is discussed in Section 1.5.2.

ii) The thylakoid membranes of cyanobacteria do not show the separation between granal and lamellar regions. Consequently, the phosphorylation-dephosphorylation mechanism proposed for regulating the distribution of excitons between the photosystems in eukaryotes cannot apply in an exactly analogous way.

iii) Whilst both plants and cyanobacteria are able to produce oxygen, there are differences in the constitution of the polypeptides bound to the lumenal face of the thylakoids, close to the PS II reaction centre, that affect water oxidation. This difference is described in detail below, Section 1.8.1.2.

C) Bacteria of the order Rhodospirillales perform anoxygenic photosynthesis and do not contain chlorophyll, but the structurally related molecule bacteriochlorophyll (Bchl). This order is divided into two sub-orders: the purple bacteria (Rhodospirillineae) containing Bchl a and b located in intracytoplasmic membranes; and the green bacteria (Chlorobiineae) containing Bchl a in the reaction centres and Bchls c, d ,e or g located in vesicles underlying the cytoplasmic membrane. Most green bacteria are rod-shaped and immotile, whereas the purple bacteria are rod, spiral or spherical in shape, and frequently flagellate.

The purple bacteria are further classified into two families. The Chromatiaceae are anaerobes which oxidise sulphide to sulphate via elemental sulphur. The Rhodospirillaceae may grow photoorgano-heterotrophically, using organic substrates such as succinate as a source of carbon and electrons; they may grow photoautotrophically, using carbon dioxide as carbon source; and some species, such as Rhodobacter (Rb.) sphaeroides and Rb. capsulata, can grow

heterotrophically in the dark, which makes them particularly important as subjects for genetic manipulation. Although some species of Rhodospirillaceae are able to utilise sulphide as a reductant, in general H_2S is toxic to them; this family is often referred to as the 'purple non-sulphur bacteria'. Detailed information is now known about the photosynthetic reaction centres of two members of this family, namely, Rb. sphaeroides and Rhodopseudomonas (Rps.) viridis, and is discussed in a separate section.

The green bacteria also divide into two families: Chlorobiaceae and Chloroflexaceae. Only one species is contained in the second of these - Chloroflexus aurantiacus - which is non-flagellate but can 'glide', and grows photolithotrophically using CO_2 and sulphide. The Chlorobiaceae use reduced sulphur compounds such as sulphide, sulphur or dithionate as their electron source. They are obligate anaerobes, obligate phototrophs and non-motile.

The purple and green bacteria have only a single photosystem, unlike oxygenic systems. The proton gradient generated across the cytoplasmic membranes of purple bacteria can only be used to drive photophosphorylation and is not able directly to reduce NADP: this is brought about by reversed electron transfer powered by ATP hydrolysis or by oxidation of exogenous substrate. This is also true of the green bacterium Chloroflexus aurantiacus. On the other hand, the family Chlorobiaceae have reaction centres similar to PS I of higher plants, and can generate acceptors with sufficiently low redox potential to reduce NADP.

1.5 Light Harvesting in Photosynthesis

Absorption of light by pigment molecules is the fundamental event in photosynthesis. The bulk of these pigments are bound by

specialised protein units, called light-harvesting complexes or antennae. The pigment molecules most widely used by oxygenic organisms are the chlorophylls: however, there are other pigments which are able to absorb in regions of the visible spectrum not covered by the absorption maxima of the chlorophylls, e.g. carotenoids, Fig. 1.2(b), and bilins, Fig. 1.2(c)

Absorption of a photon in the antenna causes an electronic transition in the pigment molecule, from a ground state to an excited singlet state. This 'excitation' can be passed from molecule to molecule within the antenna, by means of radiationless transfer. The initial photochemical event, though, is the 'trapping' of excitation by transfer to the 'special' chlorophyll molecules located in the reaction centre: this excitation event is followed by the oxidation of this chlorophyll. In the antenna of PS II in higher plants trapping of excitation by the reaction centre occurs within a few hundred picoseconds. Recent analysis of excitation transfer and trapping dynamics suggests that transfer is fast compared with trapping, and that excitation can be viewed as being 'delocalised' over the antenna and reaction centre; a further implication is that the excitation is likely to have been in the vicinity of the reaction centre several times before trapping and productive charge separation [27].

1.5.1 Light Harvesting Complexes in Higher Plants

Higher plants and green algae have antennae complexes, termed LHC I and LHC II, associated with photosystems I and II. Photosytem II is also closely associated with a complex array of Chl-containing light-harvesting antenna proteins: CP47 ('CP' = chlorophyll-binding polypeptide; '47' = molecular weight, in kDa) and CP43, which bind

chlorophyll a, and CP29, which binds both chlorophylls a and b. These tightly-associated proteins account for approximately 50% of the 'pigment bed' associated with PS II. LHC II is less tightly associated with the PS II reaction centre. It is also composed of several different polypeptides, and binds both Chl a and b. LHC II has been postulated to regulate the distribution of excitation to the two reaction centres, PS II and PS I. LHC II can be phosphorylated by a 64kDa kinase located in the thylakoid, whose activity increases with increased activity of PS II. It is dephosphorylated at a constant rate by a phosphorylase. The consequence of this phosphorylation is for LHC II to dissociate from the PS II and to migrate from the grana to the lamellae, thereby reducing the transfer of excitation of this reaction centre.

LHC I, which binds chlorophyll a, is tightly associated with the PS I reaction centre. It does not show the phosphorylation-dependent association-dissociation of LHC II.

1.5.2 Light Harvesting in Cyanobacteria

In cyanobacteria Chl b is absent, as are the polypeptides associated with binding this pigment, e.g. LHC II. There are analogues of CP47 and CP43 associated with PS II, as in higher plants. Up to 50% of the light-harvesting capacity, and as much as 25% of the cell's dry weight, is made up by chromophoric proteins called phycobiliproteins. These assemble into larger complexes, of total molecular weight $\approx 10^4$kDa, called phycobilisomes, Fig. 1.4.

Phycobiliproteins consist of two dissimilar polypeptides, termed α and β, of molecular weight ≈17 and ≈18 kDa, which are thought to associate as hexamers with composition $(\alpha.\beta)_3$, which appear disc-like under the electron microscope.

The pigmentation of phycobiliproteins is due to binding of

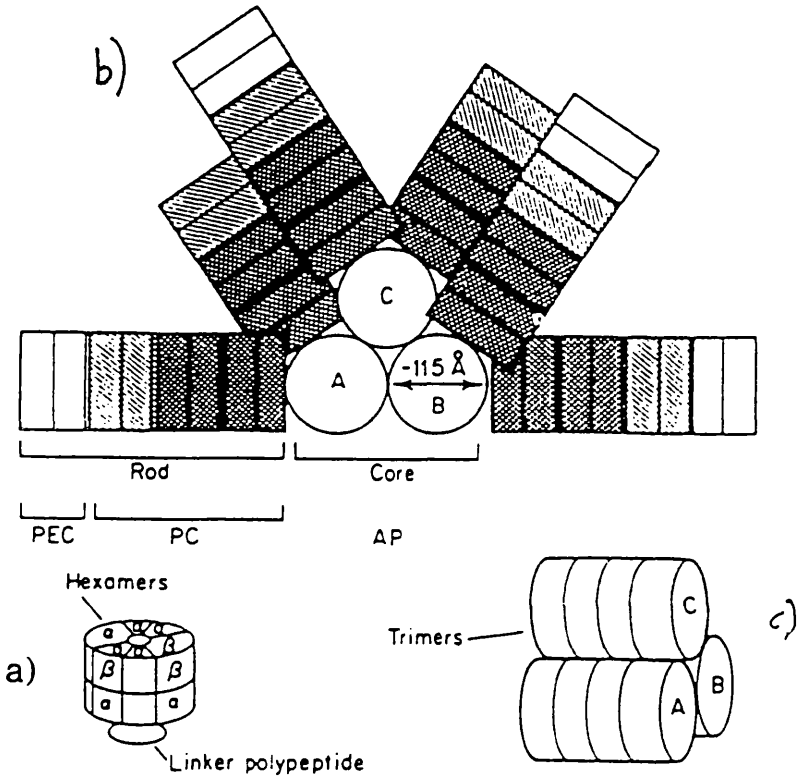

Figure 1.4 Structure of a Phycobilisome

The hemidiscoidal phycobilisome is built up from (a) disc-like hexamers, $(\alpha.\beta)_3$, of phycocyanin (PC) or phycoerythrin (PEC) which stack through a linker polypeptide into rods, (b). These are arranged around a core of two or three allophycocyanin (APC) tetramers (c). Excitation is transferred from the periphery towards the APC core. [From Zuber, H. (1986) TIBS, 11, 414.]

bilins, which are a group of related linear tetrapyrroles (compared with chlorophylls, which are cyclic tetrapyrroles). The chromophores are covalently bound to the polypeptides through a thioester link. There are three main phycobiliproteins: phycoerythrin (PE, A_{max} = 565nm), phycocyanin (PC, A_{max} = 620nm) and allophycocyanin (APC, A_{max} = 650nm); quantitatively less important biliproteins include allophycocyanin B (APCB) and allophycocyanin 1 (APC1), that absorb with A_{max} = 670nm.

The phycobiliproteins transfer excitation from shorter- to longer-wavelength absorbers, as follows:

PE ----> PC ----> APC -- (APCB) --> APC1 ----> Photosystem II

Phycobilisomes contain two or three 'core' cylinders, each of four APC discs. From this core, radiate six cyliders, forming a hemidiscoidal stucture. In species that produce PE, the peripheral discs of these cylinders consist of PE, whereas the proximal discs consist of PC. Synecchococcus leopoliensis, for example, cannot produce PE, and adapts to low or red light by manufacturing phycobilisomes with larger cylinders. Other species can adapt to red light by replacing the short-wavelength absorber PE with the longer-wavelength absorber PC.

The cylinders of phycobiliprotein are associated with various linker polypeptides which are necessary to maintain the structure of the phycobilisome. The wavelengths at which the various pigments absorb is determined in part by their environment: in the phycobilisome, the same pigments towards the periphery absorb with shorter wavelength than closer to the APC core. This assists flow of excitation towards the reaction centre. The phycobilisome is anchored to the thylakoid membrane by means of APC1, which has a

molecular weight in S. leopoliensis of 75kDa.

1.6 The Reaction Centre of Purple Non-Sulphur Bacteria

Elucidation of the redox components and the sequence of electron transfer in the reaction centres of purple non-sulphur bacteria occurred earlier than the corresponding work on PS II. This was because a stable isolated reaction centre preparation from these prokaryotes, i.e., one free from light-harvesting components (which make up the bulk of the pigmentation in photosynthetic systems, and therefore complicate the interpretation of optical spectra), was available many years before a corresponding preparation of isolated photosystem II [28]. In recent years the three-dimensional structures of two bacterial reaction centres, those of Rps. viridis and Rb. sphaeroides, have been determined at <0.3nm resolution (see [29], [30], [31], [32]). The detailed structural and thermodynamic information now available has given impetus to theoretical work which aims to account for the direction, speed and efficiency of photochemical electron transfer. For a recent review of the structure and function of purple bacterial reaction centres see [33].

The reaction centre of the purple non-sulphur bacteria is an integral membrane-spanning protein complex consisting of three polypeptides referred to as L, M and H (i.e., Light, Medium and Heavy, referring, in the case of Rps. viridis, to their apparent molecular weights of 24, 28 and 35kDa: the real molecular weights, calculated from primary sequences are, respectively, 30.4, 35.9 and 28.5kDa; and for Rb. sphaeroides the corresponding real values are 31.4, 34.5 and 28.0kDa). The development of crystallisation techniques applicable to membrane proteins (for review see [34]) has permitted structural analysis of these proteins using X-ray crystallography. The first structure of a membrane protein to be

described at atomic resolution (recently to .23nm [35]) was that of the reaction centre from Rps. viridis, followed shortly by that of the related structure from Rb.sphaeroides (to .28nm). The 3-D structures of the reaction centres are similar, insofar as the arrangement of L,M and H polypeptides and the disposition of the electron-transfer cofactors. The important differences are the presence in Rps. viridis of: 1) an additional cytochrome subunit, containing four heme groups; 2) bacteriochlorophyll b instead of bacteriochlorophyll a; and 3) menaquinone rather than ubiquinone as first stable electron acceptor. A simplified diagram showing electron transfer through the purple bacterial reaction centre is shown in Fig. 1.5.

The three subunits have, in total, eleven transmembrane helices: the L and M subunits each has five, and the H subunit has one. This result confirmed predictions based on the distribution of hydrophobic amino-acid residues in the primary sequence. The L and M subunits are in close contact: together they form a cylindrical core, bounded by two α-helices from each polypeptide, having an elliptical cross-section with axes of $\approx$4nm and $\approx$7nm. The four α-helices bordering this core region each has a histidine residue which together are thought to provide ligands to a ferrous iron. The two subunits are related by a quasi two-fold symmetry axis, which is perpendicular to the plane of the membrane.

The H chain makes contact with the L-M complex on the cytoplasmic side of the membrane. Loss of this subunit impairs electron flow from Q_a to Q_b [36]: this result is interpreted as giving a role to the H-subunit in maintaining the structure of the L-M complex, and it is proposed that when H is not bound the binding constant of Q_b at its site is lowered.

The periplasmic face of the L-M complex binds the cytochromes

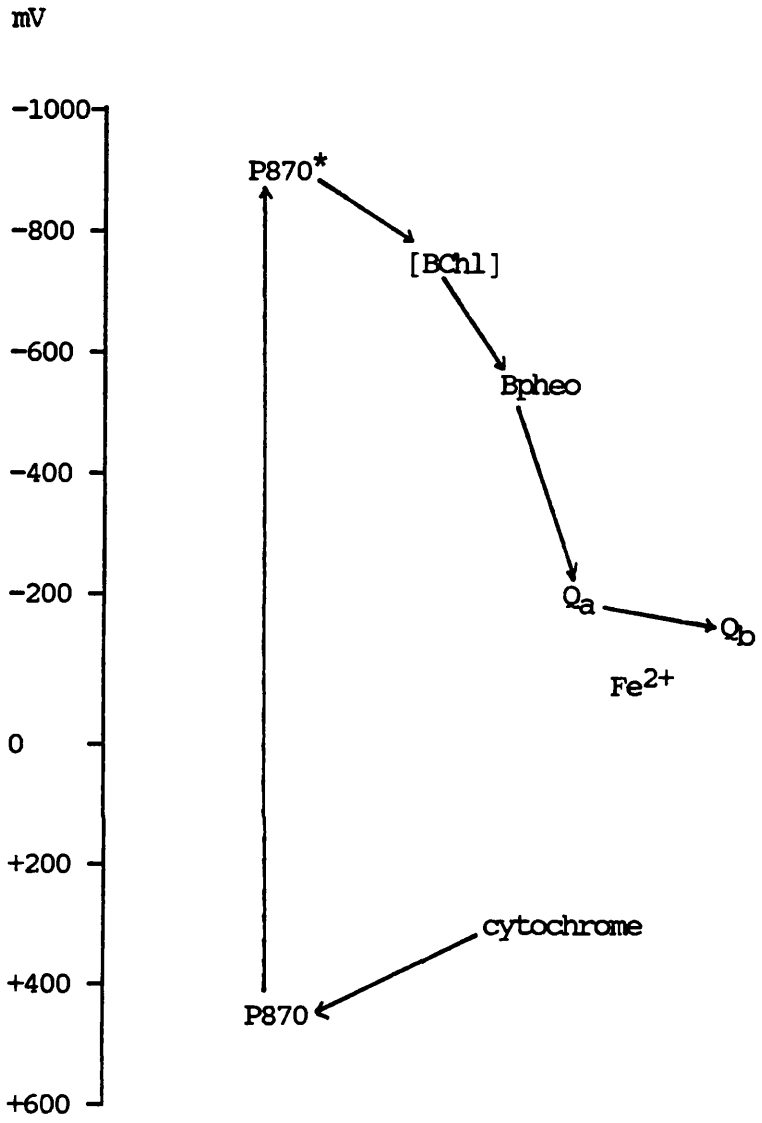

Figure 1.5 Diagram of Electron Transfer in the Reaction Centre of Purple Non-Sulphur Bacteria

The simplified picture applies to Rb. sphaeroides and to Rps. viridis. It has only recently been shown, in Rb. sphaeroides, that electron transfer from P870* to bacteriopheophytin (Bpheo) involves bacteriochlorophyll (BChl). The important differences between the two species are the presence in Rps. viridis of: a four-heme cytochrome, instead of a single-heme cytochrome c, as donor to $P870^+$; menaquinone, not ubiquinone, as the primary stable acceptor, Q_a; and BChl b replacing BChl a. The role of the iron atom is not clear: it can be replaced by other divalent metal ions, e.g. Cu^{2+}, without loss of electron transfer from Q_a to Q_b.

that are the secondary donors to the oxidised Bchl dimer: in Rb. sphaeroides this is cytochrome c_2, and in Rps. viridis it is a four-heme cytochrome, which crystallises as an integral part of the reaction centre.

The following cofactors are present in the reaction centre: four bacteriochlorophylls, two bacteriopheophytins, two quinones and one non-heme iron. The cofactors are arranged along two branches, called 'A' and 'B' in Rb. sphaeroides and 'L' and 'M' in Rps.viridis. The arrangement of the cofactors like that of the L-M complex, reveals quasi two-fold symmetry: the axis extends from the non-heme iron to the Bchl dimer (D_A and D_B), forming the 'special pair', which constitutes the primary donor of the reaction centre. After optimising the symmetry axis, the root-mean-square deviation between the positions of the rotationally-related atoms is ≈0.1nm.

Two bacteriochlorophylls, D_A and D_B, overlap to form the dimer, P870: the distance between ring centres is 0.7nm, and the average perpendicular distance between overlapping parts is ≈0.3nm in Rps.viridis, and ≈0.35nm in Rb.sphaeroides. Adjacent to the Bchl dimer along each branch are two Bchl monomers, B_A and B_B, that assist electron transfer from the primary donor to the bacteriopheophytin, BpheoA and BpheoB. Optical studies [37] had suggested that only one of these plays an active role in electron transfer, and this is now thought to be the BpheoA molecule.

An electron is transferred from the primary donor to BpheoA in less than 5ps: this is fast given the average distance of 1.7nm between the ring centres of the donor and BpheoA molecules, and the consequently small overlap of electron density. A role for monomeric Bchl, B_A, has been suggested by femtosecond time resolved spectroscopy of Rb. sphaeroides reaction centres, where a transient attributed to $P870^+.B_A^-$, with a rise time of 3.5 ± 0.4ps, has been

detected prior to reduction of BpheoA ($P870^+.B_A^-$.BpheoA ---> $P870^+.B_A$.BPheoA-, with time constant of 0.9ps ± 0.3ps) [38]. There is also the possibility that this rapid transfer is assisted by conserved tyrosine residues or by the phytyl chain of B_A, which has van der Waals contacts with the BpheoA molecule; this view is challenged by Dutton, who suggests that the rate of electron transfer is affected only by distance.

The rates of electron transfer are different along the two branches of the purple bacterial reaction centre. This is due to the slight asymmetry in the following ways. 1) There is an inherent asymmetry in the special pair itself, one of the tetrapyrroles is puckered, the other flat; 2) there is greater overlap between the dimer and B_A than B_B; 3) BpheoA is approximately 0.15nm closer to B_A than BpheoB to B_B; 4) There is an asymmetric distribution of charged amino acid residues between L and M; 5) The phytyl and isoprenoid chains of the cofactors are not symmetrical. The rate along the A branch is estimated to be greater than 20 times the corresponding rate along the B-branch.

An iron atom (Fe^{2+}) is situated between the two quinone molecules. This atom is coordinated to four histidine residues and the bidentate carboxylate ligand of a glutamate residue, forming a distorted octahedral complex. These five residues are conserved between Rps. viridis and Rb. sphaeroides. In Rb. sphaeroides, the iron lies closer to Q_b than to Q_a, by approximately 0.2nm.

The electron is transferred from BpheoA to Q_a in approximately 220 ± 40ps [38]. Conserved tryptophan residues (Trp-M252, or Trp-M250) may assist in this process: replacement of the corresponding residue with valine in Rb. capsulatus inhibits photosynthetic growth. However, this is not necessarily due to a slowing of the rate of electron transfer [39].

Electron transfer from Q_a to Q_b occurs in about 100μs. In Rb. sphaeroides both quinone acceptors are ubiquinone molecules, and therefore the vectorial electron flow arises from differences in the two protein microenvironments: Q_b is surrounded by more polar residues than Q_a, and the non-heme iron is closer to the secondary quinone, both of which might stabilise the negative charge at Q_b. In Rps. viridis the iron is symmetrically positioned, therefore will not stabilise either semiquinone more than the other; however, the primary quinone is a menaquinone.

1.7 Redox Potentials and Electron Transfer

The tendency of a chemical species to lose or gain electrons is measured by its standard electrode potential, E^o. E^o is a precisely defined thermodynamic quantity, related to the standard free energy change between oxidised and reduced forms of the species. It is a convention to relate E^o to the hydrogen electrode, which is assigned (arbitrarily) an E^o of 0mV. Convention then dictates that redox couples with negative E^o are more easily oxidised, and those with positive E^o are more easy to reduce. Comparison of two half cell electrode potentials enables the prediction of the equilibrium position of a redox reaction between two redox active species.

For a half reaction:

$$Ox + n.e^- \longrightarrow Red,$$

The observed 'half-cell' potential, E, is related to E^o by the Nernst equation:

$$E = E^o + \frac{R.T}{n.F} \ln \frac{[\ Ox\ ]}{[\ Red\ ]}$$

Where R is the universal gas constant (8.314 $J.K^{-1}.mol^{-1}$), T the thermodynamic temperature and F the Faraday constant (9.65×10^4 $C.mol^{-1}$). When the oxidised and reduced forms are present in their standard states, i.e. at equimolar concentration, standard temperature and pressure, E is equal to E^o. For other defined conditions, this value is also called the midpoint potential, E_m.

In cases where the oxidised and reduced forms have very different acid-base properties, the observed value of E is seen to be dependent on the pH at which the measurement is made. In general, $pK_a(red) >> pK_a(ox)$: for example, if respective values of pK_a are 11 and 3, then reduction at pH 7 will also involve protonation. For a single-protonation, this leads to a modified form of the Nernst equation:

$$E = E_m + \frac{R.T}{n.F} \ln \frac{[\ Ox\ ].[\ H^+\ ]}{[\ Red\ ]}$$

If [Ox] = [Red], a conversion made from $\log_e$ to $\log_{10}$, and the various constants multiplied out (assume T = 293K), the observed midpoint potential will vary by $\approx$ -59mV per pH unit increase.

There are several reasons why it is useful to know the redox potentials of components involved in electron transfer.

1) The most-often given reason for determining the E_m values of components in electron transport systems is that this information helps one to determine in which order components are reduced. In terms of the acceptor side of the PS II reaction centre, therefore, the argument is that a more reducing component will come 'before' a more oxidising one in the sequence: so, pheophytin, with a potential of -600mV, is assumed to be the first acceptor from the excited chlorophyll, and reduces Qa next in line. However, this information

alone is not strictly sufficient to show the order of transfer. This is because the redox potential predicts only the ratio of reduced to oxidised forms at equilibrium, and this is independent of mechanistic considerations. It is necessary that overall the redox potentials favour electron transfer in the 'correct' direction.

That having been said, a theory has been developed to account for the observed rates of electron transfer [40] which takes account of the differences in midpoint potentials of the participating species. However, the involvement is not simple: it is noted that the difference in midpoint potentials is almost invariably favourable to electron transfer in the observed direction. In addition to a dependence upon the distance between redox sites, the principal rate determining factor is viewed as the conformational changes in the protein that bring the oxidising and reducing species into the same 'activated geometry', prior to the actual electron hop.

2) Since the redox potential is related in a simple way to the free energy of the redox reaction, it is possible, through knowledge of the redox potentials, to calculate the energy losses at each transfer step. This sort of consideration is used in detailed evaluation of the quantum efficiency of photosynthesis.

1.8 Photosystem II

Some of the properties of photosystem II have been mentioned in the earlier part of this introduction, and in this section these will be described in more detail. A recent review of all aspects of PS II structure and function is [41].

PS II is the part of oxygenic photosynthesis which catalyses the light-induced transfer of electrons from water to plastoquinone (PQ); simultaneously there is a net movement of four protons from the stroma to the thylakoid lumen. This can be represented by the

equation:

$$4H^+(s) + 2PQ + 2H_2O \xrightarrow{4h.v} 2PQH_2 + O_2 + 4H^+(l)$$

As in all photosynthetic reaction centres, trapping of the excitation at the reaction centre results in the photooxidation of a special pigment; in the case of PS II, the special chlorophyll pair denoted P680 and often referred to as the primary donor. Components of the acceptor and donor complexes of PS II are then defined depending on whether they receive electrons from the excited singlet state of P680 ($P680^*$), or rereduce the oxidised $P680^+$. Figure 1.6 illustrates the donor and acceptor components of PS II, together with their proposed redox potentials. However, this simple definition is complicated by the fact that, in cyclic electron transfer, reduced components of the acceptor side can donate electrons to $P680^+$.

Overall, PS II has to couple the four-electron oxidation of water on the donor side with the two-electron reduction of PQ on the acceptor side, by means of the single-electron photochemistry in the reaction centre.

1.8.1 Polypeptide Composition of PS II

PS II is a multi-subunit complex: 2-dimensional electrophoresis suggests it may comprise over 22 polypeptides [42]. The complex may be viewed in terms of four functional parts: (i) the reaction centre complex, containing the primary reactants and plastoquinone-reducing components; (ii) the polypeptides associated with the oxygen-evolving complex, consisting of hydrophilic proteins bound to the lumenal surface of the thylakoid membrane; (iii) a proximal antenna; and (iv) a distal antenna. This section will describe in more detail (i) and (ii), the antennae having been described in an earlier section. A

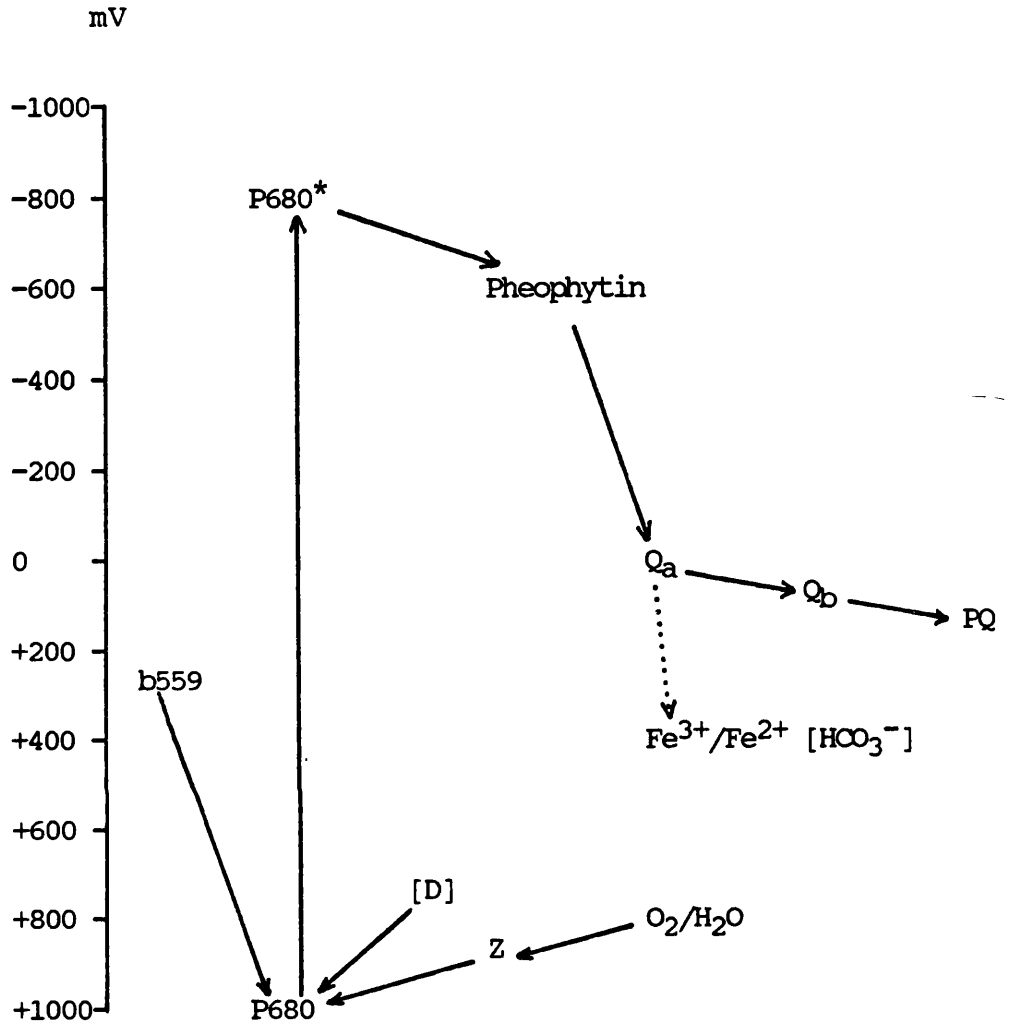

Figure 1.6 Diagram of Electron Transfer in Photosystem II

The similarities between the models shown here and in Figure 1.5 can be seen: electron transfer from the primary donor, P680*, proceeds through pheophytin to the stable acceptors, Q_a and Q_b, which are plastoquinones. Q_b mediates transfer of electrons to free plastoquinone, located in the membrane phase. There is also a non-heme iron (which is redox active under certain conditions) to which a bicarbonate anion is thought to ligate for electron transfer to occur. Z and D are tyrosine residues: Z is thought to mediate rapid electron transfer to $P680^+$ from the water-oxidising complex; D may play a role in the deactivation of S-states. The physiological role of cytochrome b559 is unclear, although it can function as a donor at low temperatures.

speculative arrangement of these is illustrated in Fig. 1.7.

1.8.1.1 The Reaction Centre Complex

Four chloroplast-encoded polypeptides appear to form the minimum structural unit capable of performing the primary photochemistry of PS II [2]: the two polypeptides D1 and D2 ('D' for 'diffuse', owing to the appearance of the bands in polyacrylamide gels), and the two apoproteins of cytochrome b559 (α and β). There is also a 9kDa phosphoprotein of undetermined function.

The assignment of D1 and D2 as the two polypeptides that bind the reaction centre components was originally made on the basis of gene sequence homology between D1 and D2 and the bacterial reaction centre polypeptides L and M [43],[44]: L shows homology with D1, [45], [46], [47] and M is homologous to D2. The structure of PS II based on the model by Trebst [48], as shown in Figure 1.8 The two core polypeptides each contains five membrane-spanning helices, labelled A - E, connected by exposed sections ('loops'). This model stresses the possible roles of conserved residues in binding the cofactors of electron transport: three pairs of histidines, in symmetry-related positions on the D and E helices of D1 and D2, were proposed to ligate to the non-heme iron and the magnesium atoms of P680; a second pair of symmetry-related histidines were suggested as ligating accessory chlorophylls.

This assignment was confirmed by the isolation of a D1/D2/cytb559 complex able to perform electron transport from an artificial donor, diphenylcarbazide, to an artificial acceptor, silicomolybdate [49], [50]. This minimal complex also undergoes basic photochemistry: it forms a chlorophyll triplet upon illumination, indicative of radical pair formation, i.e., $P680^{+}.Pheo^{-}$. The exact stoichiometry of redox cofactors remains

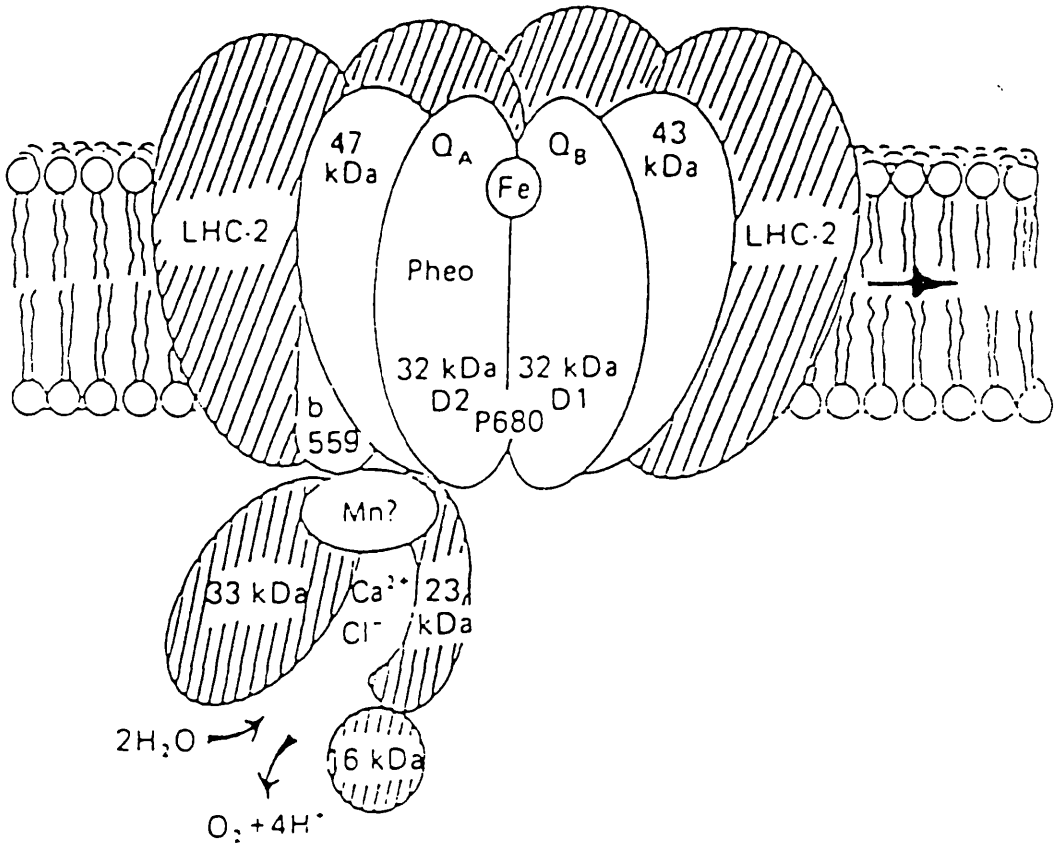

Figure 1.7 Proposed Model for the Arrangement of the Polypeptides in Photosystem II

The reaction centre of photosystem II consists of the D1/D2 heterodimer, which binds the electron transfer cofactors P680, pheophytin, Q_a and Q_b, as well as the non-heme iron. Z and D (not shown) are tyrosine residues of D1 and D2, respectively. CP43 and CP47 are believed to form the tightly-associated antenna of PS II, whereas LHC-2 appears to dissociate following phosphorylation. Shaded polypeptides are coded for by nuclear genes and unshaded by the chloroplast genome.[From Gounaris, K., Barber, J. and Harwood, J.L. (1986) Biochem. J., 237, 313.]

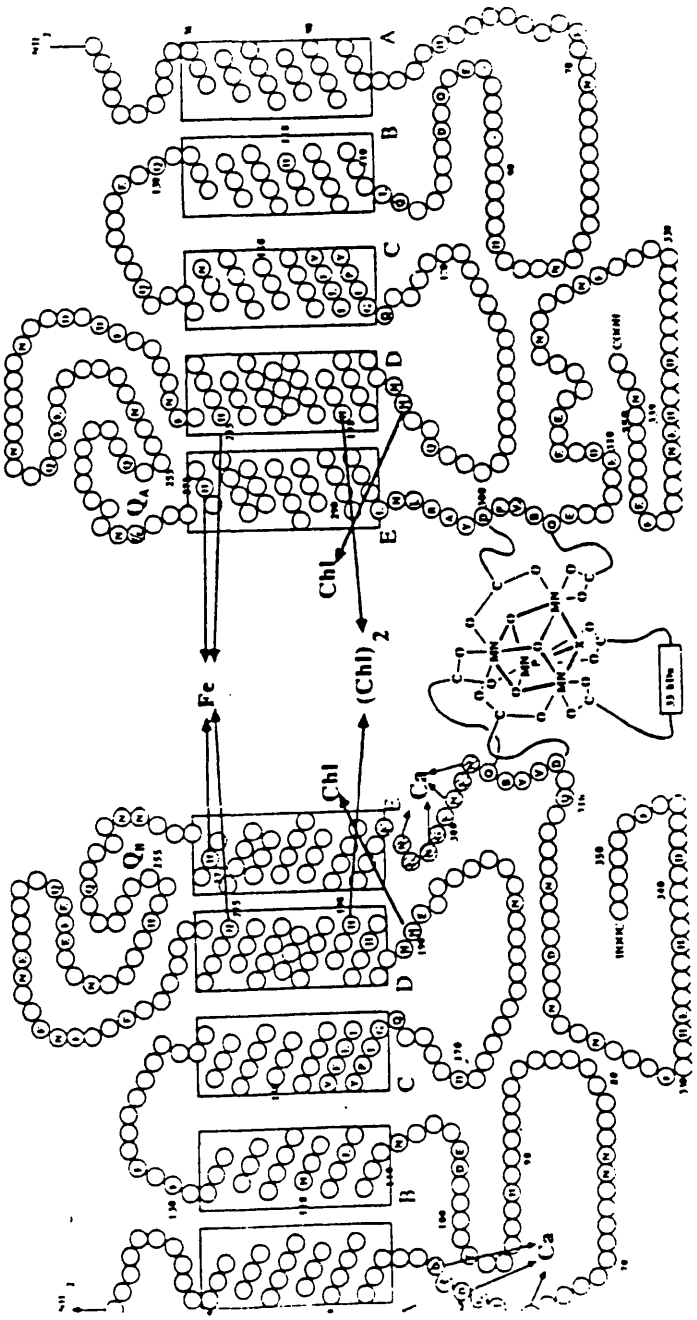

Figure 1.8 Proposed Structure of D1/D2 Reaction Centre of Photosystem II

The figure shows a hypothetical structure for the manganese complex involved in water oxidation as well as its ligation to the D1/D2 heterodimer and 33kDa extrinsic polypeptide. The folding pattern of D1/D2 in the membrane is taken from [48]. The diagram indicates the five transmembrane helices proposed for D1 and D2, and the symmetry-related ligation of P680, ancillary chlorophylls and non-heme iron. [From Dismukes, G.C., (1988) Chemica Scripta, 27a]

uncertain but is thought to be, per reaction centre, four or five Chl a molecules, one or two pheophytin and one β-carotene. There are no quinone molecules associated with this isolated reaction centre.

The D1/D2 polypeptides, by analogy with the L and M polypeptides from Rps. viridis, are believed to form a membrane-spanning heterodimer.

1.8.1.2 The Oxygen-Evolving Complex

Associated with the oxygen-evolving complex in higher plants and algae, are three polypeptides with apparent molecular weights 33, 23 and 16 kDa, bound extrinsically to the lumenal surface of the thylakoid membrane and closely to the polypeptides of the reaction centre itself. There is a fourth polypeptide, with molecular weight ≈5 kDa that is also proposed to be a part of this complex. Their role is believed to be to regulate the ionic cofactor requirements and exchange of reactants of water oxidation. It is clear that there are equal amounts of 33, 23 and 16 kDa polypeptides, and cross-linking patterns suggest 2 copies of each per PS II [51].

The relative positions of the three polypeptides have been investigated using cross-linking, protease and immunological methods, which have indicated that the 33kDa polypeptide lies adjacent to the reaction centre, whereas the 23 and 16 kDa polypeptides appear to mask the 33kDa from the aqueous lumen. These two smaller polypeptides also cross-link with components of the proximal and distal antennae.

The extrinsic polypeptides can be depleted to different degrees by various ionic treatments, and characterisation of the depleted systems can give information as to the functions of the polypeptides. Washing with 1M Tris at pH 8.0 results in the loss of all three polypeptides, with almost total loss of oxygen evolution. Washing

with 2M sodium chloride removes only the 23 and 16 kDa components. Loss of the two smaller polypeptides under certain conditions can lead to a 50% decrease in oxygen evolution, which can be restored by addition of Ca^{2+} or Cl^-: these polypeptides are viewed as having a Ca^{2+}/Cl^- concentrating function, regulating the binding affinities of these two ionic cofactors to their functional sites.

Cyanobacteria have a polypeptide analogous to the 33kDa polypeptide of plants: in three species of cyanobacteria, P.laminosum, Synechococcus leopoliensis (Anacystis nidulans) and Anabaena variabilis, immunoblotting assays with antibodies raised against the chloroplast proteins indicated counterparts to the 33kDa polypeptide; a 34kDa polypeptide from S. vulcanus partially replaced activity of the 33kDa polypeptide from depleted chloroplasts; finally, there is similarity in the gene-sequences for these polypeptides in spinach and cyanobacteria. This polypeptide is thought to have a role in stabilising the manganese complex central to the water oxidising function. On the other hand, no counterparts have been found in cyanobacteria for the 16 or 24 kDa polypeptides. A 9 kDa polypeptide has been identified in P.laminosum as being necessary for maximum oxygen-evolving activity, which when removed, slows, but does not inhibit, a dark step in the S-state transitions [52]. It does not appear to have an activity comparable to the Ca^{2+} or Cl^- concentrating activity of the 16 and 24 kDa polypeptides of higher plants.

1.8.2 The Primary Donor, P680

The absorption difference spectrum of the primary donor in PS II was first measured by Doring and coworkers, who observed bleachings at 682 and 435nm. From this it was suggested that P680 was a modified form of chlorophyll a [53]. The redox potential of

the $P680^+$/P680 couple has been estimated at +1100mV.

The exact nature of P680 is still unclear. The epr signal due to $P680^+$ has a g-value of 2.0026 and linewidth of ≈0.8mT, which is similar to Signal I from chloroplast preparations identified by Commoner [54]. Signal I, assigned to $P700^+$ from PS I, has a g-value of 2.0025 and a linewidth of 0.75mT. This compares with a similar epr signal, seen following the in vitro oxidation of chlorophyll, which has a g-value of 2.0026 but a width of 1.4mT. The narrower linewidth of Signal I was attributed to a chl dimer [55].

An analogous narrowing occurs in the signal equivalent to Signal I from Rb. sphaeroides, compared with epr signal from Bchl oxidised in vitro. In the $Bchl^+$ monomer, the unpaired electron exists over a π-conjugated system and may interact magnetically with different nuclei. If it is assumed that the participating nuclei are identical, and ignoring other line-broadening mechanisms, the otherwise discrete epr line is broadened by a product $A.\sqrt{N}$, where N is the number of interacting nuclei and A is a measure of the strength of the electron-nuclear interaction. If the electron is then delocalised equally over the π-systems of two identical molecules, it is argued that the electron then interacts with twice the number of nuclei, i.e., $N_2 = 2.N_1$, but that the strength of the interaction, A_2, is only equal to $\frac{1}{2}.A_1$ since the electron spends only half the time in the vicinity of each nucleus. The ratio of monomer:dimer linewidths is thus $A_1.\sqrt{N_1} : \frac{1}{2}.A_1.\sqrt{(2N_1)}$, or, $\sqrt{2} : 1$, which agrees closely with the experimental observation for the epr signal of oxidised reaction centre Bchl.

However, this semi-quantitative argument cannot be applied generally: the narrowing of the epr signals from Rps. viridis reaction centre compared with $Bchl^+$, and from PS II compared with Chl^+, differs from this ideal value, suggesting that the assumptions

made for a symmetric dimer are incomplete. There is further epr evidence for a monomeric P680: the zero-field splitting parameters for the spin-polarised triplet are consistent with a monomeric chlorophyll [56],[57].

1.8.3 Components of the Donor Complex to $P680^{+}$

1.8.3.1 The Oxygen-Evolving Complex

The four-electron gate on the donor side was first shown by Joliot and co-workers [58] by measurement of the oxygen yield from dark-adapted chloroplasts as a function of single turnover, saturating Xenon-lamp flashes. The oxygen yield showed a damped oscillatory pattern with a periodicity of four, beginning after the third flash. This observation led directly to the 'S-state cycle' model of Kok ([59], and Figure 1.9) which proposed five discrete S-states (labelled S_n, where n = 0,1,2,3 and 4), where S_0 is least oxidised and S_4 defined as the state which spontaneously reacts to release oxygen and regenerate S_0. The majority of PS II centres in a dark adapted sample are in S1. In the light of recent knowledge, the S-states have come specifically to refer to successive oxidation states of the manganese complex (including possible oxidation of ligands to the metal ions, rather than the metal ions themselves) believed to be the active site of water oxidation in PS II.

It has been established that each PS II reaction centre contains four manganese, all of which are required for oxygen evolution [60]. It is believed that these form a protein-bound complex which is the catalytic site of water oxidation, often referred to as the oxygen-evolving complex (OEC) . The arrangement of the manganese has been partially characterised, primarily through X-ray and epr spectroscopy.

A low-temperature epr signal, referred to as the 'multiline'

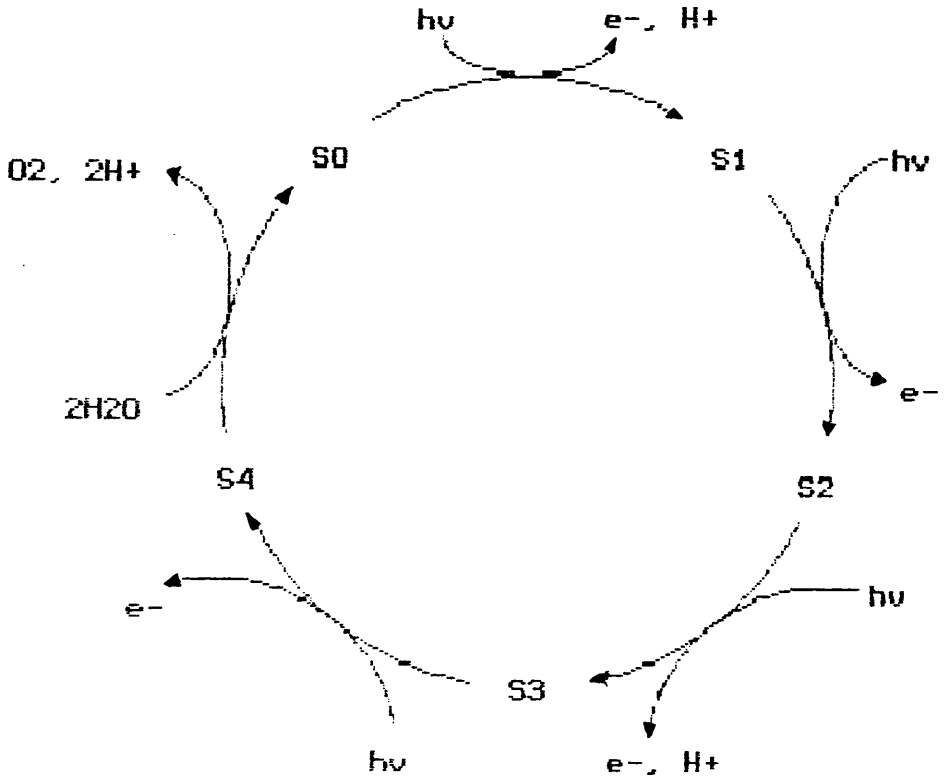

Figure 1.9 Model of the 'S-state Cycle' for Accumulation of Four Positive Charges

Bessel Kok originally proposed five S-states, where S_0 was the least oxidised and S_4 defined as the state which undergoes a spontaneous reaction to yield oxygen. Photooxidation of P680 (single-electron chemistry) causes the stepwise change in the S-states. In the light of recent knowledge, the term S-state refers to any the successive oxidation states of the manganese complex, including possible oxidations of the ligands to the metal ions themselves (e.g. S2 ——> S3). Release of oxygen from dark-adapted PS II after three flashes, suggests S1 as the dark stable form. Shown in the diagram is also a proposed proton release pattern. [Based on diagram from Rutherford, A.W. (1989) TIBS, 14, 227-232.]

signal, having 16 or 19 partially resolved hyperfine lines, has been attributed to the S_2 state of the cycle described above [61]. This signal can be generated by continuous illumination of dark-adapted PS II at 200K, freezing-under-illumination in the presence of DCMU, or by saturating single turnover laser flash. A number of models have been put forward to account for this observed lineshape. The multiline spectrum is similar to spectra observed from di-μ-oxo bridged Mn(III)Mn(IV) complexes, and arguing by analogy, it has been suggested that the OEC might have a similar structure.

In these artificial complexes, the spins of the two manganese ions interact via strong antiferromagnetic exchange coupling, giving a species with an effective ground state electronic spin of $S=\frac{1}{2}$. This state has an epr signal that is nearly isotropic, centred close to g=2. The signal is split into 16 lines, due to the interaction with the non-equivalent $I=5/2$ manganese nuclei.

The S_2 multiline signal is proposed to arise from an analogous pair of exchange coupled manganese nuclei, and the splitting from interaction with two (or more) manganese nuclei. However, successful modelling of the 19-line multiline signal has not yet been achieved.

A second epr signal arising from the S2 state, centred at g=4.1 [62], [63] can be formed as well as the multiline signal, the relative yields depending upon various factors: ethanol, ethylene glycol and glycerol inhibit formation of the g = 4.1 [64]; whereas illumination at 140K [65], or addition of F^- following extraction of Cl^- [66], decrease yield of the multiline. The interpretation of this signal is also ambiguous: either it arises from an $S=3/2$ ground state produced by a modified spin-coupling pattern within a tri- or tetranuclear complex, or, it could be due to monomeric Mn(IV).

Analysis of the extended X-ray absorption fine structure (EXAFS) arising from the manganese complex has been done by several

groups. Klein, Sauer and co-workers have found that the average manganese coordination environment includes a Mn-(N,O) distance of 0.175 - 0.18nm, a disordered shell of oxygens or nitrogens at 0.215nm from the Mn and a Mn-Mn distance of 0.27nm, reviewed in [67]. The technique is not sufficiently sensitive to discriminate between types of low atomic weight scatterers, e.g. nitrogen and oxygen, and therefore the two are invariably mentioned together: exact assignment requires other information. The shorter Mn-(N,O) distance has been assigned to a di-μ-oxo bridging ligand, Mn-O-Mn, based on comparison with dinuclear manganese models; and the longer Mn-(N,O) distance to terminal, non-bridging ions. The detection of Mn at 0.27nm is evidence of at least a dinuclear cluster, but is no proof of any higher nuclearity.

There have also been reports of a second shell of manganese scatterers at 0.33nm: this feature was observed to show significant dichroism, and on this basis was deduced to be aligned close to the membrane normal [68], [69]. It has been proposed that this longer distance could arise from a single Mn atom within an asymmetric cluster of more than two Mn atoms.

Simulations of EXAFS have indicated that tetranuclear cubic [70] or 'butterfly' [71] arrangements are unlikely, although bi-, tri- or highly disordered tetranuclear structures have not been ruled out. On the basis of the X-ray and epr work the following suggested arrangements have been put forward: a single Mn tetramer [72], [73], [74]; a single Mn dimer with one or two adjacent Mn monomers [75]; or a pair of Mn dimers [76], [77].

Information on the valence state of the Mn can be extracted from X-ray absorption spectra by analysis of the K-absorption edge: not only by determination of the edge-energy (which varies with ligand field for a given oxidation state), but also by the 'edge-

shape'. It appears that the average oxidation state in S_1 is Mn(III), with one Mn being oxidised on conversion to S_2. The organisation of S_3 does not appear to differ from that of S_2, in terms either of its coordination environment or oxidation state [78]. Accepting that some component of the complex is oxidised at each point of the S-state cycle, it has recently been proposed that a histidine might form the charge-storage component on the transition from S_2 to S_3 [79].

1.8.3.1.1 The Mechanism of Water Oxidation

Little is known about the mechanism by which the manganese complex brings about oxidation of water. It is assumed, at least, that the complex is able to bind the two water molecules in an orientation permitting formation of the dioxygen bond. However, the sequence of binding of water to the S-states is not known. There are two lines of evidence suggesting that water binds directly, at some point in the cycle, to the manganese:

1) Ammonia, a water analogue and potent inhibitor of water oxidation, has been shown by the technique of electron spin echo envelope modulation (ESEEM) [80], and inferred from its modification of the multiline signal [81], to bind directly to manganese in the S_2-state.

2) The linewidth of the S_2-multiline is broadened in samples of PS II incubated with $H_2{}^{17}O$ [82] , from which it was inferred that oxygen ligates directly to Mn, in the form of $O_2{}^{2-}$, OH^- or H_2O.

Recent results of Plijter and coworkers [83] suggest that water oxidation occurs as a kinetically and mechanistically distinct process from that of charge accumulation by the manganese complex.

1.8.3.2 Z and D

An epr signal having a g-value of 2.0046 and a partially-resolved hyperfine lineshape, termed Signal II, was identified in the 1950s by Commoner [54]. Several components of this signal have since been distinguished on the basis of their kinetic decay times. A component, termed Z, believed to be the interface between the reaction centre and the water-oxidising complex, gives rise to a signal with fast re-reduction kinetics, termed Signal II_{vf} (very fast) [84]. In the native state, Z^+ is reduced rapidly by the OEC, with times that are S-state dependent; in preparations where the OEC is damaged the reduction of Z^+ is slower, and the corresponding component of the epr spectrum is called Signal II_f (fast) [85].

A third component of the spectrum is due to a different component of the donor complex, called D, whose oxidised form, D^+, gives rise to a dark-stable component of Signal II, called signal II_s (slow) [86]. D was shown to be able to reduce S_2 and S_3 with rate constants of approximately $1s^{-1}$; the normal, oxidised state has also been shown to oxidise S_0 to S_1 [87].

Interpretation of several lines of evidence suggested that the signal arose from a plastoquinone radical: for example, extraction of plastoquinone and reconstitution with deuterated quinone led to a narrowing of the signal [88]; and more recently, the partially-resolved hyperfine has been attributed to the 2-methyl group on the $PQH_2^{\cdot +}$.

This assignment presented a number of difficulties:

1) Extraction of plastoquinone did not result in complete extraction of the original Signal II, necessitating data manipulation to obtain the spectrum from deuterated D^+.

2) Quantification of plastoquinone in the reaction centre indicated that there was insufficient quinone to account for Z, D and the

acceptor quinones.

3) $PQH_2^{\cdot +}$ is not an accurate model for the observed spectra of Z^+ and D^+: the g-value is higher than those of a range of model quinones, with values in the range 2.0034 - 2.0038, and the hyperfine characteristics could not be observed in oriented quinone samples.

The spectra of Z and D are now assigned to two redox active tyrosines which are a part of the D1 and D2 polypeptides. Barry and Babcock first showed the involvement of tyrosine [89], by using a method selectively to deuterate tyrosine in Synechocystis, in vivo, which led to alteration of the dark-stable Signal II. Deuteration of methionine, the precursor to plastoquinone, caused no such change. From the original assumption that Z and D were identical chemical species, since their spectra were identical, it was argued that both would be tyrosine residues.

Two tyrosine residues to account for this result were suggested by the model of PS II proposed by Trebst [48] and D is now assigned to Tyr-160 of the D2 polypeptide, and Z to the symmetry-related residue of the D1 polypeptide, Tyr-161. This assignment was made by site-specific mutagenesis of the two amino-acids. Replacement of Tyr-160 of D2 by a phenylalanine, in Synechocystis sp., results in a mutant capable of growing photosynthetically, but lacking the dark-stable epr signal of D^+ [90], [91]. Tyr-161 of D1 was confirmed as the component Z by similar mutation of this residue, following deletion of all three copies of the psbA genes encoding this polypeptide. This mutant showed the stable epr signal due to D^+, but was unable to grow photosynthetically. Its fluorescence characteristics indicated disruption of the forward electron flow to $P680^+$ [92].

The exact role of D in vivo is not known. Its slow kinetics indicate that it is not a part of the main electron transfer pathway;

and the survival of mutants from which it has been deleted show that has no obligatory role. An ancillary role in photoactivation, by which a functional manganese complex is assembled, has been proposed [93].

1.8.3.3 Cytochrome b559

Associated with the reaction centre core is at least one heme protein, cytochrome b559 (cyt b559). The apoprotein of cyt b559 consists of two polypeptides of molecular weight ≈4 and ≈9 kDa, and it has been proposed that the heme is bound by histidine ligands supplied by the two adjacent subunits [94]. It is known to be photooxidised by $P680^+$ at 77K, but its exact role in vivo is still uncertain. It is not thought to be a component of the main electron-transfer chain, since the kinetics of its photooxidation at room temperature are slow and the extent of the reaction small. There are several suggestions, which are not necessarily incompatible with each other: 1) In reaction centre core particles it may have structural role; 2) A role in the assembly of a functional Mn complex; 3) protection of PS II from photoinhibition, by reducing chlorophyll oxidised by $P680^+$. 4) Cyt b559 can be reduced by components of the acceptor side of PS II, which may indicate a role in cyclic electron transfer.

On the basis of its redox potential, cytochrome b559 exists in two (or three) forms: a high potential form, with E_m = +370mV, and a low potential form, with an E_m between +60 and +80mV. These two forms may be distinguished by the g-values of the epr signals arising from their oxidised states (Fe^{3+}). A third intermediate form has also been reported, with E_m of +240mV. A shift from the high to low potential forms had been correlated with damage to PS II, but exceptions to this have been found.

1.8.4 The Electron Acceptor Complex of Photosystem II

1.8.4.1 Pheophytin

The first acceptor from $P680^*$, called the intermediate or transient acceptor owing to the rapidity of its reduction and reoxidation, is thought to be a pheophytin molecule, i.e., a molecule with a chlorophyll structure, but missing the central coordinated magnesium ion. This proposal was first made by Klimov and co-workers on the basis of the light-induced bleaching of absorbance bands at 420nm and 680nm, and the appearance of absorbances at 450nm, 660nm and at >695nm. These changes implied the reduction of either pheophytin or chlorophyll: the bleaching of two less intense bands at 518nm and 545nm are characteristic of pheophytin [95]. This component is identical with an intermediate I proposed by Rademaker et al, [96]. Its midpoint potential is
-610mV.

This component has an epr spectrum with a signal centred at g = 2.0035 and having a linewidth of 1.25mT, similar to that of the anion radical of pheophytin *in vitro*. Samples under reducing conditions (-450mV) which are subsequently illuminated at 220K give rise to a low-temperature spectrum in which the epr signal from pheophytin is split by ≈5mT around g = 2.0020 [97]. There is an analogous signal arising from $Bpheo^-$ in bacterial reaction centres (which preserve their functional donor cytochrome), attributed to an interaction between the Bpheo anion and the singly-reduced electron acceptor, a menaquinone-iron complex ($MQ^-.Fe^{2+}$) [98].

The kinetics of reduction of this component ($P^*I \longrightarrow P^+I^-$) have been measured at 3ps in the D1/D2/cytb559 preparation, based on the rise time of an absorbance band at 820nm from the state P^+I^-[99]. A second estimate for this rate, obtained at low temperature by

photochemical hole-burning, is given as 1.8ps [100]. These values are comparable to those obtained for the purple bacterial reaction centre described in Section 1.6.

1.8.4.2 The First Stable Acceptor, Qa, (Plastoquinone)

Under normal conditions, the primary acceptor, Q_a, is a one-electron acceptor. Formation of this semiquinone is not thought to be accompanied by a protonation of the semiquinone. The time constant for Q_a reduction from pheophytin has been inferred to be 350 ± 100ps [101].

The increase in chlorophyll fluorescence yield following the photoreduction of a component of PS II was the first evidence for the existence of Q_a ('Q' for 'quencher') [102]. Reduction of this component was also accompanied by the shift of an absorbance band at 546nm. Later, on the basis of increases in an absorbance close to 320nm, Q_a was tentatively assigned to a plastoquinone (PQ) molecule [103]. The complete absorption reduced-minus-oxidised difference spectrum for sub-chloroplast fractions at room temperature was determined by van Gorkom [104]. The shape, position and amplitude of absorbance changes indicated the reduction of one bound plastoquinone per reaction centre.

Extraction of both plastoquinone and ß-carotene with 2% hexane/methanol causes the loss of two properties [105]: firstly, the ability at low temperature to form the $P680^+$ cation; and secondly, the observation of the shift in an absorbance at 550nm of ß-carotene, indicative of charge separation in the reaction centre. Readdition of PQ restores the ability stably to photooxidise P680; whereas readdition of the carotene alone restores neither capability. The interpretation of this result is that PQ is responsible for the stabilisation of the charge-separated state in PS II, i.e.,

$P680^+.I.PQ^-$, whilst ß-carotene has no direct role in the primary photochemistry.

Confirmation of PQ as a part of the acceptor complex was made by the detection of an broad epr signal, analogous to a similar signal from reaction centres of purple non-sulphur bacteria having a g-value of 1.8, in a highly-active PS II preparation from the unicellular green alga Chlamydomonas reinhardtii [106]. The fluorescence properties of these PS II particles indicated that only the primary acceptor was bound. A similiar signal has since been discovered in PS II preparations from higher plant and cyanobacteria [107], [108]. The lineshape and g-value of the g=1.8 signal in purple bacteria has been ascribed to the magnetic coupling of the semiquinone with the non-heme ferrous iron, and the interaction has been modelled in some detail [109]: the signal from PS II is likewise attributed to such an interaction. Because of this interaction, the primary acceptor is often referred to as a quinone-iron complex, Q_a-Fe^{2+}.

A second epr signal due to this complex was discovered later in higher plant PS II [110]. The g-value (g = 1.9) and lineshape of this signal distinguish it clearly from the g = 1.8 form, and indicate differences in the local environment of the complex in the two cases. This signal is similar to one due to the Q_a-Fe^{2+} complex of the purple bacterium Rhodospirillum rubrum [111], [112]. In particular, it was noted that the signals were interconvertible: the g = 1.8 form is favoured, in the higher plant preparations, at low pH (6.3 compared with 7.5), and under conditions in which bicarbonate is depleted from the samples.

In theory, any of the properties of Q_a that are dependent upon its redox state can be titrated, and estimates made of the midpoint potential of the species. The potential of the species, however, is

the cause of some controversy. The curve of the fluorescence yield due to Q_a shows two waves [113], with midpoints at pH 7 of -240mV and -30mV, both of which show a pH dependency of -60mV per pH unit, indicating protonation accompanying the reduction. The two steps have been known historically as Q_l and Q_h, indicating low and high potentials. Two interpretations of this result have been either that: 1) there is in addition to Q_a a parallel acceptor, but with a different midpoint potential, whose reduction causes the observed rise in fluorescence; 2) there is no additional acceptor, but two distinct populations of PS II, in which the primary acceptors have different midpoint potentials.

This heterogeneity is not observed in all experimental situations: it is not detected in titrations of the carotenoid bandshift at 550nm (which may only mean that it does not give rise to a transmembrane electric field) [114], which titrates in one step with an $E_{m\ 7}$ of -40mV [115], [116]. Neither does titration of the fluorescence yield from PS II isolated from P. laminosum show two steps [117].

Titration of the epr signals arising from PS II has also resulted in a somewhat confused picture: two steps in the reduction of the g = 1.8 signal were seen in formate-treated PS II from spinach, and assigned to Q_h and Q_l [118]. On the other hand, titration of the same signal from PS II extracted from Chlamydomonas reinhardtii showed only the single, higher potential, step [119].

In this thesis the redox properties of epr signals arising from the acceptor side of PS II isolated from P.laminosum are extensively investigated. The interpretation of these conflicting results will therefore be discussed more fully later.

A third epr signal with a g-value of ≈1.6 has also been attributed to an interaction between the Q_a-semiquinone and the non-

heme iron [120]. This will be discussed below, as the characterisation of this signal occupies a large part of the present work.

1.8.4.3 The Second Stable Acceptor, Qb, (Plastoquinone)

As in the reaction centre of purple non-sulphur bacteria, a second quinone accepts an electron from Q_a. The existence of this species was proposed simultaneously, but independently, for both bacterial and PS II reaction centres [121], [122], [123]. This molecule acts as a two-electron carrier, i.e. undergoes double reduction and protonation to give the quinol [124] when the molecule dissociates from the reaction centre and exchanges with plastoquinone of the pool. Electron transfer from Q_a to Q_b and Q_b^- has two different time constants, ≈100μs and ≈400μs respectively.
Recombination can occur with oxidised S-states, with time constants for back-reaction with S_2 and S_3 measured at ≈30s, whilst for S_1 the time-constant is of the order of hours.

The rate of electron transfer from Q_a to Q_b is affected by the presence of bicarbonate [125], [126]. Depletion of bicarbonate either by exposure to low pH or certain anions (e.g., formate) leads to a slowing of the rate: in dark adapted chloroplasts depletion by formate causes a 4-fold slowing at the first saturating flash, and 20-fold after subsequent flashes. This effect is reversed by addition of bicarbonate. There are three areas of uncertainty with respect to the mechanism of this 'bicarbonate effect':
(1) The nature of the active species is also not known, since bicarbonate in solution exists in equilibrium with carbon dioxide and carbonic acid.
(2) The bicarbonate anion has been suggested to act either as an allosteric regulator or as a participating species in protonation

reactions associated with the reduction of Q_b to quinol.

(3) The bicarbonate ion has been argued to bind directly to the non-heme ferrous ion located between the two quinones, mimicking the ligation by glutamate in the purple non-sulphur bacteria. An alternative proposal was for the formation of a carbamate species, by binding of carbon dioxide to a lysine residue.

Although a g = 1.8 epr signal, similar, though not identical, to that assigned to the interaction between Q_a^--Fe^{2+}, has been attributed to the interaction between Fe^{2+}-Q_b^- in purple bacteria [128], [129] no analogous signal has been seen in PSII. This signal was titrated and an E_{m8} of +70mV given to the couple Q_b/Q_b^- in Rps. viridis [130]. However, a signal similar to the g = 1.9 has been tentatively assigned to this interaction [131].

The redox potentials of the two secondary plastosemiquinone redox couples from PS II have not been directly measured. However, estimates of the equilibrium constants for the electron-transfers between Q_a and Q_b and Q_{b-} have suggested a span of ≈80mV between the Q_a/Q_a^- and Q_b/Q_b^- couples in chloroplasts, which is close to that of Rb. sphaeroides, reviewed in [132].

1.9 Aims of this Thesis

The properties of the electron acceptor complex of PS II isolated from the thermophilic cyanobacterium P. laminosum were studied. Having detected a g = 1.9 signal, attributable to the Q_a^--Fe^{2+} interaction, it was attempted to characterise the conditions for its formation, and also its redox potential. At the same time, an epr signal with g = 1.6 was detected, and a substantial part of the work described here was directed towards characterising this signal.

The final chapter of the thesis describes EXAFS measurements of the manganese water-oxidising complex of PS II.

2. MATERIALS AND METHODS

2.1. Isolation of Photosystem II-Enriched Particles from Phormidium laminosum

Oxygen-evolving preparations of PS II have been isolated from a number of cyanobacteria. The first of these was from the lysozyme-sensitive filamentous species Phormidium laminosum [133]. The method used in this thesis differs from the original preparation by use of a different detergent and a different means of concentrating the PS II particles.

2.1.1. Growth of P. laminosum.

P. laminosum was grown on Medium D of Castenholtz, [134]. This medium is prepared as a x10 stock solution, shown in Table 2.1, and diluted to working strength when required.

P. laminosum was grown routinely in 10, 5 and 0.8 litre cultures. The 0.8 litre cultures were grown under air in 1.5l conical flasks at 45°C in a Gallenkamp orbital incubator (shaking speed, 40 cycles.min^{-1}). Illumination was by means of five fluorescent tubes. Larger cultures were grown in glass jars sparged with a filter-sterilised mixture of 5% CO_2/95% air (flow rate, 4l.min^{-1}) and placed on magnetic stirrers. Illumination for each jar was provided by a single 150W flood lamp. Light intensities were gradually increased during growth to a final value of 3000 lux.

2.1.2 Preparation of Thylakoids from P. laminosum

Cultures from either 10 or 5 litre jars were harvested by filtration using a Millipore Pellicon cassette system: a starting volume of ≈50l could be reduced to approximately 1.5l, from which

Table 2.1 Composition of x10 Stock Castenholtz Medium D

Compound	Conc.	($g.5l^{-1}$)
nitrilotriacetic acid	6.5mM	6.15
calcium sulphate (hydrated)	3.3mM	3.0
magnesium sulphate (hydrated)	4.0mM	5.0
sodium chloride	1.5mM	0.4
potassium nitrate	10mM	5.15
sodium nitrate	80mM	34.5
di-sodium hydrogen phosphate (hydrated)	1.60mM	1.60

As indicated, 5 litres of the above are made; this volume is to include:

i) 50ml of a 1mM solution of iron(III)chloride ($0.3g.l^{-1}$)

ii) 25ml of a micronutrient solution containing:

	Conc.	(l^{-1})
manganese sulphate (hydrated)	14 mM	3.01g
zinc sulphate (hydrated)	2.0mM	0.5g
boric acid	8.0mM	0.5g
copper(II)sulphate (hydrated)	100μM	25mg
sodium molybdate (hydrated)	100μM	25mg
calcium chloride (hydrated)	200μM	45mg
conc. sulphuric acid	5mM	0.5ml

* * *

This solution is diluted 10-fold, and corrected to pH 8.2 with sodium hydroxide, prior to autoclaving and use.

the cyanobacteria were pelleted by centrifuging for 10min at 16,000 x g (10,000 r.p.m using a Sorvall RC 5B with 6x400 rotor). The supernatant was discarded and the pellet washed twice in 0.5M sorbitol, 10mM $MgCl_2$, 10mM HEPES, 5mM K_2HPO_4, pH 7.5 (Buffer A). The cells were resuspended into Buffer A containing 12.5mM EDTA: 0.25g lysozyme is added per 250ml of suspension, and the whole was mixed rapidly (1-2s) in a blender. The homogenate was then transferred to a 500ml conical flask and incubated at 37°C for 1-2h. The extent of degradation of the cell wall was monitored by microscopy, and the reaction stopped by addition of cold Buffer A when spheroplasts were clearly visible. Spheroplasts were concentrated by centrifuging for 7min at 3,000 x g at 4°C, the supernatant discarded, and the pellet washed a second time in cold Buffer A. Lysis of the spheroplasts was achieved by resuspension and incubation in Buffer B, i.e., Buffer A without the sorbitol osmoticum. This suspension was homogenised in a hand-held glass homogeniser, then placed on a magnetic stirrer, in the dark and on ice, for 30min. Thylakoid membranes are then harvested by centrifuging at 25,000 x g for 15min at 4°C. This pellet is washed twice in the same buffer containing 25% (v/v) glycerol (Buffer C) before resuspension in a minimal volume of Buffer C. Membranes are stored at liquid-N_2 temperature.

2.1.3 Assay of Chlorophyll from P. laminosum Thylakoids and Photosystem II Particles

As described in Section 1.4, cyanobacteria have Chl *a*, but not Chl *b*. Extinction coefficients for chlorophyll *a* are given in [135], and the method here assumes Chl *a* to have a molecular weight of 893.5Da and an extinction coefficient, in 80% (v/v) acetone, at 663nm of 73,300$cm^{-1}.M^{-1}$ (i.e. 82.04 $cm^{-1}.g^{-1}.l$).

Thylakoids were thawed and chlorophyll extracted from 100μl into 10ml 80% (v/v) acetone. Absorbance at 663nm was measured in a 1cm path-length quartz cuvette against an 80% acetone blank, and related to the chlorophyll concentration by the expression

$$[Chl] = [Abs(663) \times ml.acetone] \div [82.04 \times \mu l.thylakoids]$$

2.1.4 Isolation of Photosystem II from P. laminosum Thylakoids

All parts of the method for isolating PS II from thylakoids should be done on ice and under green-filtered light in a light-restricted room.

Thylakoid membranes were re-homogenised and treated with the zwitterionic detergent N-dodecyl-N,N-dimethylammonio-3-propane sulphonate (SB12) [136]. Additions were made to the membranes of a 10% (w/v) stock solution of detergent and Buffer C to give a final concentration of 0.5% (w/v) SB12 and a chlorophyll concentration of 1mg.ml^{-1}. The mixture was stirred in the dark and on ice for 40min, before centrifuging at 250,000 x g for 1h using a Sorvall OTD-B ultracentrifuge and T865 titanium rotor (50,000 r.p.m). The supernatant was collected, and for each 5ml was added 1ml of 50% (w/v) poly(ethylene glycol) 6000 (PEG 6000), and PS II particles concentrated by centrifuging for 2h at 250,000 x g and 4°C. The pellet was resuspended in Buffer C containing 5mM EDTA, 1.2ml 50% (w/v) PEG 6000 added per 5ml suspension and centrifuged for 1h at 100,000 x g and 4°C. The pellet was washed again in Buffer C (without EDTA), and the PS II particles finally concentrated by addition of 1.5ml PEG 6000 per 5ml suspension, and centrifuging for 1h at 250,000 x g and 4°C. The particles were resuspended in a minimal volume of Buffer C and stored at 77K until used.

2.2 Isolation of PS II-Enriched Membranes from Spinach.

PS II enriched membranes were isolated from market spinach, Spinacia oleracea, for use in an EXAFS study of the manganese centre in PS II. A method was used based on that of Berthold, et al., [137], with the modifications of Ford and Evans, [138]. The modified protocol includes a period of dark incubation of thylakoids in Mg^{2+}-containing buffer. This step is believed to promote the tight stacking of the membranes, such that PS II is contained largely within the stacked, and PS I in the unstacked regions, of the membrane. Separation then relies on the differential detergent solubilisation of the different parts of the membrane.

Isolation of thylakoids was routinely performed in a cold room, under green-filtered light. All solutions should be kept at 4°C. Broken chloroplasts are light-sensitive; therefore light should be restricted as far as possible.

De-ribbed spinach leaves were ground in 330mM sorbitol (as an osmoticum), 20mM MES, 200μM magnesium chloride, pH 6.5 and approximately 1mM ascorbic acid. The brei was filtered through nine layers of muslin: approximately 2 litres of filtrate were centrifuged for 5 min at 3000 x g and 4°C. The supernatant was discarded and the pellet resuspended in excess 5mM (hypotonic) magnesium chloride for 1min, to lyse the chloroplasts. An equal volume of 660mM sorbitol, 20mM MES, 200μM magnesium chloride, pH 6.5 was added, followed by centrifugation for 20min at 3000 x g and 4°C. The pellet was resuspended to ≈4mg Chl.ml^{-1} in 5mM magnesium chloride, 15mM sodium chloride, 20mM MES, pH 6.3 ('resuspending medium') and left on ice in the dark for 90min. 20% (w/v) Triton TX-100 and resuspending medium were added to give a final concentration of 5% (w/v) Triton and a chlorophyll concentration of

2mg.ml^{-1}. The suspension was stirred and kept dark for 25min, then centrifuged for 30min at 40,000 x g. The pellet was finally resuspended into resuspending medium containing 20% glycerol, as cryoprotectant. Particles were stored at 77K until required.

2.3 Chlorophyll Assays

Chlorophyll in spinach PS II particles was calculated using methods derived from [135]. The formulae assume the following extinction coefficients, with units of cm^{-1}.mg^{-1}.l (in 80% (v/v) acetone): Chl *a*, 82.04 and 16.75 ; Chl *b*, 9.27 and 45.6 (at 663 and 645nm). Molecular weights of Chls *a* and *b* are 893.5 and 907.5, respectively, from which molar extinction coefficients can be calculated.

Chlorophyll was extracted from 50μl of a chloroplast suspension or PS II preparation into 10ml 80% (v/v) acetone. The suspension was mixed before filtering through Whatman No.1 filter paper. Absorbances were measured in a 1cm path-length quartz cuvette at 645 and 663nm against an 80% acetone blank. The chlorophyll concentration and chlorophyll *a* to *b* ratio were then determined using the following formulae:

(1) [Chl *a*] = $[(0.0127 \times A_{663}) - (0.00258 \times A_{645})] \times 200$ mg.ml^{-1}

(2) [Chl *b*] = $[(0.0229 \times A_{645}) - (0.00467 \times A_{663})] \times 200$ mg.ml^{-1}

The derivation of these equations is straightforward, and is shown in Appendix A.

2.4 Measurement of Oxygen Evolution

The rate of oxygen evolution from PS II particles was measured using a Clark-type oxygen electrode.

Samples were maintained at a constant 18°C by means of a water-jacket and a thermostatic pump. Illumination was by means of a 1kW photographic lamp, with a serum bottle of water placed between the lamp and the sample, to minimise heating of the electrode. Measurements were made in resuspending medium (spinach) or Buffer C (P. laminosum), at chlorophyll concentrations of approximately 10$\mu g.ml^{-1}$, such that light was saturating.

Oxygen-evolution data are typically recorded in units of μmol $O_2.mg^{-1}$ Chl.h^{-1}.

2.5 Absorption Spectroscopy

Absorption spectra from the different fractions from preparations were recorded at room temperature using a Phillips PU 8740 UV/VIS scanning spectrophotometer. 1ml quartz cuvettes with 1cm path-length were used.

2.6 SDS Polyacrylamide Gel Electrophoresis

The polypeptide composition of fractions from the preparation of P. laminosum were determined using vertical SDS-PAGE by the method of Chua [139].

The separating gel was a 15% (w/v) acrylamide, 0.4% (w/v) N,N'-methylenebisacrylamide slab gel which contained 0.13% (w/v) SDS, 6M urea (equivalent to 36% w/v) and 85mM Tris-HCl, pH 9.18, polymerised using a fresh 0.06% (w/v) solution of ammonium persulphate and 0.07% (v/v) N,N,N',N'-tetramethylethylenediamine (TEMED). A 1-2cm stacking gel, containing 6% (w/v) acrylamide, 0.16% (w/v) N,N'-methylenebisacrylamide, 0.4% (w/v) SDS, 0.125mM Tris-HCl, pH 6.8 and 36% (w/v) urea, was polymerised as above onto the top of the separating gel.

Samples were solubilised overnight at room temperature in 4%

(w/v) SDS, 5% (v/v) mercaptoethanol, 5% (v/v) glycerol, 0.2% (v/v) bromophenol blue, 36% (w/v) urea and 95mM Tris-HCl, pH 6.8.

The running buffer contained 2M glycine, 0.1% (w/v) SDS and 0.375M Tris-HCl, pH 8.3. The gel was run using a constant current of 15mA for approximately 6h. Gels were stained with Coomassie Brilliant Blue in 10% acetic acid and 10% methanol, and finally destained in 10% acetic acid and 10% methanol.

2.7 Tris-inactivation of Photosystem II

Samples of PS II for use in kinetic optical spectrophotometry were incubated at 1mg.ml^{-1} Chl, 0.8M Tris-HCl, pH 8 for 1h at 4^{o}C. Following this, PS II was collected by centrifuging for 30min at 40,0000 x g. Samples treated in this way are inhibited for oxygen-evolution.

2.8 Kinetic Optical Spectrophotometry

The lay-out of apparatus used to measure time-resolved absorbance changes at 820nm is shown in Figure 2.1. Absorbance changes at 820nm (an increase in absorbance occurs upon photooxidation of P680) were measured at room temperature in a 1cm path-length, 'four-sides-clear' quartz cuvette. A purpose built single-beam spectrophotometer was used, as in [140]. A large-area, silicon photodiode, type PIN 10-D (United Detector Technology, Optilas, U.K.) was employed as a detector, coupled to a low-noise differential amplifier (EG/G Princeton Applied Research, Model 113). The limit of resolution of this apparatus was of the order of 5μs. The measuring beam was provided by a 250W tungsten filament lamp powered by a Constant D.C. source (Model ASC 3000PC).

Signals were recorded with a Datalab 920 transient recorder and averaged with a Datalab 4000B signal averager.

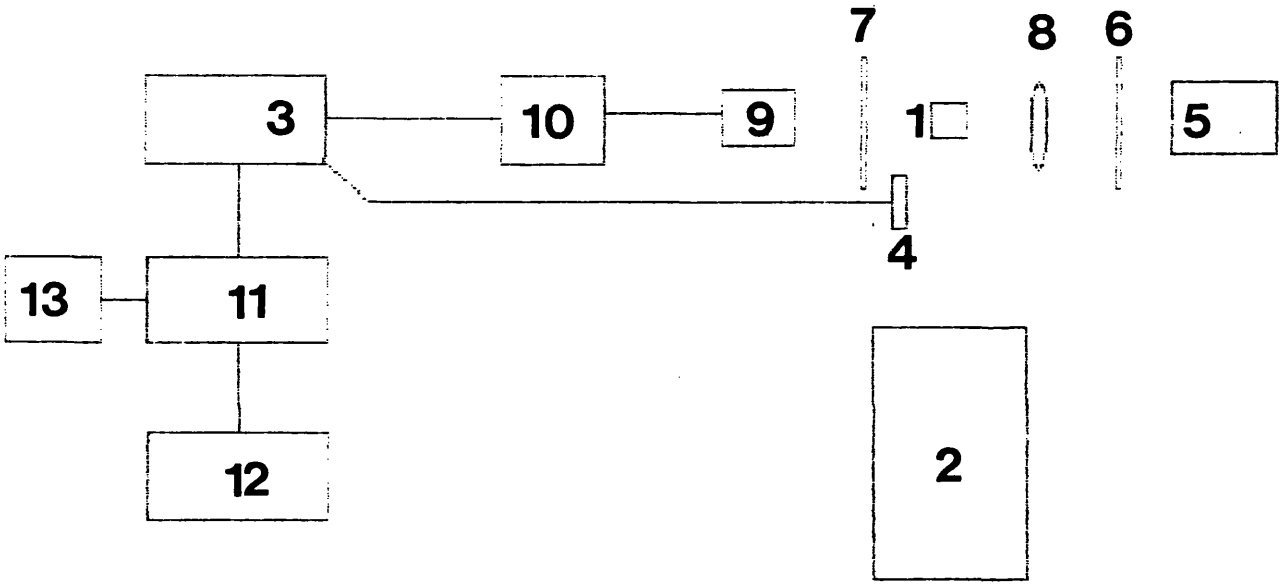

Figure 2.1 Schematic Diagram of Kinetic Spectrophotometer

The diagram represents apparatus used to measure absorbance changes at 820nm (due to oxidation and rereduction of P680) in the μs - ms time range. Excitation of sample (1) is provided by a 800ps pulse (337nm) from a nitrogen laser (2). The laser simultaneously triggers a transient recorder (3) by means of a photodiode (4). A measuring beam is provided by a tungsten lamp (5), passed through 820nm filters, (6) and (7), and focussed by a lens at (8). The measuring beam is detected by a photodiode (9) coupled to an amplifier (10), which passes the time-resolved signal to the transient recorder. Transients are stored by a signal averager (11) and output to an oscilloscope (12) or an X-Y plotter (13).

Samples of tris-inactivated PS II from P. laminosum were resuspended to 75$\mu g.ml^{-1}$ in 5mM magnesium chloride, 10% (v/v) glycerol and one the following buffers: 20mM MES, pH 6.0; 20mM Tris or tricine, pH 8.0; and 20mM glycine, pH 10.0. Optical redox titrations were performed in a quartz cuvette built and used as in [141]. Redox potential was monitored continuously using a Russell microplatinum rod combination electrode (CMMP Pt 57, Russell pH Ltd., U.K.). The following redox mediators were used at 20μM concentration (figures in brackets indicate E_{m7}, mV): thionine (+60), methylene blue (+11), indigotetrasulphonate (0), Janus Green (-96), phenosaffranine (-255), saffranine T (-289), benzyl viologen (-311), diquat (-350) and methyl viologen (-436). Control experiments were also performed in the absence of mediators.

2.9 Electron Paramagnetic Resonance (EPR) Spectroscopy

2.9.1 Practical Aspects of EPR Spectroscopy

EPR spectroscopy was performed using a Jeol FelX X-band commercial spectrometer (9.4GHz microwave frequency, 100kHz field modulation frequency) fitted with an Oxford Instruments ESR 9 cryostat. Liquid helium was used to cool samples to temperatures in the range 4-20K. Samples (0.3 or 0.4ml) were analysed in calibrated quartz tubes of internal diameter 3mm. Sample concentrations, given in mg $Chl.ml^{-1}$, and EPR conditions, such as temperature, microwave power and modulation amplitude, are given in the appropriate text or figure legend.

Several different illumination regimes were used throughout this thesis. Particular details are again given in the appropriate text, but in general conditions were as follows:

(1) Illumination at 77K was performed in a silvered dewar, with samples immersed in liquid nitrogen. Illumination was by means of

a 1000W light source above the dewar, from a distance of approximately 70cm, for 5 or 10min.

(2) Samples were illuminated at 200K for 10min, in an ethanol/dry ice bath in an unsilvered dewar, partially surrounded by aluminium foil. Illumination was from the side, by means of a 1000W light source, and samples were rotated through 180^{o} after 5min to ensure equal irradiation.

(3) Samples illuminated at room temperature for 1min using the same light source as above, held at a distance of 1m from the samples (to avoid heating) which were rotated continuously.

(4) Illumination of samples inside the spectrometer cavity was by means of a Barr and Stroud 150W light source and fibre optic light guide inserted in the front of the cavity.

2.9.2 Introduction to EPR Theory

EPR spectroscopy is a technique to detect and to some extent to characterise chemical species with unpaired electrons, also known as paramagnetic species. In this thesis reference is made to the following species: free radicals, possessing one unpaired electron; triplet states, possessing two strongly coupled unpaired electrons; and certain oxidation states of transition metals which have unpaired electrons in their d-orbitals. The simplified lay-out of an epr spectrometer is shown in Figure 2.2.

The basic principles of epr are as follows. Most molecules have *singlet* ground states, i.e., total electron spin equal to zero, $\underline{S} = 0$, and are not detected by the epr method: this state includes, for example, molecules with paired electrons. On the other hand, species that have a single unpaired electron (for example, oxidised chlorophyll or singly-reduced quinone) have a *doublet* ground state, with total electron spin $\underline{S} = \frac{1}{2}$. The terms

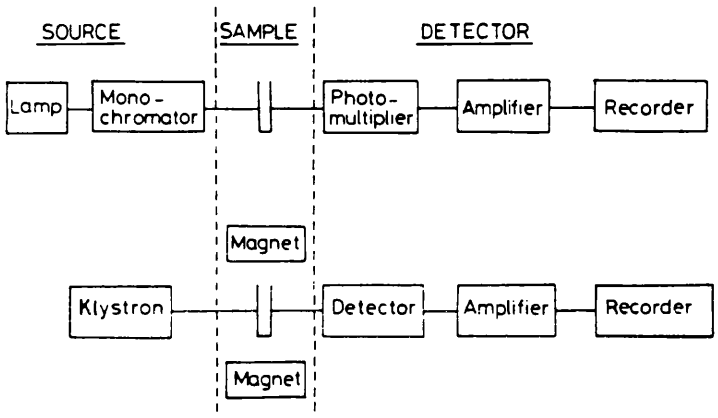

Figure 2.2

The figure shows schematic diagrams of an EPR spectrometer (lower) compared with an absorption spectrophotometer (upper). In the spectrophotometer, light is passed through the sample and changes in the intensity (due to electronic transitions in the sample) are detected. In the EPR spectrometer, a beam of microwaves passes through the sample in a magnetic field and changes in intensity (due to electron spin transitions) are detected. The Jeol Fe1-X spectrometer uses a Gunn diode rather than a klystron as the source of microwaves [From Evans, M.C.W. (1977) In: Topics in Photosynthesis (Barber, J., ed.) 2, 435, Elsevier.]

singlet, *doublet*, *triplet*, etc, refer to the total electron spin, but not directly (as does the value of $\underline{S}$): rather, these terms refer to the *spin multiplicity*, which is equal to $2\underline{S} + 1$. For example, for $\underline{S} = 1$, (i.e. two unpaired electrons) the spin multiplicity is 3, and the state is referred to as a triplet.

In the simplest case, when a doublet is placed in a magnetic field, it gives rise to two possible states, Figure 2.3(a), with different energies corresponding to the electron spin quantum numbers $\underline{m}_S = +\frac{1}{2}$ and $\underline{m}_S = -\frac{1}{2}$:

$$E(\underline{m}_S) = g.\mu_B.\underline{B}.\underline{m}_S$$

where $E(\underline{m}_S)$ is the energy, $\underline{B}$ is the magnetic flux density, μ_B is the Bohr magneton (9.27408×10^{-24} J.T^{-1}) and g, a dimensionless parameter known as the 'g-value'. For practical reasons, the system is bathed in radiation of a fixed frequency *f*, and the magnetic field swept until the resonant condition:

$$h.f = E(\tfrac{1}{2}) - E(-\tfrac{1}{2}) = g.\mu_B.\underline{B}$$

is reached, when a strong, resonant absorption occurs (h = Planck's constant = 6.626×10^{-34} J.s). Magnetic field modulation methods are used to improve the signal-to-noise ratio: the resulting spectra are presented as a first derivative of the absorption spectra.

At X-band, i.e., ≈9GHz, resonance occurs typically in the region of 0.3T. 9GHz corresponds to a wavelength of approximately 3cm, hence the technique is a form of microwave spectroscopy. It is seen by inspection of these equations that the energy separation between the $\underline{m}_S = \frac{1}{2}$ and $\underline{m}_S = -\frac{1}{2}$ states is linearly proportional to

the strength of the magnetic field.

For a 'free' electron, g has been determined to be 2.002319. In many free radicals, including oxidised chlorophyll, the unpaired electron behaves almost as a free electron, and g-values are close to this figure. Consequently, for a fixed frequency, the magnetic field positions at which resonance occurs are similar for these species. But for many molecules and ions, the electron experiences not only the applied field ($\underline{B}$), but a sum of the applied field, local and induced fields. The consequences of this are that the magnetic field positions of the absorption peaks (epr signals) vary, in some cases quite significantly. The position of an absorption is, then, characterised by the effective g-value, which can be calculated from the resonance condition, $h.f = g.\mu_B.B_{obs}$, where B_{obs} is the observed magnetic field position at which absorbance occurs (for some transition metal complexes, g-values of >8 are known).

There are several causes of deviation of measured g-values from that of the free electron. For isolated paramagnetic species, interaction of the electron spin with contributions from its orbital motion can introduce *anisotropy* into a spectrum, which is characterised by three g-values (g_x, g_y and g_z). Orbital contributions from d-electrons in transition metal complexes (e.g., high-spin $\underline{S}$=5/2 Fe^{3+}, Figure 2.3(b); this type of epr is seen in the spectra from the non-heme iron of PS II) can be substantial. Interactions between the electron spin and adjacent magnetic nuclei may introduce *hyperfine* structure into a spectrum, causing deviations in the g-value dependent upon the nuclear magnetism and the strength of the coupling between it and the electron spin. Interactions between two or more paramagnetic centres can also influence the shape of an epr spectrum through spin-spin coupling.

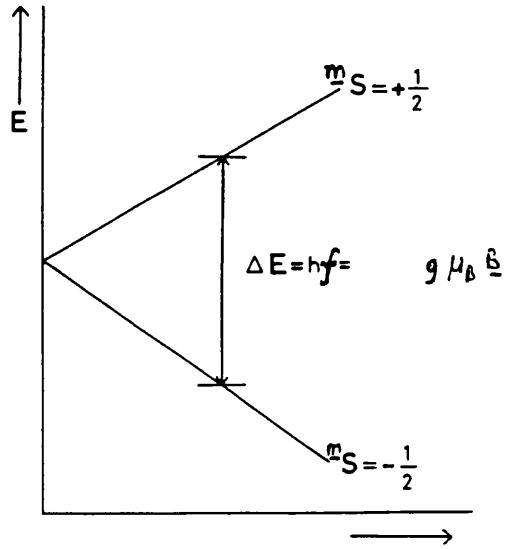

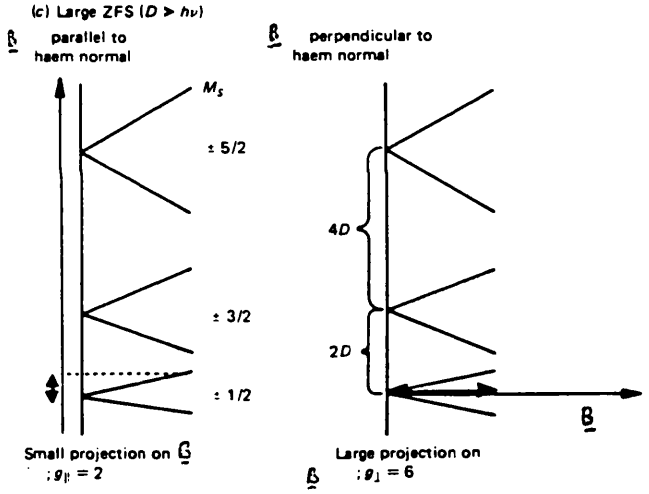

Figure 2.3 Energy Level Diagrams for S = 1/2 and S = 5/2 States

(a) In the case of an S = 1/2 system, application of a magnetic field separates two spin substates ($m_S = +1/2$, $m_S = -1/2$). The energy difference is linearly proportional to the strength of the applied magnetic field, B. For a fixed microwave frequency, the field is swept, and absorption occurs when the resonance condition, $h.f = g.\mu_B.B$, is met.

(b) More complex epr can arise from an S = 5/2 system, e.g. high spin Fe^{3+}. In a magnetic field, there are six spin substates. However, if at zero field the interactions with surrounding ligands are strong, the substates are non-degenerate: a highly anisotropic signal is observed from the lowest ($m_S = \pm 1/2$) component.

2.9.2.1 Spin Relaxation and Power Saturation Studies

Net absorption of electromagnetic radiation requires a difference in populations between the lower ($m_S = -\frac{1}{2}$) and upper ($m_S = \frac{1}{2}$) energy levels. The ratio of populations in the two states of an epr transition is given by the Boltzmann distribution:

$$[N_{\frac{1}{2}}]/[N_{-\frac{1}{2}}] = \exp -[\ (E(\tfrac{1}{2}) - E(-\tfrac{1}{2}))\ /\ k.T\ ]$$

where k is the Boltzmann constant (1.381×10^{-23} $J.K^{-1}$); T, the thermodynamic temperature and N, the population of each state. For energy separations corresponding to ≈9.5GHz, the value of $[N_{\frac{1}{2}}]/[N_{-\frac{1}{2}}] \approx 0.998$, i.e., only a small fraction of electrons contribute to the absorption. Microwave-induced transitions from the lower to the higher energy states reduce the population difference, causing a fall in signal intensity at higher microwave powers, a phenomenon known as *saturation*. The power at which a particular epr signal saturates is governed by the rate at which the system relaxes from the excited state, characterised by the spin relaxation times T_1 and T_2. T_1, the *spin-lattice* relaxation time, is a measure of the relaxation of electrons from the higher energy state through transfer of energy to vibrational modes ('phonons') in the surroundings ('the lattice'). The *spin-spin* relaxation time T_2 is due to a dephasing of the spins through spin-spin and other interactions.

The intensity of an epr line, I, as a function of power is given by:

$$I = [\ k.\sqrt{P}\ ]/[\sqrt{(1 + P/P_{\frac{1}{2}})^b}]$$

where k is a constant proportional to the number of spins; P is the microwave power; $P_{\frac{1}{2}}$ is the power at half-saturation, proportional to the spin-lattice relaxation time, T_1; and b is the inhomogeneity

parameter, varying 1 - 4 with increasing homogeneity (the terms *homogeneous* and *inhomogeneous* refer to mechanisms determining an epr lineshape) [142]. A convenient way to present power saturation data is to plot log(I/√P) against log P. In the non-saturating limit this plot yields a straight line parallel to the abscissa (log(I/√P) = log k); as saturation occurs the plot curves downwards and becomes a straight line of slope -0.5b. $P_{\frac{1}{2}}$ is determined by extrapolating these lines to their point of intersection.

For practical purposes, if power saturation is not accounted for, serious errors in quantitation may occur. The phenomenon is valuable if two signals overlap: if one is easily saturated and the other is not, then use of higher power favours observation of the less easily saturated signal.

2.9.2.2 Temperature Dependence of EPR Signals

All of the spectra recorded in this thesis were obtained at low temperature. From the Boltzmann distribution, it can be seen that the lower the temperature, the greater the difference in populations of the $m_S = +\frac{1}{2}$ and $m_S = -\frac{1}{2}$ states, leading, in principle, to an increase in the absorption. The signal should increase in intensity as 1/T. However, at lower temperatures the spin-relaxation processes tend to be slower. There are two consequences of this: (i) signals saturate at lower powers than they do at higher temperature; (ii) signals tend to be sharper at lower temperatures (since linewidths are related to T_1 and T_2). Optimising signal shapes and sizes has to be done empirically.

2.10 EPR Redox Potentiometry

Redox potentiometry was performed essentially as described in [143]. The sample vessel was enclosed by a water jacket maintained

at 10°C by a Churchill thermostatic pump. Samples were kept anaerobic by continuous flushing with oxygen-free nitrogen: gas from the cylinder was scrubbed by passing through a Drechsel bottle containing 1% (w/v) sodium dithionite, 2.5mg/200ml methyl viologen in 0.1M Tris-HCl pH 8; and through a second containing 0.1M Tris-HCl pH 9. The redox potential was measured using a microplatinum rod combination electrode (CMMP Pt57, from Russell pH, Ltd., UK). The electrode was calibrated using three anaerobic solutions: a saturated solution of quinhydrone in 0.1M potassium hydrogen phosphate, pH 7 at 25°C (E_m = +286mV); an equimolar (5mM) solution of potassium ferricyanide and potassium ferrocyanide in 50mM Tris-HCl, pH 8 at 25°C (E_m = +420mV); estimation of the end-point of a titration of benzyl viologen (colour change: clear ---> purple) in 0.1M potassium hydrogen phosphate, pH 7 at 25°C. The value for the end-point at pH 7 is -311mV, but this is difficult to determine precisely.

Redox potential was altered and maintained by additions of freshly prepared 1% or 0.25% (w/v) solutions of sodium dithionite in 50mM Tris-HCl, pH 8 and 0.05M potassium ferricyanide in 50mM Tris-HCl, pH 8. The stock solution of sodium dithionite is kept anaerobic throughout the course of the titration. pH was also continuously monitored, and adjusted by additions of 0.1M sodium hydroxide or 0.1M hydrochloric acid. Samples were poised at any given potential for a minimum of 10min, to allow equilibration of the membrane- and protein-bound redox components with the bulk phase.

Redox mediators were normally used at 20μM concentration, although control titrations using 5μM and 50μM were also performed. For titrations of the primary quinone in the range +100mV -->-450mV the mediators given in Section 2.8 were all used, whereas for

titrations of the secondary quinone, in the range +200mV -->- 100mV, only the first four of the above list were used.

Titrations were routinely performed in almost total darkness: LED displays from electrodes were masked by green filters; green-filtered light was used when samples were taken, but otherwise kept turned off. Samples were frozen to 77K and kept in darkness until analysed.

2.11 Extended X-ray Absorption Fine Structure (EXAFS)

2.11.1 Practical Aspects of EXAFS Spectroscopy

PS II from spinach was prepared as described above (Section 2.2). Samples were washed in resuspending medium containing 12.5mM EDTA, to remove extraneous manganese, and centrifuged for 30min at 40,000 x g. This pellet was resuspended in resuspending medium, without EDTA, and finally concentrated by centrifuging for 1h at 250,000 x g. The pelleted sample is used for EXAFS measurements. The PS II particles used in the EXAFS studies had activities of between 400 - 500 μmol O_2/mg.chl/hr.

2.11.1.1 Estimation of Chlorophyll in EXAFS Samples

The estimation of chlorophyll in the pellet was performed as follows. A small sample of the pellet was put into a clean, dry 10ml volumetric flask and resuspended carefully to 10ml using resuspending medium containing 20% v/v glycerol from a 20ml volumetric flask. The concentration of chlorophyll is calculated as follows:

Let W_1 = weight of 20ml flask, empty

W_2 = weight of 20ml flask + resuspending medium

W_3 = weight of 20ml flask + remaining resusp. medium

therefore: density of resusp. med, D = $(W_2 - W_1) \div 20$ $g.ml^{-1}$

volume of resuspending medium added to pellet, V = $(W_2 - W_3) \div D$ ml

therefore, volume of pellet = 10 - V ml.

The chlorophyll concentration in the pellet can then be calculated, since the dilution is known to be $10 \div (10 - V)$. We estimated the chlorophyll in the EXAFS sample to be 52mg.ml^{-1}

2.11.1.2 Estimation of Manganese

PS II membranes were incubated with Triton X-100 at a ratio of 4% (w/v) detergent: 1mg.ml^{-1} chl. 0.3ml of this was placed in an epr tube, and 10M hydrochloric acid added to a final concentration of 0.2M. The concentration of manganese is then estimated by comparison of the intensity of the six-line hexa-aquo Mn^{2+} epr signal with a range of standard solutions of $MnCl_2$ in 0.2M hydrochloric acid. The detergent solubilisation step facilitates complete extraction. Using this method, we estimated the concentration of Mn in the pellet to be ≈800μM.

In addition to this method, the concentration of Mn can be estimated directly from the EXAFS experiment, since the height of the absorption edge is proportional to the concentration of the absorbing species. In these experiments, the two values were in agreement.

2.11.1.3 Estimation of P680

P680 is estimated in a tris-washed sample of PS II by monitoring the extent of the absorption change at 820nm following a saturating laser flash.

From these various determinations we concluded the EXAFS sample to have a chlorophyll:P680 ratio of ≈ 350:1 and a manganese

content of ≈ 5 Mn per reaction centre.

2.11.2 Introduction to EXAFS Theory

The details of EXAFS theory are rather abstruse and this section will attempt to provide only a superficial review: further information can be found in [144].

EXAFS is a technique, developed over the past two decades, which relates modulations in the X-ray absorption spectrum of a particular atomic or ionic species ('the absorber') to the number, type and positions of adjacent atoms ('the scatterers', which occupy 'shells' around the absorber). In principle, distances between atoms can be determined to an accuracy of 0.01-0.02Å, which compares well with crystallographic resolution of a few tenths of an Ångström unit. An important advantage of the technique is its applicability to non-crystalline samples. The drawbacks of the technique as applied to biological samples are: (1) a requirement for a high concentration of absorber, which for proteins with metal centres, such as PS II, is not always easy to achieve; (2) the poor resolution of atoms more than a few Ångström units from the absorbing atom; (3) an error of roughly 15-20% in calculations of the numbers of atoms around the absorber; and (4) inability to distinguish low atomic weight scatterers, for example, oxygen and nitrogen.

Absorption of X-rays by atoms generally decreases as the energy of the incident X-ray increases (i.e. its wavelength shortens), except at a certain discrete value, called the absorption edge, which corresponds to the minimum energy capable of ionising an inner (K) shell electron. If the electron is ionised by X-radiation of greater-than-edge energy, the behaviour of the ejected electron (termed 'the photoelectron') can be viewed as a

by the energy of the incident photon, see Figure 2.4. If other atoms surround the absorber, the photelectron wave is backscattered, and the backscattered waves interfere with the outgoing waves: this interferes with the absorption process itself. Constructive interference between the outgoing and backscattered waves (which to a first approximation occurs if the absorber and scatterer are separated by an integral multiple of wavelengths) is associated with maxima in the X-ray absorption coefficient.

EXAFS of dilute samples can be measured using apparatus represented in Figure 2.5. White (i.e. polychromatic) X-radiation from the synchrotron source is monochromated by reflection from pairs of silicon (2,2,0) crystals, according to Bragg's Law: adjusting the angle of incidence alters the wavelength emitted. The intensity of the incident beam is estimated by the first ionisation chamber, which contains an argon/helium mixture. The absorption (and hence transmitted intensity) is detected by a fluorescence detector: the K-shell hole left by the photo-electron is filled by a p-electron from the L-shell, emitting an X-ray photon of a fixed energy less than that of the incident photon, and the detector is thus tuned to this wavelength. The incident and transmitted intensities are used to find the absorption coefficient, μ_x, using the Beer-Lambert Law.

The magnitude of the EXAFS is obtained from the measured value of $\mu_x(E)$ by subtraction of the background, μ_o, and normalising: $\chi = [\mu_x(E) - \mu_o]/\ \mu_o$. The background is difficult to measure, and is usually fitted by means of a polynomial, called a spline function, usually of third-order; higher order polynomials, whilst fitting the background accurately, also tend to fit the EXAFS, and information can be lost. It has proved very difficult

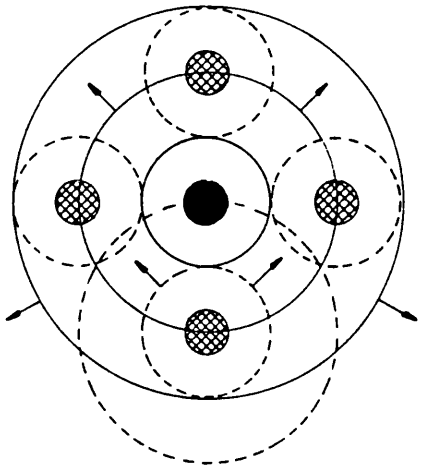

Figure 2.4 A Schematic Representation of the EXAFS Process

An atom (filled circle) absorbs X-rays, emitting a photoelectron wave which is back-scattered by neighbouring atoms (hatched circles). The solid circles denote outgoing electron waves and the broken circles back-scattered electron waves. Constructive or destructive interference, corresponding to absorption maxima and minima, occur when the waves overlap. This is a function of the wavelength of the photoelectron, and the distances and type of the neighbouring atoms.

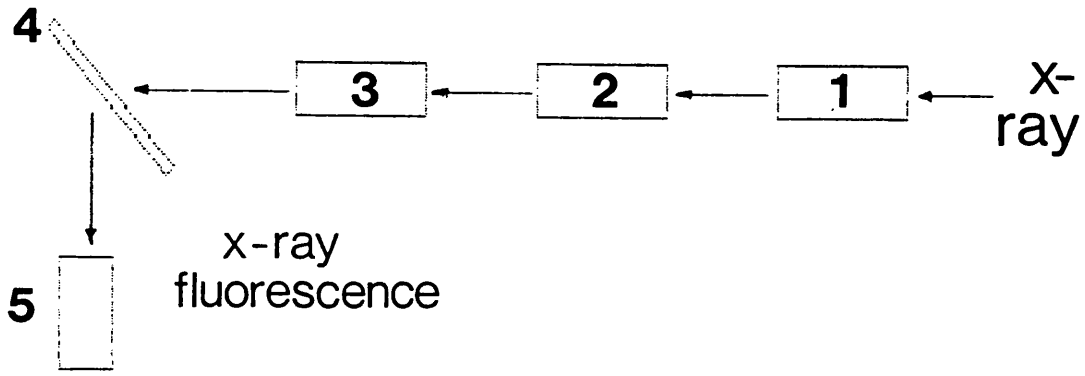

Figure 2.5 Schematic Diagram of Apparatus for Measurement of EXAFS

Intense, white X-radiation from the synchrotron source passes first through a silicon crystal monochromator, (1). The wavelength of radiation passed to the sample is changed by altering the angle of incidence on the crystal planes. The monochromated beam is focussed by a mirror of glass coated with Pt (2). The intensity of the incident beam is gauged by the Ar/He ionisation chamber, (3): ionisation of the gas atoms allows a current, proportional to the X-ray intensity, to flow across the chamber. A 'window' of sample is placed at 45° to the incident beam: the fluorescent X-rays are measured at 90° to the incident beam, by a solid-state Ge detector (5).

to automate this step in the analysis of EXAFS data, and background fitting is somewhat subjective.

The formula describing the amplitude of the EXAFS is a complex oscillatory function, which contains terms, for the jth shell, relating to the coordination number (N_j), distance (R_j^{-2}), variations in this distance (the Debye-Waller term, in turn related to the r.m.s. displacements, σ_j, about the equilibrium position), and a sinusoidal modulation of this amplitude by a function which is dependent upon the energy of the photo-electron, the distance (R_j) and 'phase shifts' which arise because the electron is emitted and backscattered from atomic potentials.

The structural information available from EXAFS (N_j, R_j, and σ_j^2) is extracted using Fourier transform methods, which convert the EXAFS function into a series of peaks in terms of absorber-scatterer distances: the amplitudes of the peaks are dependent upon the nature of the atoms and their positions can be related to real distances. The experimentally determined Fourier transform is then fitted by a theoretically-derived Fourier transform for particular arrangements of scatterers (an assumption is made that the properties, e.g. phase shifts, are transferable and invariant in systems which are chemically similar). This model Fourier transform can then be back-transformed to produce a theoretical EXAFS spectrum, which can be compared with the experimental data.

3.1 Properties of P. laminosum Thylakoids and Photosystem II.

Thylakoid membranes and membrane particles enriched in PS II were routinely prepared by the the method described in Section 2.1. The method described in this thesis differs slightly from that previously published [108], not only for the detergent used, but also because no DNAaseII was found to be needed for preparation of an homogeneous thylakoid suspension. In the earlier method, this enzyme was added to the spheroplast lysate, after incubation in hypotonic buffer, as an aid to homogenisation of the fibrous extract. It was found that DNAaseII, applied under the conditions of ionic strength and temperature used in this method, could not by itself homogenise the suspension, nor was it helpful to the mechanical methods (glass homogeniser, magnetic stirrer) used.

At all stages of the purification, the different fractions were monitored for chlorophyll content, specific and total activites of oxygen evolution: results of a typical purification are shown in Table 3.1. Typical rates of oxygen evolution from isolated PS II particles were between 1000 and 2000 μmol.O_2/mg.chl/h.

The absorption spectra from different fractions are shown in Fig. 3.1. Figs. 3.1(a) and (b) are spectra from thylakoids and PS II extracted with 80% acetone, respectively. Both spectra show similar profiles, with peaks at 433, 618 and 664nm, attributable to chlorophyll *a*; a fourth peak at 482nm is possibly due to a carotenoid component. There is a shoulder at 417nm, which may be due to pheophytin. Figs 3.1(c) and (d) show spectra from thylakoids and PS II extracted with distilled water. The positions

Step	Tot.vol. (ml)	Tot.Chl. (mg)	Spec.Ac. µmol/mg/h	Tot.Ac. µmol/h	Yield (%)
Thylakoids	69	121	380	45,980	(100)
SB12 Fractionation pellet (PS I)	[ ]	83.3	116	9660	21
SB12 Fractionation, supernatant (PS II)	101	21.7	1400	30,380	66
PS II, PEG 6000 precipitate	15	18.7	1300	24,310	53

Table 3.1 Typical Specific Activities and Yields Associated with Isolation of PS II from P. laminosum

Yields are given as the percentage of the total activity recovered in a particular fraction relative to the total activity of the thylakoid extract. Notes: (i) a part of the pellet (row 2) cannot be resuspended; this may contribute to the loss of tot.chl and tot.activity. (ii) the PS II activity is labile, even at 4°C, hence a part of the loss of spec.activity on PEG precipitation; in addition PEG precipitation did not always recover all of the chlorophyll from the supernatant, as shown.

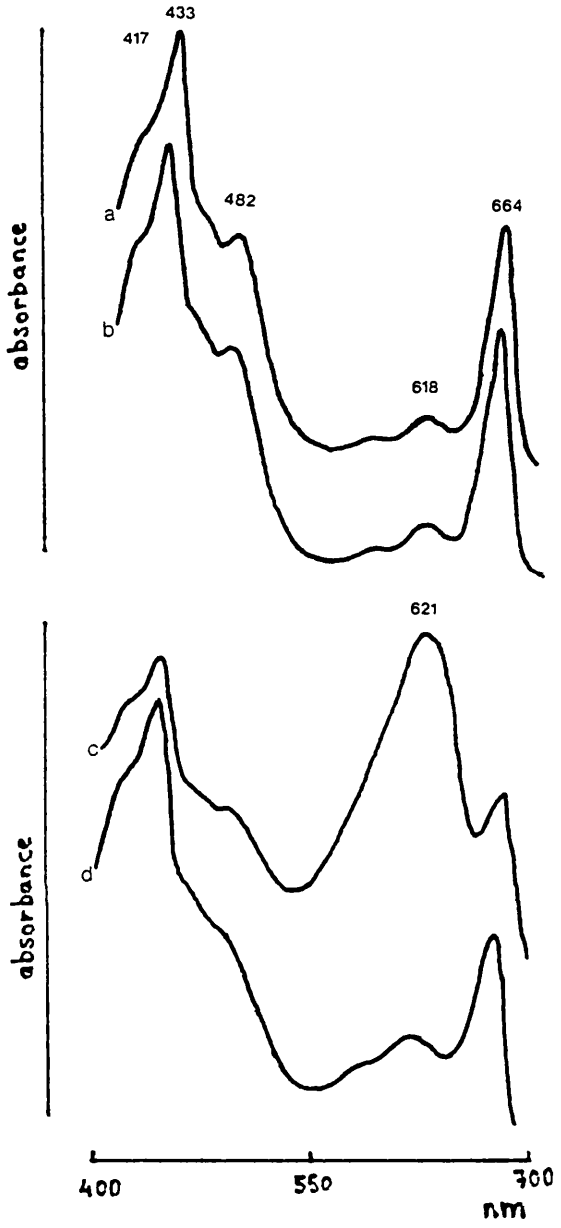

Figure 3.1 Absorption Spectra of P. laminosum Thylakoids and Photosystem II Particles

Figs. (a) and (b) show absorption spectra from thylakoids and PS II, respectively, extracted with 80% acetone. Chl *a* is indicated by peaks at 433 and 664nm; pheophytin is suggested by the 417nm shoulder; and carotenoid by the peak at 482nm. There is little difference between the organic soluble pigment profiles of the two fractions. This contrasts with Figs. (c) and (d), which are distilled water extractions of the two fractions: in the thylakoids, (c), can be seen a large contribution from phycocyanobilin at 621nm which is lost in the course of isolating PS II.

of the chlorophyll peaks are altered slightly, and the relative heights of the strong absorbances in the red and blue parts of the spectrum are changed, which may only indicate an alteration in the extinction coefficients in water. The carotenoid peak at 482nm is small in this extraction. The most significant difference is the loss of the peak at 621nm in the PS II compared with the thylakoid fraction, which represents loss of the water-soluble phycocyanobilin.

SDS-polyacrylamide gel electrophoresis was used to follow the polypeptide profiles of various fractions, and an example is shown in Fig. 3.2. As can be seen from the gel, following detergent-solubilisation and centrifuging many of the bands that appear in the PS II-enriched supernatant (track 4) also appear in both the thylakoid (track 2) and unsolubilised fractions (track 3); this indicates a less than 100% efficient isolation. Samples were loaded onto the gel at a fixed chlorophyll concentration (1.5mg.ml^{-1}) and it can be seen that bands of approximate molecular weight 66, 43, 33 and 31 kDa were intensified in the PS II fraction. The two polypeptides of cytochrome b559 are too small to have been resolved in the gel shown. The 33kDa band may represent the D1 and D2 polypeptides; the 66kDa band may arise from an aggregate of these two polypeptides. Track 2 shows a faint band at ≈ 70kDa, which is possibly the CP1a polypeptide of PS I; there is also a strongly-staining band at ≈ 130kDa, which presumably represents unsolubilised material.

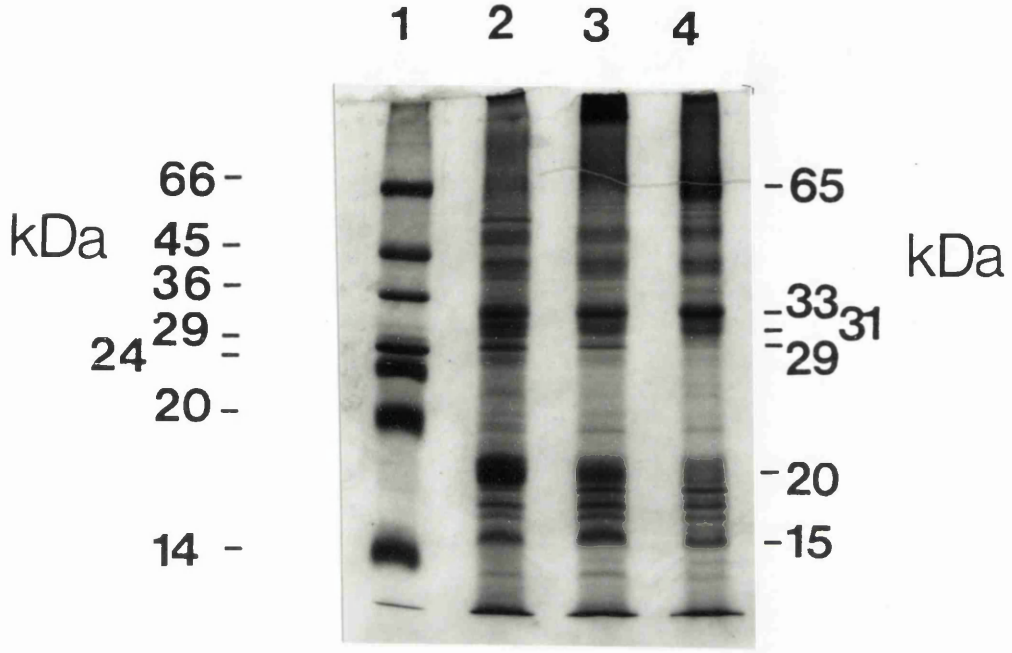

Figure 3.2 Polyacrylamide Gel Electrophoresis of Fractions from the Isolation of P.laminosum Photosystem II

Molecular weight markers were run in Track 1, and their weights given at left. Polypeptides of the thylakoids are shown in Track 2. The PS II-enriched fraction (Track 4) has several intensified bands, notably at ≈66kDa (aggregate of D1/D2) and 33kDa (D1 and D2). The PS I-enriched fraction (Track 3) shows a prominent band at 29kDa, and intensified bands at ≈20 and ≈15kDa. Track 3 shows, too, that not all the putative PS II polypeptides have been isolated by this method.

3.2 Detection of EPR Signals from Q_a^--Fe^{2+} in PS II from P. laminosum

As described in Section 1.8.4.2, two epr signals have previously been attributed to the interaction between Q_a^--Fe^{2+} in photosystem II purified from a variety of sources. Of these two signals, only the g = 1.82 form has been observed in P.laminosum PS II [108],[145], the observation of the signal requiring high levels of the herbicide 3-(3,4-dichlorophenyl)-1,1-dimethylurea (DCMU) or the ADRY reagent carbonyl cyanide *m*-chlorophenylhydrazone (CCCP).

In this section the properties of the epr spectra from the iron-semiquinone component in P. laminosum PS II isolated using a zwitterionic detergent, SB 12, are described. In particular, the results report detection of the g = 1.9 form of the Q_a^--Fe^{2+} signal in isolated PS II particles from P. laminosum, previously detected in preparations from higher plants [110].

All samples of P. laminosum PS II were dark-adapted for 4h at 4°C. Where chemical additions were made to epr samples, ethanolic solutions were used, except in the case of sodium formate, which was added from a 2M aqueous solution. The final concentration of ethanol was 1% (v/v).

The epr spectrum from a 4h dark-adapted sample of P. laminosum PS II, Fig. 3.3(a), shows no signals characteristic of semiquinone-iron components, either at g = 1.82 or g = 1.9, indicating the oxidation in the dark of any Q_a^- to Q_a. All of the spectra shown in these figures are noisier than is ideal: each spectrum is the average of three scans, but this clearly seems not to have removed the noise.

Following illumination at 77K of samples at pH 7.5 to which no additions had been made, the broad g = 1.9 signal can be seen, arrowed in Fig. 3.3(b). This signal may be attributed to an

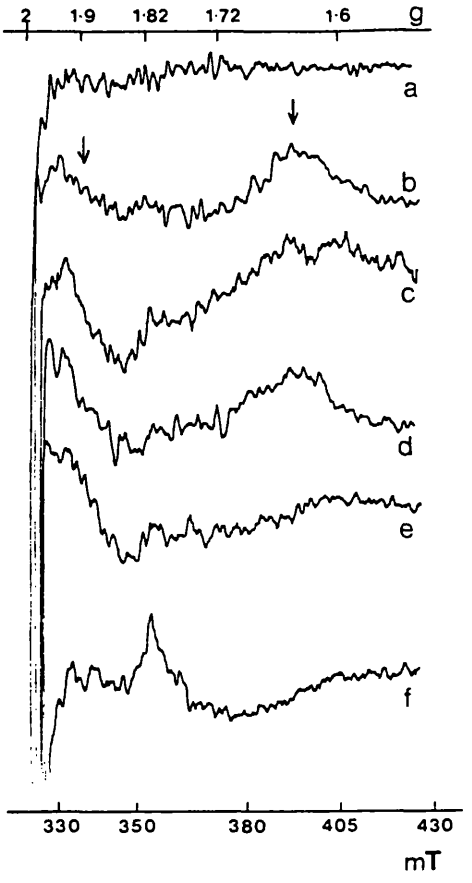

Figure 3.3 EPR Spectra from the Semiquinone-Iron in P. laminosum PS II

(a) PS II dark adapted for 4h; (b-f) following 5min illumination at 77K. (b) no additions (the g = 1.9 and g = 1.6 signals are marked); (c) +100μM DMBQ; (d) +100μM CCCP; (e) +500μM DCMU; (f) +100mM sodium formate (g = 1.8 arrowed). Chlorophyll concentration, 0.5mg.ml^{-1}. EPR conditions: temperature, 4K; microwave power, 10mW; modulation width, 1mT.

previously reported in higher plant PS II [110]. In addition, there is a broad resonance with an approximate g-value of 1.6, arrowed.

Additions of either 100μM 2,6-dimethyl 1,4-benzoquinone (DMBQ) or 100μM CCCP markedly increase the intensity of the g = 1.9 signal obtained following 77K illumination, Figs. 3.3(c) and 3.3(d). The effects of these two agents on the g = 1.6 resonance are different: DMBQ decreases significantly the intensity of this signal, whereas CCCP has little apparent effect. DMBQ is one of a class of compounds that is able to accept electrons from PS II, via the Q_b-binding site: it would be capable of oxidising any native Q_b-semiquinone to the quinone. CCCP 'deactivates' oxidising equivalents at the PS II donor side (e.g. the higher S-states of the OEC) perhaps by mediating the oxidation of semiquinone.

The lower yield of the g = 1.9 signal in untreated, compared with DMBQ- and CCCP-treated, samples may therefore be rationalised by bound Q_b^- decreasing the g = 1.9 resonance through magnetic interactions.

The effects of addition of the herbicide DCMU, a competitive inhibitor of native Q_b at its binding site, are illustrated in Fig. 3.3(e). Following 77K illumination, the size of the g = 1.9 signal was again increased in size, and, conversely, the g = 1.6 was decreased in size, compared with the untreated samples. Freezing-under-illumination of a sample treated with 500μM DCMU also gives rise to the g = 1.9 signal, in contrast to the result reported in [145]. The need for a high DCMU concentration (500μM) may be to displace both quinone and semiquinone forms of Q_b from the binding site. An effect of DCMU in reducing the size of a small g = 1.6 resonance has been observed in higher plant PS II [146].

Addition of 100mM sodium formate to samples has the effect observed in Fig. 3.3(f). 77K-photoreduction of Q_a in these samples yields the g = 1.82 form of the iron-quinone signal. There is no substantial yield of the resonance at g = 1.6. As discussed below,

this effect on the epr spectrum of P. laminosum PS II suggests that formate replaces bicarbonate at its binding site.

3.2.1 DISCUSSION

3.2.1.1 EPR Signals at g = 1.9 and 1.8 in P. laminosum

The results from these experiments show that P. laminosum PS II isolated using the zwitterionic detergent SB12 gives rise to both previously reported forms of the Q_a^--Fe^{2+} epr signals. It differs from the previously reported preparation of PS II from this cyanobacterium, in which, at the same pH (7.5), only the g = 1.82 epr signal could be detected. The earlier epr work was performed on PS II fractionated from the thylakoids using the non-ionic detergent, lauryl dimethylamine oxide (LDAO); this detergent is a mild oxidising agent. In contrast to the present work, freezing-under-illumination of LDAO-isolated PS II treated with 500μM DCMU did not lead to formation of the g = 1.9 signal, but instead to the g = 1.82 signal [108].

The g = 1.9 and g = 1.82 forms of the iron-semiquinone signal have been shown to be interconvertible: pH 6.5 favours detection of the g = 1.82 form, whereas at pH 7.5 the g = 1.9 form predominates [110]. Two other conditions have also been shown to increase the yield of the g = 1.82 signal [146]: (i) depletion of CO_2 (and therefore of bicarbonate as well) from samples of PS II; (ii) addition of formate, HCO_2^-, which increases the amplitude of the signal 12-fold compared with untreated samples. Formate ions are thought to inhibit electron transfer through the quinone acceptors of PS II by replacement of the bicarbonate ion from a ligation site at or near the non-heme iron [147]. Because the epr signals detected from bicarbonate-depleted samples and formate-washed samples are similar in terms of g-value and linewidth, it is

suggested that loss of bicarbonate affects the configuration of the Q_a^--Fe^{2+} complex: symptomatically, the g = 1.9 resonance is lost when bicarbonate is displaced.

The conclusion from this result is that the isolation of PS II from P. laminosum using SB12 conserves bicarbonate at its binding site. This state can be represented Q_a^--Fe^{2+}-[HCO_3^-], where bicarbonate is ligated either at, or close to, the non-heme iron. As noted in Section 1.8.4.3, there is controversy as to the nature of the active species. Bicarbonate has been proposed to act as a bidentate ligand to the non-heme iron, in a way analogous to the residue Glu M232 in the reaction centre of purple non-sulphur bacteria: the physiological advantage to oxygen-evolving organisms in replacing the acidic side chain of an amino acid with an exchangeable anion is not clear, although a mechanism by which electron transfer is made sensitive to the presence of carbon dioxide (through a negative feedback loop) can be envisaged.

The exact mechanism by which bicarbonate enhances the rates of electron transfer from Q_a to Q_b is equally controversial: one proposed mechanism is that it participates in the protonation reactions accompanying reduction of Q_b to Q_b^- [148], or Q_b^- to Q_bH_2 [149].

3.2.1.2 The EPR Signal at g = 1.6

The displacement of bicarbonate, by formate, causes the alteration of the Q_a^--Fe^{2+} signal from g = 1.9 to g = 1.8. It can also be seen from Fig. 3.3(f) that there is no yield of the g = 1.6 signal in these samples, suggesting that binding of formate also prevents the generation of this signal. It also may imply that bound bicarbonate is a necessary condition for seeing this resonance at g = 1.6: to show this, experiments would be required

in which bicarbonate was depleted from PS II, but not replaced with a competing anion; evidence for this has only recently come from oxygen-evolving core preparations from higher plant PS II (J. Nugent, personal communication).

The spectrum from PS II treated with 500μM DCMU also shows an almost total loss of the g = 1.6 resonance and a corresponding increase in the intensity of the g = 1.9 signal. As discussed above, detection of the g = 1.8 signal from P. laminosum PS II prepared using LDAO also required addition of DCMU [108], [145]. It was argued that, by analogy with the demonstrated effect of Q_b-semiquinone to suppress the g = 1.8 Q_a^--Fe^{2+} signal in purple bacteria [150], preparations of PS II from P. laminosum might conserve some native Q_b, thereby masking the Q_a^--Fe^{2+} signal. Further indirect support for the idea that the presence of Q_b may (e.g. if present as a semiquinone) affect the epr signals from the interaction between Q_a^- and Fe^{2+}, comes from the fact that the g = 1.8 signal was first seen in a PS II preparation from the alga C. reinhardtii, in which it had been shown from the fluorescence properties that Q_b was not present [106].

A speculative conclusion is that in P. laminosum PS II, which (i) preserves bicarbonate and (ii) native Q_b (in some form), 77K photoreduction of Q_a leads to formation of the g = 1.6 resonance. Disturbing the bicarbonate with formate favours formation of the g = 1.8 signal; and disturbing the Q_b, while preserving bicarbonate, leads to the g = 1.9 resonance.

Further indirect support for the influence of Q_b-semiquinone is provided by the result with DMBQ. This compound could alleviate the effect of Q_b either by replacement, or by an *in situ* oxidation, of the native semiquinone, which by the above model would cause a relative increase in the g = 1.9 signal intensity. The observed

result is consistent with this, although the g = 1.6 signal is not entirely removed.

An alternative view for the assignment of the g = 1.6 signal, not involving a contribution from some state of Q_D, was put forward by McDermott et al [120], using PS II isolated from a different cyanobacterial species of the genus Synechococcus (the precise species and strain are unspecified). This group also observed several of the properties which are reported in this thesis: for example, the attenuation of the signal in the presence of formate or DCMU. The effect of the former was ascribed to the modification of the ligation at the non-heme iron. However, no firm correlation was made by these workers between the effect of DCMU and the state of occupancy at the Q_D site.

This group measured the illumination-temperature dependence of the g = 1.6 signal and found that between 77-200K the g = 1.6 signal was formed (optimally at ≈180K) in preference to the g = 1.8, but that at higher temperatures the conventional g = 1.8 form was preferred. Consequently, the g = 1.6 signal was assigned to a conformationally-excited state of Q_A^--Fe^{2+} that could not relax at the lower temperature. The possibility that lower yield of the g = 1.6 signal at warmer temperatures might be due to electron transfer to Q_B^- was not considered, but could also account for the apparent yields of the different forms.

It may be significant that in PS II from Synechococcus, the yield of g = 1.6 signal is inversely proportional to the g = 1.8 form of the Q_A^--Fe^{2+} signal. This may not accord with the results in P. laminosum given above (no g = 1.6 signal in either formate-treated samples or reported in untreated LDAO-isolated particles) which indicate that bicarbonate binding may be a necessary condition for observation of the g = 1.6 signal. The result from

Synechococcus may therefore show that it is only when formate is bound that the g = 1.6 signal is not detected. However, even this statement must be qualified, since in [120] what is referred to as the 'g = 1.8' is admitted to be a mixture of g = 1.8 and g = 1.9 forms and it may be possible that the g = 1.6 arises from only a fraction of the centres in the sample.

There are important differences in the PS II preparations used: (i) the source species are not the same; (ii) the detergents used to fractionate the membranes are different ([120] reports use of octyl-ß-glucoside); and (iii) the pHs are not the same, the PS II from Synechococcus was kept at pH 6.3, compared with pH 7.5 for the P. laminosum preparation. Point (iii) is perhaps the most significant, since the g = 1.8 and 1.9 signals were shown in plant PS II to be the low and high pH forms, respectively, of the Q_a^--Fe^{2+} signal. It has not been possible to induce the g = 1.8 in PS II from P. laminosum by lowering the pH (J. Nugent, unpublished result).

3.3 Determination of the Midpoint Potential of the Primary Semiquinone-Iron in P. laminosum PS II

Epr titrations of the primary semiquinone-iron from P. laminosum (isolated using LDAO) have been reported previously [108], [145] although described as 'difficult', owing to the presence of the oxidising detergent; however, a value of the midpoint for the Q_a/Q_a^- couple of ≈ 0mV was determined. This value was close to that established for Q_h (+30mV) from fluorescence titrations of PS II from P. laminosum [117].

In formate-washed PS II from peas, a two-step titration of the g = 1.82 signal has been observed, with midpoints at ≈ 0mV and -250mV [118]. The implications of these two steps has been the subject of some debate, in particular whether they are evidence for an extra tightly-bound quinone acceptor, or whether they were due to a population of PS II where Q_a, in a fraction of centres, was either (i) insulated from the bulk phase, or (ii) in a different conformation that caused it to have a different midpoint potential.

Using the P. laminosum preparation described above, the redox properties of the bicarbonate- and formate-bound states of PS II was investigated.

3.3.1 Titrations of EPR Signals from Q_a^--Fe^{2+}

In contrast to the results obtained from spinach PS II particles, redox titration of the primary semiquinone-iron complex from Phormidium laminosum in the formate-bound state at pH 7.8 (giving the g = 1.8 signal, Fig. 3.4) shows only one major step over the potential range +100 to -300mV, Fig. 3.5 The data points have been fitted to a Nernst curve assuming a single-electron redox reaction, and a value for the midpoint of the Q_a/Q_a^- couple determined at approximately 20mV. Given the error in this type of

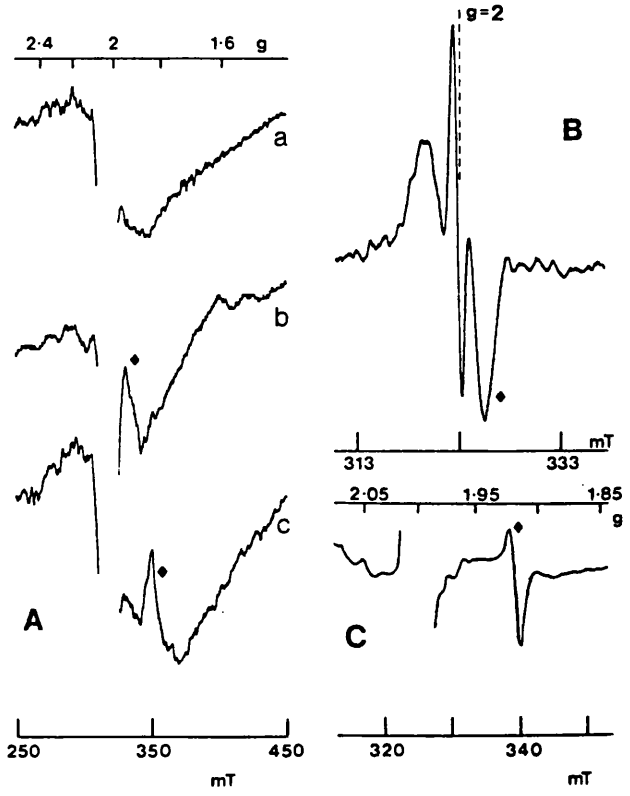

Figure 3.4 EPR Spectra from Redox Titrations of P. laminosum PS II

(A) native sample poised in darkness at +100mV (a) and at-100mV (b) showing an increase in the g=1.9 signal. (c) shows a spectrum from a sample containing 100mM sodium formate poised at-100mV. (B) -100mV, 200K-illumination minus dark difference spectrum showing doublet EPR signal from I^{-}-Q_a^{-}-Fe^{2+}. (C) Sample frozen under illumination showing the g=1.92 signal, also observed at low potentials. Chlorophyll concentration $1mg.ml^{-1}$. EPR conditions: temperature: A and B, 5K; C, 15K; microwave power: A and C, 10mW and B, 25mW; modulation width, 1.25mT. Peaks measured are indicated by the diamonds.

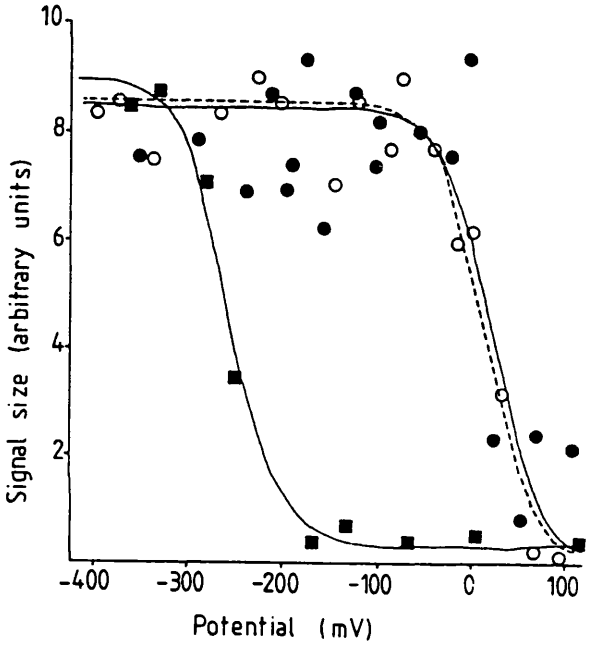

Figure 3.5 Redox Titrations of Acceptor Components of P. laminosum PS II

Titrations were performed in darkness; samples were maintained at pH 7.8. Signal intensity before illumination of the semiquinone-iron signals in the presence (g=1.8, open circles) and absence (g=1.9, filled circles) of sodium formate, and of the g=1.92 signal (filled squares) are shown. Curves are drawn assuming a one-electron redox event, with midpoints as follows: +20mV (g=1.8); +27mV (g=1.9) and -255mV (g=1.92).

titration (approximately ±15mV), this result is consistent with the figure determined for LDAO-extracted P. laminosum PS II [145]. The midpoint potential of this step also agrees closely with that of the component with midpoint of ≈ 0mV, termed Q_h, in the higher plant titrations [118]. It should be emphasised that no second step corresponding to the -250mV step (known as Q_l) seen in pea PS II was observed in this titration: a result in agreement with the fluorescence titrations of P. laminosum where Q_l was also not seen.

It was also possible to titrate the g = 1.9 form of the Q_a^--Fe^{2+} signal in this preparation, Fig. 3.4. No titration of this signal has previously been reported. The result is also shown in Fig.3.5, where again the data has been fitted to a Nernst curve assuming single-electron transfer. The midpoint potential of the g = 1.9 form is +27mV at pH 7.8. This value is not significantly different from the figures already cited for the midpoint of Q_a/Q_a^-.

Although the Q_a^--Fe^{2+} signal did not show a low potential step, a change in the epr spectrum is observed as the potential is lowered. This is due to the presence of a previously-reported component, with g-value of 1.92, which titrates with a midpoint potential of approximately -270mV, Figs. 3.4 and 3.5 [151],[152]. Unlike the semiquinone-iron signal on which it is superimposed, this signal is seen optimally at temperatures of approximately 14K, and can be very easily titrated.

A method of indirectly measuring the midpoint potential of the Q_a/Q_a^- couple is to monitor the formation following low-temperature illumination of the 'split' $Pheo^-$ radical signal. This signal has previously been observed in isolated bacterial reaction centres and PS II from higher plants. It can be generated specifically after 200K illumination, in PS II from P. laminosum

either untreated or in the presence of 500μM DCMU. In untreated samples, this signal was seen to have two steps in its titration curve, Fig. 3.6 The first step, accounting for some 75-80% of the total, titrated with E_m of approximately +35mV. Accepting the error in these titrations, it is not unreasonable to say that this step occurs in parallel with the reduction of Q_a, as monitored directly by the increase in size of the g = 1.9 or 1.8 $Q_a^{\cdot-}$-Fe^{2+} signals.

A second step, accounting for a smaller fraction of the maximum signal size, is also observed in the titrations of the split signal. The precise midpoint potential of this second, low-potential step was difficult to determine: it was observed to vary between particular preparations over the range -150 to -250mV. This inaccuracy may only reflect the fact that the changes in signal size are relatively small, and therefore errors in signal measurement are more significant. However, it was apparent from repetitions of the titration that an increase in signal size occurred at the lower potential; and that it was also not merely a problem of sample equilibration. The presence of this second step in the titration can most straightforwardly be explained by positing an additional, low-potential acceptor, operating either in series or in parallel with the Q_h-component. In these experiments, there was no evidence that this second acceptor was another quinone-iron component, since in neither of the direct titrations of this species was a low-potential step seen. This is certainly in agreement with the models for PS II structure, based on that of the purple bacterial reaction centre [48], which do not indicate a third quinone binding site that has the necessary orientation to the non-heme iron to give rise to these particular epr signals.

At the lower limit of the potential that could be sustained

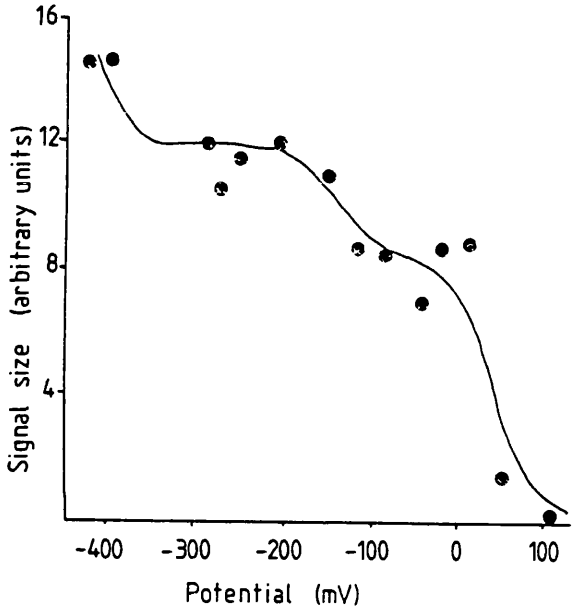

Figure 3.6 Redox Titration of the Formation of 'Split Signal' arising from the state I^{-}-Q_a^{-}-Fe^{2+}

The split signal can be generated following 10min 200K-illumination of untreated PS II samples. Assuming one-electron reductions, two steps have been fitted to this data, with midpoints at +35mV and -150mV. The high potential step probably corresponds to reduction of Q_a; the low potential step is less well-defined, but may reflect an involvement, in a fraction of centres, of the component giving rise to the g=1.92 signal. There is also evidence for a third step at potentials below -400mV, but it was not possible to fit this.

by titration with sodium dithionite at this pH, i.e. approximately -430mV, there appeared to be a further increase in the yield of the split signal. It was also observed in titrations of both the g = 1.8 and g = 1.9 signals that at such low potentials there was a further decrease in the size of the semiquinone-iron signals. However, no complete titrations were performed (i.e. by raising the pH the redox potential of dithionite is lowered) to establish a value for these midpoints. The loss of Q_a^--Fe^{2+} signals at low potentials has been attributed by van Mieghem, et al, to double reduction of quinone [153]: this would not, however, account for an increase in the size of the split-signal, which relies on a contribution from Q_a-semiquinone. In addition, although attempts were made to measure the yield of triplet in these samples, by continuous illumination at 4K in the epr cavity, none was detected.

Several attempts were made to titrate the pheophytin split signal in the presence of 100mM sodium formate, but the signal is narrowed under this condition to such an extent, that it could not be sufficiently distinguished from the large radical signal(s) at g $\approx$ 2 to allow quantitation. The same effect of the formate anion on the pheophytin split-radical signal has previously been noticed in preparations of PS II from spinach [146] and from C. reinhardtii [119].

3.3.2 Kinetic Optical Redox Titrations

The principle of this technique is as follows: an increase in the extinction coefficient at 820nm of P680 occurs following photooxidation. Changes in the absorption at 820nm are measured as a function of time; if the fast donors (specifically, the water-oxidising complex) are inactivated, $P680^+$ is re-reduced by back-

reaction from the components of the acceptor complex. Successive chemical reduction of the acceptors causes changes in the back-reaction kinetics by changing the acceptor from which the back-reaction occurs.

The time-resolution of the equipment used was of the order of 5μs: clearly, unless the fast donors to $P680^+$ are inactivated, e.g. through tris-washing, the primary donor will be re-reduced before the first point in the decay curve is measured. Even in a situation where these exceptionally fast donors have been inactivated, $P680^+$ is still capable of oxidising other components of the donor complex (D, cyt b559 or a chlorophyll), on time-scales at least comparable, if not faster than those of the back-decays of electrons from the acceptor complex. It is, therefore, by no means a trivial, but not an impossible, task to assign the kinetic components that make up a decay curve to real elements of the PS II reaction centre.

The decay of the $P680^+$ cation following actinic laser flash in tris-washed samples at +20mV, pH 8.0 is shown in Fig. 3.7(a). The curve of the decay is most easily fitted with a single exponential decay, with $t_{\frac{1}{2}}$ of between 2 and 3ms. At approximately 150mV, the signal is too small to be resolved easily, but as the potential is lowered the size of the signal increases, which can be fitted by a Nernst curve. The midpoint at pH 8.0 of the increase in this absorbance component is approximately 0mV. In the presence of 100μM DCMU, shown in Figure 3.8, the midpoint potential of this component is approximately +25mV. Titration of the millisecond component in the decay kinetics in the absence of redox mediators gives an identical value for this midpoint, thereby ruling out the possibility that what is being measured is simply donation by a redox mediator that is reduced with a similar

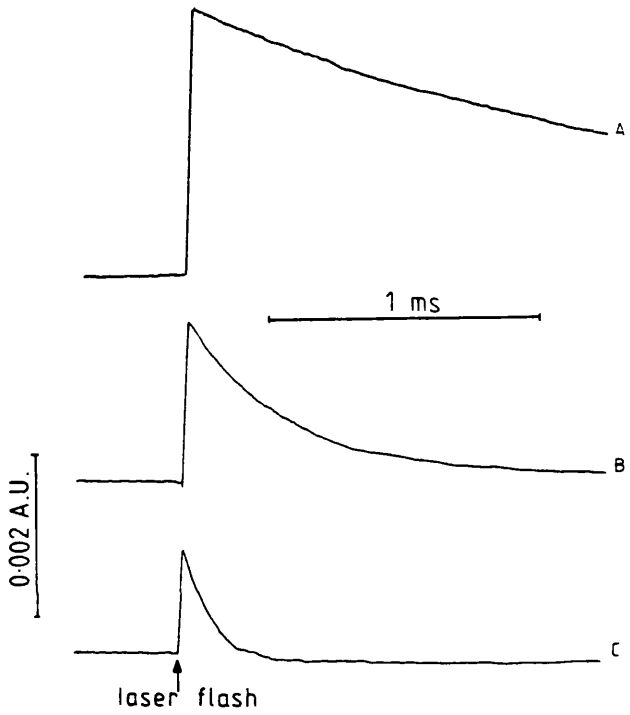

Figure 3.7 Absorbance Changes at 820nm due to Oxidation-Reduction of P680

The absorbance changes were taken from Tris-washed PS II from P. laminosum in the presence of 100μM DCMU, pH 8, at room temperature. Each measurement is averaged over 32 excitations, using an 800ps pulse 337nm nitrogen laser-light. Chlorophyll concentration: 7.5μg.ml^{-1}, path length, 1cm. Redox potentials: (A) 20mV, (B) -240mV, (C) -350mV. Two kinetic components were distinguished, with decay half times of 2-3ms (100% contribution in A) and 200μs (100% contribution in C).

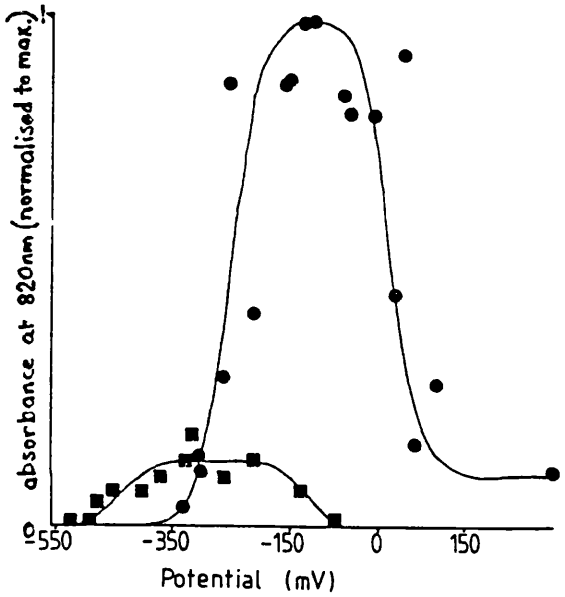

Figure 3.8 Redox Titration of Absorbance Changes at 820nm in P.laminosum PS II

PS II particles were treated as in Figure 3.7. Decay half-times of 2-3ms (filled circles) and 200μs (filled squares) were fitted to absorbance transients, and each's contribution to the decay then fitted to theoretical one-electron Nernst curves. Each measurement is the average of 32 excitations. Midpoint potentials are, for the ms component, 20mV (rise) and -250mV (loss) and -150mV (rise) and -400 (loss) for the μs component.

midpoint potential. It is seen, therefore, that the millisecond component in the optical titrations has a midpoint similar to those of the semiquinone-iron signals in the epr titrations, and of the component Q_h in titrations of the fluorescence yield.

In the epr titrations, a component with a midpoint potential of -250mV was noted; the amount of this component varied between preparations. There is no evidence from SDS-PAGE as to what this component might be - for example, a labile polypeptide component of the PS II preparation, which is lost even through minimal variations in the isolation procedure. Despite this variable stoichiometry of the acceptor composition, there is no corresponding variation in, for example, the rates of oxygen evolution seen in these preparations. The obvious conclusion from this is that this component has no essential role to play in electron transfer from water to the plastoquinone pool in P. laminosum.

The titration of the millisecond component is completed at lower potentials, by observing its loss, with an approximate midpoint of -250mV. Again, however, it should be noted that this value was subject to variation: partial and complete loss of the millisecond component were observed, in individual experiments, to titrate with a midpoint of -100mV. This probably reflects an experimental error, e.g. poor equilibration of redox components. Again, however, it is observed that the titration of the component giving rise to the g = 1.92 signal occurs with a midpoint potential in the region of -250mV at pH 8.0 (although this feature was never subject to the variability of the -250mV component in the kinetic titration); this value is also close to the proposed second step in the titration of the Q_a^--Fe^{2+}-I^- split signal. Therefore, it is possible that the loss of the ms component of the decay kinetics is

due to the reduction of the same component that gives rise to the g = 1.92 signal, which was suggested also to affect the titration of the split signal at low potentials.

A component of the decay kinetics, which is characterised by a $t_{\frac{1}{2}}$ of approximately 200μs, rises with a midpoint potential of about -150mV Figs. 3.8(b), (c) and 3.9. The precise value for the E_m is difficult to determine, since the signals are small. This component is lost as the sample is reduced, with an E_{m8} of ≈-400mV. This value corresponds with that attributed to an unidentified component, U, observed in redox titrations of the triplet yield in PS II from spinach [154]. Again, a simple explanation for this result would be that an additional electron acceptor also functions with a midpoint potential lower than that of Q_a in PS II from P. laminosum; but, alternatively, the double reduction of Q_a has been proposed to account for U [153]. The existence of such an acceptor in P. laminosum has previously been inferred, since the epr signal arising from the spin-polarised reaction centre triplet can only be observed in samples reduced with excess sodium dithionite at pH 10. From samples in which only the Q_a had been reduced there was seen only a small yield of triplet, suggesting that a further electron transfer event from pheophytin to the acceptor complex could take place [145].

3.3.3 DISCUSSION

Redox titrations of the g = 1.8 and g = 1.9 epr signals from the semiquinone-iron component in P. laminosum both indicate a homogeneous population of centres, where the Q_a/Q^- couple has an $E_{m7.8}$ of ≈ +25mV. Titration of the epr signal arising from the interaction between reduced pheophytin and Q_a^--Fe^{2+} supports this, but suggests the population of centres is heterogeneous with

respect to an unidentified low-potential acceptor, with $E_{m7.8} \approx$ -250mV.

There have been previous measurements of the midpoint potential(s) of primary semiquinone-iron acceptor in isolated PS II by following the change in the intensity of the g = 1.8 epr signal arising from this complex. It has been used as a measure of the reduction of the quinone in PS II preparations from C. reinhardtii, P. laminosum, pea and spinach. However, the measurement of the midpoint potential for the 'native' g = 1.9 signal has not been previously reported in the literature. Titrations of both the g = 1.8 and g = 1.9 epr signals show the semiquinone-iron species to be reduced in a single step, at pH 7.8, with a midpoint potential of approximately +25mV. This is in contrast to the result obtained in formate-washed pea PS II, where titration of the semiquinone-iron form giving rise to the g = 1.8 showed two steps in the titration [118]. On the other hand, it is in agreement with the results of the titration of chlorophyll fluorescence in P. laminosum [117], and it is tempting to conclude simply that what is being observed is a species-dependent difference between the two types of photosystem II. Exactly what, if any, significance this difference may have in terms of the physiology of the two types of organism is less obvious.

The midpoint potential value of approximately +25mV suggests that this component is identical with the Q_h component from fluorescence titrations. In the epr titrations there is no evidence for a second semiquinone-iron component functioning between pheophytin and Q_a, equivalent to the component Q_l of fluorescence titrations of higher plant PS II [113].

Replacement of bicarbonate in its binding site by formate at, or close to, the non-heme iron is known to inhibit electron

transfer between the primary and secondary quinones of PS II [125]. As discussed in Section 3.2, in PS II from P. laminosum, the epr signals arising from the two states Q_a^--Fe^{2+}-[HCO_3^-] and Q_a^--Fe^{2+}-[HCO_2^-] indicate that binding of formate displaces the native bicarbonate anion. The resulting inhibition of electron transfer cannot in this case be due merely to alteration of the midpoint potential of the Q_a/Q_a^- couple; although the possibility that it affects, for example, the midpoint potential of the Q_b/Q_b^- couple cannot be ruled out. However, if such a hypothetical raising of the redox potential of Q_b/Q_b- was brought about through a change in the position of the iron following bicarbonate binding, it is likely that an opposite effect on the potential of Q_a/Q_a^- would also occur. The result from the two titrations of the states Q_a^--Fe^{2+}-[HCO_3^-] and Q_a^--Fe^{2+}-[HCO_2^-] show that whilst formate binding affects the electronic and magnetic properties of the complex, this does not translate into an effect on the redox potential of the quinone moiety.

The role of bicarbonate has been suggested to be to facilitate protonation reactions at the secondary quinone [149]. It has also been shown to lower the redox potential of the non-heme iron of higher plant PS II: in samples which retain bicarbonate, as judged by the g = 1.9 form of the Q_a^--Fe^{2+} signal, oxidation of the iron by ferricyanide (E_m = +420mV) is possible, whilst this is prevented by formate treatment [156].

Whilst no low-potential quinone-iron acceptor was detected in P. laminosum, a component with midpoint potential at approximately -250mV was observed in both epr and kinetic optical titrations. Following reduction of Q_a, P680 is rereduced with a half-time of approximately 2-3ms. This component of the decay was lost by titrating through -250mV, similar to the midpoint potential of the

g = 1.92 signal. The nature of this component is not known, although it has been suggested that it arises from an iron-sulphur centre [151]. It can be easily distinguished from the semiquinone-iron signal at g = 1.9 since the latter is observed best at temperatures below 8K, whereas the g = 1.92 is seen most prominently at temperatures over 10K. The g = 1.92 signal can be photoinduced by illumination of P. laminosum PS II at 293K, consistent with the component functioning as an electron acceptor in the kinetic optical titrations performed at room temperature. On the other hand, the epr signal is not photoinduced at low temperature (77K). The component does not appear to be essential for electron transport from pheophytin or Q_a to the plastoquinone pool, since variations either of the g = 1.92 epr signal size or the proportion of the 2-3ms component of the decay kinetics were not correlated with any similar changes in the oxygen evolution activity [152]. A further problem with assigning a functional role to the species giving rise to these effects, is that in the titrations of the fluorescence yield there seems to be no step at ≈ -250mV corresponding to that seen in these epr and optical titrations.

The simplest explanation for these observations is that following reduction of the quinone-iron component (Q_h) at approximately 0mV, electrons are transferred from pheophytin to the g = 1.92 component. Since the component does not appear to be essential for forward electron transfer to Q_b, it is likely that it functions in parallel with Q_a.

The variable fraction of the split signal paralleling the -250mV step most probably reflects variable amounts of this component occurring in these preparations. To show this, however, it would be necessary to be able to produce a preparation with a

definite yield of the g = 1.92 signal correlated to a definite yield of the split signal.

The presence of a component with midpoint potential -400mV was detected in the optical titrations, and suggested by the titration of the split signal. This potential is similar to that of component U, identified previously in titrations of the spin-polarised triplet yield in spinach PS II. In that work, triplet was only detected by illumination at 4K in which U was reduced: this contrasted with titrations in purple bacteria, where the triplet is generated in parallel with the reduction of Q_a [157]; and also in isolated reaction centre preparations, which lack all quinone acceptors, where the spin-polarised triplet can be generated at all potentials between +400 and -500mV [158]. It has been recently shown that the component U probably corresponds to the double reduction of Q_a (i.e. $Q_a^- \longrightarrow Q_a^{2-}$), as this step could be correlated also with a decrease in yield of the g = 1.82 signal arising from primary semiquinone-iron [153]. Interestingly, it had been shown previously, that the spin-polarised triplet could be generated in PS II from P. laminosum only upon reduction with excess dithionite in samples poised at pH 10. However, a full confirmation that the μs component of the decay kinetics and the indications from epr titration of the split signal and semiquinone-iron signals in P. laminosum are due to a second reduction of Q_a remains to be achieved: in particular, double reduction of Q_a would not account for the increase in the split-signal at potentials lower than -400mV.

These results are summarised in Figure 3.9.

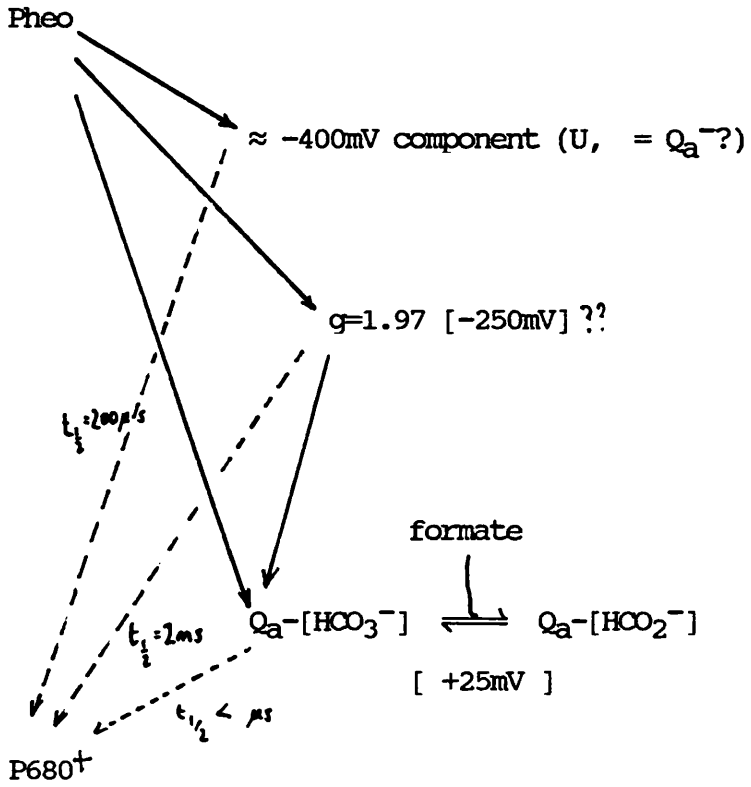

Figure 3.9 Summary of Possible Electron Acceptor Components in Photosystem II of P. laminosum

3.4 Determination of the Midpoint Potential of the D^+/D Couple in P. laminosum by Titration of Signal II(slow)

3.4.1 RESULTS

It was observed in the titrations of the quinone acceptors of P. laminosum PS II described above, that a sharp feature at $g \approx 2$, (which is not clearly resolved using the wide-field, 1.25mT modulated spectrum) decreased with decreasing potential, between +100 and 0mV. The effect of this reduction was studied more accurately by using lower microwave power (0.1mW) and modulation amplitude (0.2mT) and by scanning a narrower field (10mT). The result of the titrations are shown in Figs. 3.10 and 3.11. Fig. 3.10(a) shows little signal II(slow) in a sample poised at -100mV, but Fig. 3.10(b) shows restoration of the signal in a sample at +200mV. The [oxidised] - [reduced] difference spectrum, Fig. 3.10(c). The size of these signals was measured as the peak-to-trough height (arrowed), to avoid possible confusion from radical signals at $g = 2$. It was observed that chemical reduction using sodium dithionite did not affect either the g-value or the linewidth of the signal, for which values of $g = 2.0056$ and 2.4mT, respectively, were obtained. The magnetic field for these measurements was calibrated using a sample of magnesium oxide doped with manganese(II) ($I = 5/2$) as a g-value standard.

Fig. 3.11 shows a Nernst curve fitted to data from a reducing titration. The curve is fitted assuming a single-electron redox reaction, justified by the close fit of the theoretical curve to the data points. From this curve, an $E_{m7.8}$ for the couple Signal D^+/D is estimated to be +75mV. Titrations were performed in both reducing and oxidising directions, with the same result. No measurements were made at pHs other than 7.8, consequently whether or not this midpoint potential is pH-dependent is not known.

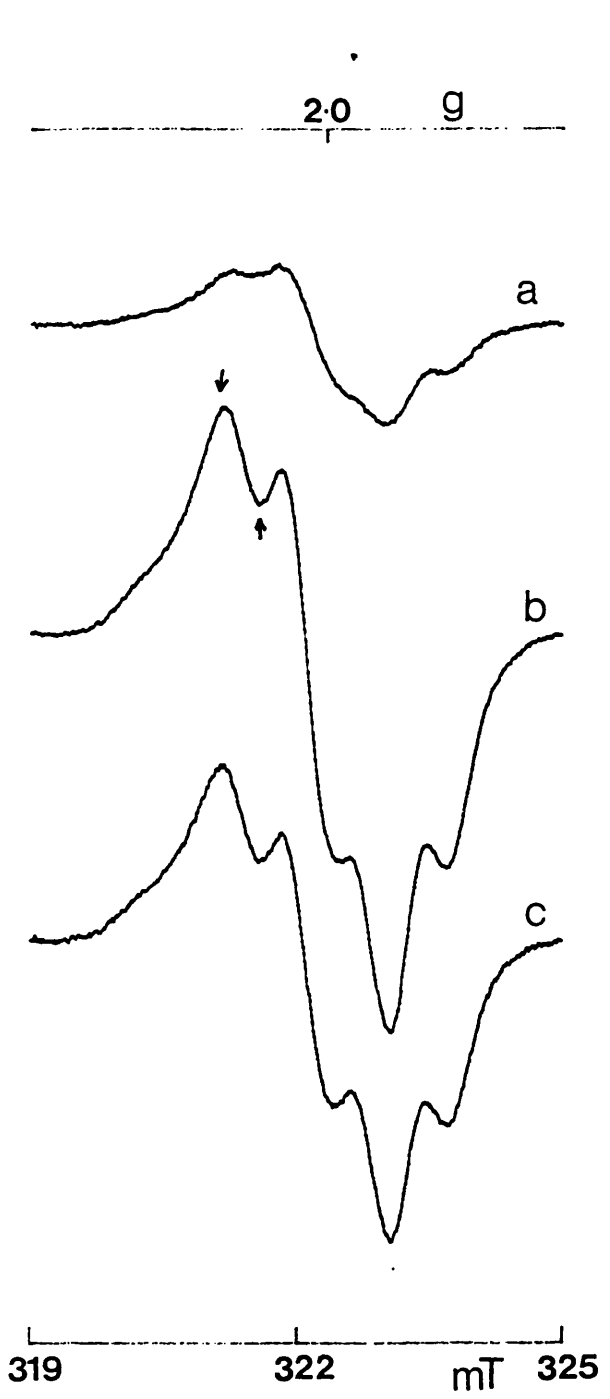

Figure 3.10 Titration of EPR Signal from D^+ (Signal $II_{(slow)}$)

The spectra are taken from a titration of P. laminosum PS II performed in the oxidising direction. (a) -10mV, (b) +100mV and (c) difference spectrum of (b) minus (a). The signal sizes were measured between the arrowed points. Although the size of Signal $II_{(slow)}$ can be increased by titration in this range, as shown, it probably does not account for 100% of centres: further increases in size can be obtained photooxidatively or by oxidation to higher potentials. Chlorophyll concentration: 1mg.ml^{-1}. Epr conditions: temperature, 14K; microwave power: 100μW; modulation width: 0.2mT.

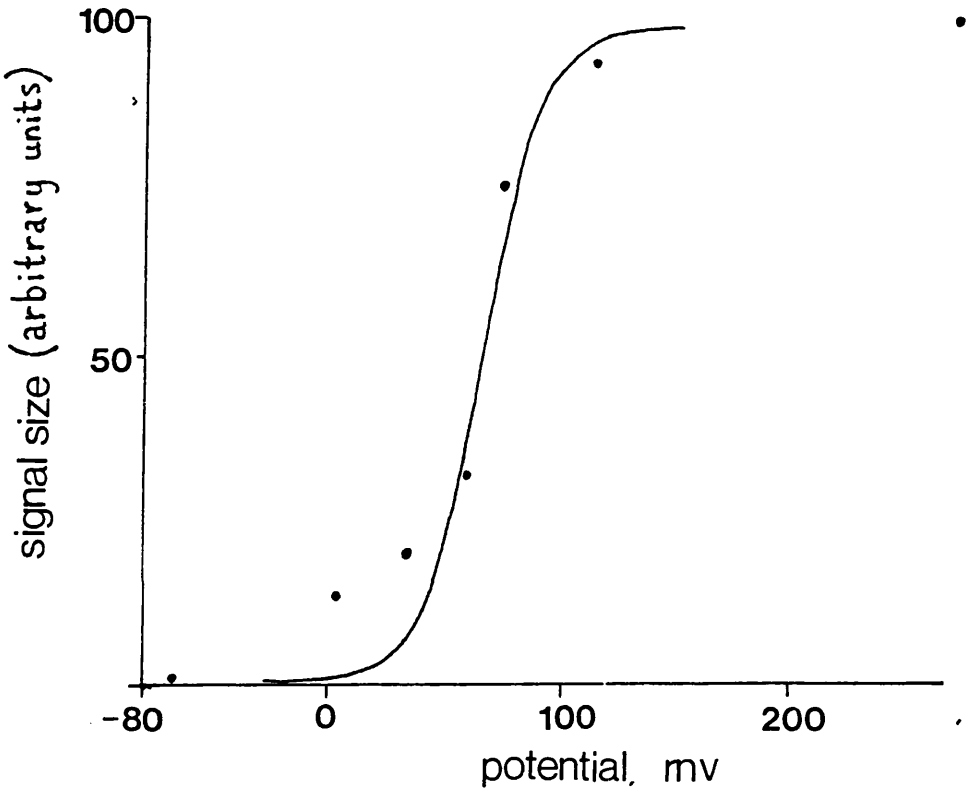

Figure 3.11 Redox Titration of D^+/D in P. laminosum PS II

The Figure shows a theoretical one-electron Nernst curve fitted to data obtained from a reducing titration of PS II at pH 7.8. Signals were measured as indicated in Fig. 3.10. The fitted curve has a midpoint potential of +75mV.

An important qualification to make regarding this result comes from observations reported later in this thesis (Section 3.6): samples poised for 4h, in the dark and at +350mV showed the epr Signal II. However, the size of the signal could be increased by illumination either at 293K, 200K or 77K, suggesting that only a fraction (≈60%) of D titrates with a midpoint of ≈ +75mV. When these titrations were first performed, the illuminated samples were not analysed for Signal II, and thus the value of 60% is derived from two different experiments.

3.4.2 DISCUSSION

The value of ≈+75mV determined in these epr titrations is substantially different from the previously determined value for the midpoint of the D^+/D couple of +760mV [159]. The earlier estimate was made using tris-washed PS II particles from fresh pea leaves, by titration not of signal II(slow), which is reported in this work and which is diagnostic of D^+, but of an epr signal that was induced by addition to these samples of an oxidising iridium salt, K_2IrCl_6. This altered epr signal was assigned to D^+ because it shared a number of properties with the conventional signal II(slow): first, the g-values of both signals are identical, at 2.0044 (different from the g-value reported here), although the altered signal has none of the hyperfine structure associated with Signal II(slow). Second, the changes in area bounded by the spectrum (directly proportional to the population changes in reduced and oxidised D) following continuous illumination and a return to darkness were quantitatively similar to those of signal II(slow).

However, the difference in potentials between these two measurements (≈700mV) is substantial. The difference between the

value in P. laminosum and any prospective value for the Z^+/Z couple in this species (which has to to be of the order of 1V to be capable of oxidising the higher S-states) is also substantial. This might reflect different roles for the component D in cyanobacterial and plant PS II, since it has been shown in PS II isolated from higher plant that D undergoes redox exchanges with different S-states [87], [93].

Clearly, the values determined for $E_{m7.8}$ for the D^+/D and the Q_a/Q_a^- in the P. laminosum PS II preparation are close, differing by only ≈20mV. It has been proposed by Nugent, et al, [160], that Q_a^- formed by illumination recombines with D^+ at 77K (in a period of days) and in thawed samples with a fast half-time (minutes). These results indicate that in higher plant PS II there is an electron-transfer pathway linking these two redox components.

It is possible that a similar pathway exists in P. laminosum PS II, and that, even if the true midpoint potential of the D^+/D couple was ≈ +750mV, the apparently low potential is the result of (i) component D^+ being in a highly insulated environment, unable to equilibrate with the bulk phase and (ii) Q_a then acting as a redox mediator for the reduction of D^+, via the hypothetical pathway.

This view can be discounted for the following two reasons: (i) the same redox behaviour is shown in by D^+/D in both oxidising and reducing titrations. If it was true that the real E_m for this couple was ≈ +750mV, no restoration of the epr signal would occur in oxidising titrations in the range -100mV ---> +100mV. (ii) Assuming that Qa functioned (below a certain potential) as an efficient mediator (i.e. equilibrated rapidly with both D^+ and the bulk phase), the pattern of reduction of D^+ would not be expected to follow a Nernst curve. Therefore, the value of +80mV does not simply reflect a mediation effect via the primary quinone. T h e

observation that reduction and oxidation did not alter the g-value or linewidth is evidence that the loss of the signal was not due to alterations in the environment of the species.

The conclusion is that this E_m is therefore real. It is not clear why only a fraction of the population should titrate with this low potential. The result is not, however, without precedent: in [118], it was reported that in PS II from peas, poised at above 0mV, the ability to photoreduce Q_a-Fe^{2+} and to generate Signal II at 5K was lost; whereas for samples poised between 0 and -100mV, 200K illumination caused an increase in the g = 1.8 signal. It was concluded that the loss of measurable photoreduction reflected a change in the donor.

3.5 Further Characterisation of the g = 1.6 signal of PS II from P. laminosum

As discussed in Section 3.2, the results of addition of agents that affect the Q_b site, or the state of ligation of the non-heme iron provide evidence that the signal seen at g = 1.6 is generated by low-temperature illumination of P. laminosum PS II centres in the states Q_a-Fe^{2+}-[HCO_3^-], or arguably without the bicarbonate, together with a requirement for conservation of native Q_b. The idea was put forward that Q_b-semiquinone was the most likely candidate, since, as a paramagnetic species, it would exert the strongest magnetic effect upon neighbouring molecules.

The first prediction that could be made from this hypothesis was that it should be possible to titrate the g = 1.6 signal, by poising of samples in the dark, and monitoring the yield of the signal after 77K illumination.

3.5.1 Determination of the Redox Properties of the g = 1.6 Signal

Figure 3.12 shows epr spectra of the iron-quinone complex in P. laminosum PS II poised in the dark. A g = 1.9 signal is obtained by poising a sample in the dark at -80mV, Figure 3.12(a). Fig. 3.12(b) shows the result of illuminating this sample at 77K. A sharp signal with g-value of approximately 1.97 can be seen, but there is no other major difference between this spectrum and (a). Fig. 3.12(c) shows a sample poised at +50mV in darkness. A smaller g = 1.9 signal can be seen at this potential. Illumination of the sample from (c) at 77K generates the prominent signal with a g-value of 1.66, and an approximate peak-to-trough width of 22mT, Fig. 3.12(d). There is an increase in the size of the g = 1.9 signal following low temperature illumination, and also the formation of the same sharp g=1.97 point seen in 3.12(b). This may reflect the

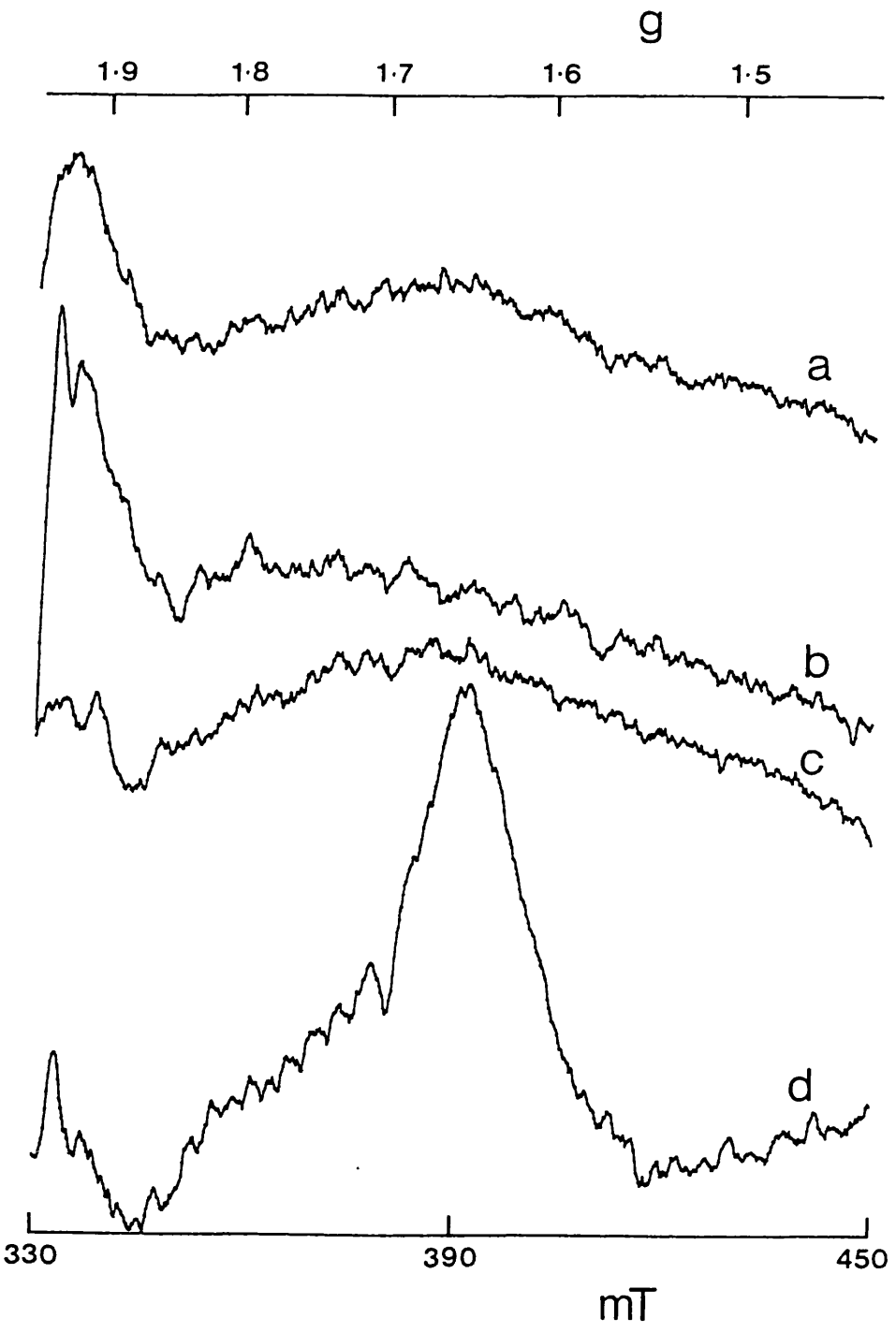

Figure 3.12 Epr spectra of the semiquinone-iron region in P.laminosum PS II

(a) Sample poised in dark at -80mV, (b) as (a) following 77K illumination. Sample poised in dark at +50mV (c), and (d) as (c) following 77K illumination. Chlorophyll concentration all 1mg.ml^{-1}. Epr conditions: temperature, 5K; microwave power, 10mW; modulation width, 1.25mT. Spectra shown are averages of three scans.

photoreduction of Q_a in centres which have not conserved the secondary quinone.

This signal is identical to the g = 1.6 signal described in Section 3.2. The reason for the improvement in the signal-to-noise, compared with the signals shown in Figure 3.3, is attributed in part to the 5-fold improved sensitivity of a new Jeol Fe1X EPR spectrometer compared with the one used to record the earlier spectra. The increased signal-to-noise permitted the measurement of the g-value and estimation of the peak-to-trough linewidth as indicated.

It indeed proved possible to measure the redox properties of the component giving rise to the g = 1.66 signal, by 77K illumination of samples poised at different potentials in the dark, as shown in Fig. 3.13. It was found to be necessary to take great care to exclude light from these samples, and to allow at least 2hr prior dark-adaption at +350mV, for satisfactory titrations to be obtained from which a value for E_m could be calculated. In samples which had been exposed to light, a substantial yield ($\leq$ 50% maximal) of g = 1.66 signal could be 77K-photoinduced at high potentials.

Titrations performed in the reducing direction show the g = 1.66 signal to rise in a single step with a midpoint potential, at pH 8.0 (E_{m8}) , of $\approx$ +60mV. As the titration proceeds, the signal then decreases in size with a midpoint of $\approx$ -10mV. In oxidising titrations, beginning at -100mV, the signal shows similar behaviour: a rise in the light-induced g = 1.66 form is followed by a decrease at higher potentials.

Comparison of the decrease of intensity of the g = 1.66 signal formed after 77K illumination, with the intensity of the g = 1.9 signal titrated in the dark is also shown in Fig. 3.13. The Nernst curve fitted to this titration of the g = 1.9 signal has a midpoint at 9mV, i.e., more negative than the figure given in Section 3.3, but within the normal error ($\pm$15mV) for this type of

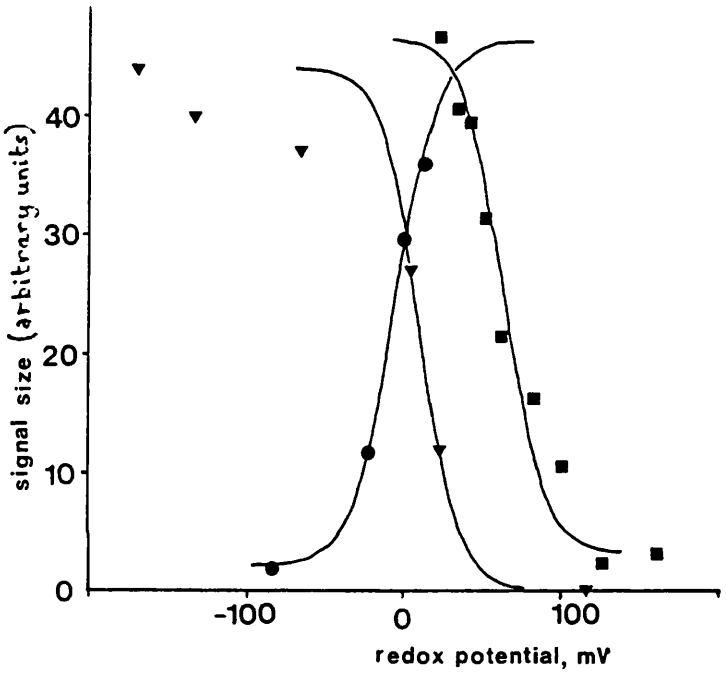

Figure 3.13 Reducing Redox Titration showing Variations in Intensities of EPR Signals from Semiquinone-Iron Components.

Squares show rise of g=1.66 signal; circles mark loss of g=1.66 signal; triangles indicate rise of g=1.9 signal in dark poised samples. g=1.66 signals can only be generated by illumination at 77K. The curves fitted are all for theoretical one-electron redox reactions, and have midpoints (pH 7.8) of: +60mV (g=1.66 rise); -10mV (g=1.66 loss); +9mV (g=1.9 rise). Epr conditions, as Fig.3.12.

titration. There appears to be an inverse relationship between the two signals, the loss of the higher field signal accompanying the rise of the g = 1.9 dark signal. This is considered further in the discussion.

The rise of the g = 1.66 signal at +60mV is accompanied by a decrease in the size of a 77K illumination-generated signal at g = 1.9. However, in these preparations the epr spectrum in the g = 1.9 region following 77K illumination is complicated by a superposition of signals which makes measurement of the broad g = 1.9 due to Q_a^--Fe^{2+} difficult. In particular, the sharp peak at g=1.97 is observed, Figs. 3.12(b) and 3.12(d), which affects the shape of the broader g = 1.9 signal formed by chemical reduction of Q_a or by photoreduction of Q_a at higher temperatures. The origin of this signal is not yet clear, although it may be due to an iron-sulphur component, present as a minor PS1-associated contaminant in these preparations.

3.5.2 pH Titrations of the g = 1.66 signal

A further prediction that stems from the hypothesis that the g = 1.66 signal arises from an interaction involving Q_b^- was that if the first reduction of Q_b was accompanied by a protonation, the midpoint potential for the rise in the g = 1.66 signal should be pH-sensitive (see Introduction).

The usual method for establishing the pH-dependence of a redox couple is to perform redox titrations at several different pH-values: in Section 1.7 it was shown that single protonation would cause a -60mV per pH unit increase. Owing to shortage of material to use in titrations, a different approach was tried (twice): it was decided to try to assess pH-sensitivity by maintaining a fixed potential and varying the pH. Samples were poised initially at

+50mV, pH 7.8, and the pH lowered by addition of 0.1M HCl. Throughout the experiment, the potential was maintained by additions of sodium dithionite or potassium ferricyanide, as described in Materials and Methods.

The result from this experiment, shown in Figure 3.14, indicates that the g = 1.66 signal is pH sensitive. However, it is difficult to make a positive interpretation of this result, since the experiment was repeated only once, but the following points seem to come out. Inspection of the Nernst equation for pH-dependent redox reactions would suggest that, if the potential is fixed, on lowering the pH, a decrease in the ratio [Ox]/[Red] would occur (assuming the potential is not so low that there is already 100% reduction, which at +50mV is not the case here). The corollary of this would be that, if what was observed in this potential range was simply reduction of Q_b, an increase in the signal size would be seen. On the other hand, if in this potential range, there is also double reduction of Q_b occurring, a decrease in pH, would also predict a decrease in the signal size; therefore, this result may provide some evidence that the loss of the signal with an $E_{m7.8}$ at ≈ +10mV is reflecting a second reduction of Q_b. A further complication is that the binding of bicarbonate, which was strongly suggested to be necessary for the formation of the g = 1.66 signal, is also pH-sensitive and may contribute to the effect (although as described in Section 3.2, this has not been shown in P. laminosum PS II). In summary, the experimental approach used does not resolve all the possible contributions which add to give the observed signal size.

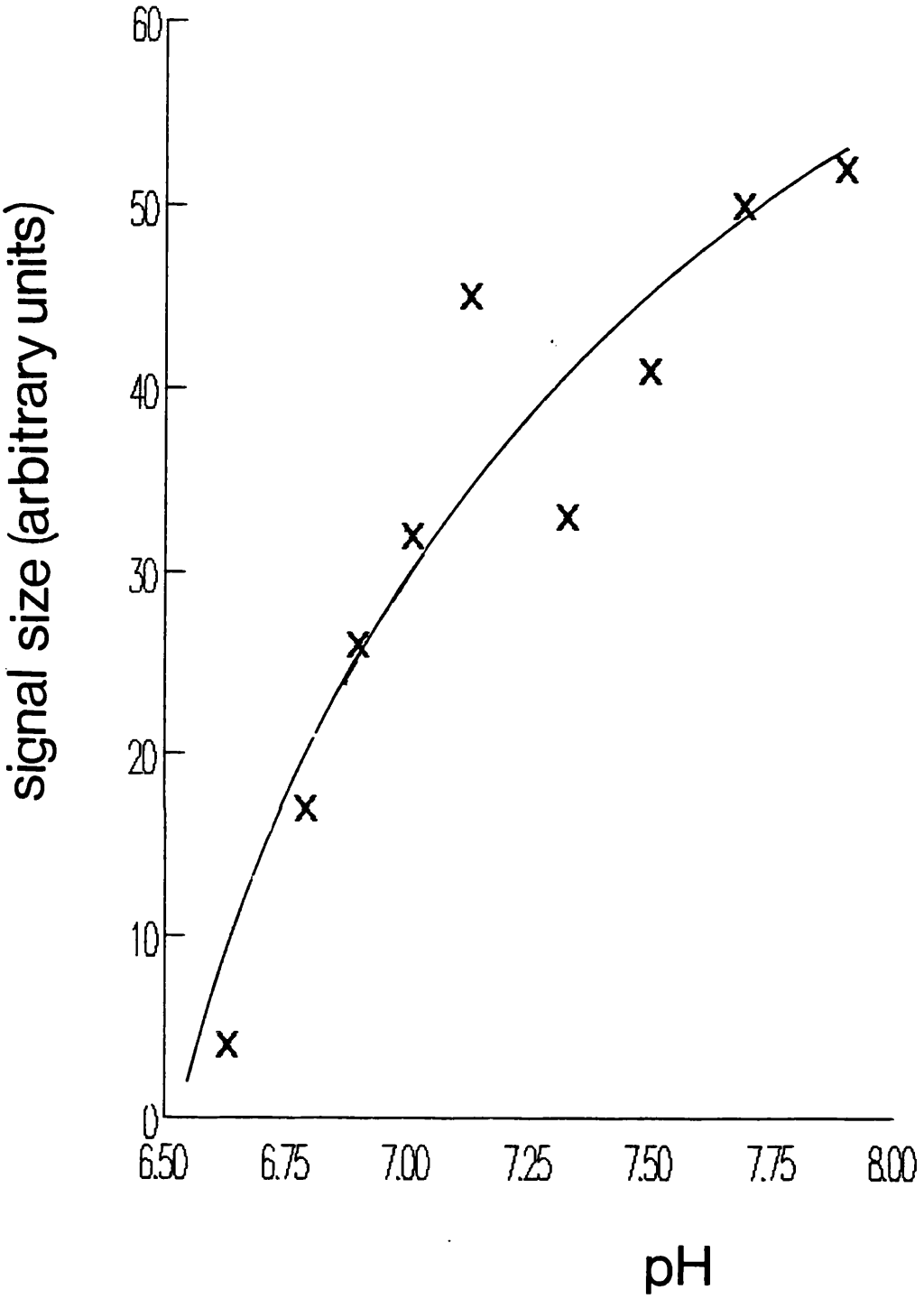

Figure 3.14 pH-dependence of the g=1.66 Signal at Constant Potential [+50mV]

The Nernst equation predicts that varying the pH whilst holding the potential constant should cause a 10-fold decrease in the ratio [Ox]/[Red] for drop in pH of 1 unit. As explained in the text, however, the situation is likely to be complex, and the curve drawn here was fitted to the points by eye.

3.5.3 Generation of the g = 1.6 Signal by Pre-Illumination of PS II at 293K

The observation that the g = 1.66 signal could in some cases be 77K-photoinduced at potentials above +100mV was investigated. Although this phenomenon was a problem with regard to obtaining clear-cut titrations of the g = 1.66 signal, it was at the same time interesting, since it suggested that one of the components (i.e. the E_{m8} = +60mV component) determining the signal showed some stability in the dark. Coupled to the observation that better titrations were obtained from PS II that had not been exposed to light, either during preparation or during the experiments themselves, it was decided to investigate whether illumination at room temperature (293K), followed by illumination at liquid nitrogen temperature could provide the right conditions for generating this signal.

Samples were dark-adapted at +350mV for 4h to allow equilibration of redox components, i.e. to allow the oxidation of any Q_a^- and perhaps of any Q_b^-. This period was followed by 1min saturating illumination at room temperature, and samples were then returned to darkness for varying intervals before freezing to 77K in the dark. (This period of darkness following 293K-illumination will be referred to as 'relaxation' and the samples as 'relaxed'). Control samples were made that were not illuminated at 293K but just frozen following the 4h in darkness (referred to as 'dark-adapted'). In addition, samples were prepared that were frozen under continuous illumination without an interval of darkness prior to freezing (referred to as 'frozen under illumination'). All of the samples were further illuminated at 77K for 10min to cause a single-electron turnover of P680. Epr spectra were taken from the samples both before and after this low-temperature illumination.

Spectra from dark-adapted samples show no distinct g = 1.9

signal prior to 77K illumination, Fig. 3.15(a), indicating little or no reduced Q_a; and after 77K illumination, they show no large yield of the g = 1.66 signal, Fig. 3.15(b).

In samples frozen under illumination, there was observed, prior to 10min 77K illumination, the g = 1.9 signal due to Q_a^--Fe^{2+}-[HCO_3^-]. 77K illumination of these samples yields no g = 1.66 signal; a result expected if the primary quinone is already in its reduced state, such that no further stable electron transfer to the acceptors can occur. This is analogous to the chemically-reduced samples seen in the titrations, where no generation of g = 1.66 occurs.

However, a high yield of the g = 1.66 signal was obtained in those samples first illuminated at 293K, allowed a period of dark relaxation and finally illuminated at 77K, Fig. 3.15(c) The time-course for this effect, Fig. 3.16, shows that approximately 60% maximal intensity of the g=1.66 signal is obtained after 1 min, followed by a slow rise in the intensity over the 135min course. Samples left for 22h in darkness in a refrigerator at 4°C showed no yield of g = 1.66 signal: the same samples did show an increase in the yield of g = 1.9, indicating that the absence of a feature at g = 1.66 was not due to the loss of electron-transfer capability.

It may appear paradoxical that the yield of g = 1.66 that could be formed 2h after 293K illumination was approximately maximal, yet only 2h was allowed for samples to relax before redox titrations were performed. However, samples used in successful titrations had had no substantial exposure to the light, and thus accumulation of the dark-stable component was presumably avoided.

In the same experiment, the pattern of oxidation of donor side components was monitored, in particular the behaviour of cytb559 and the tyrosine residue, D. This was necessary in order to

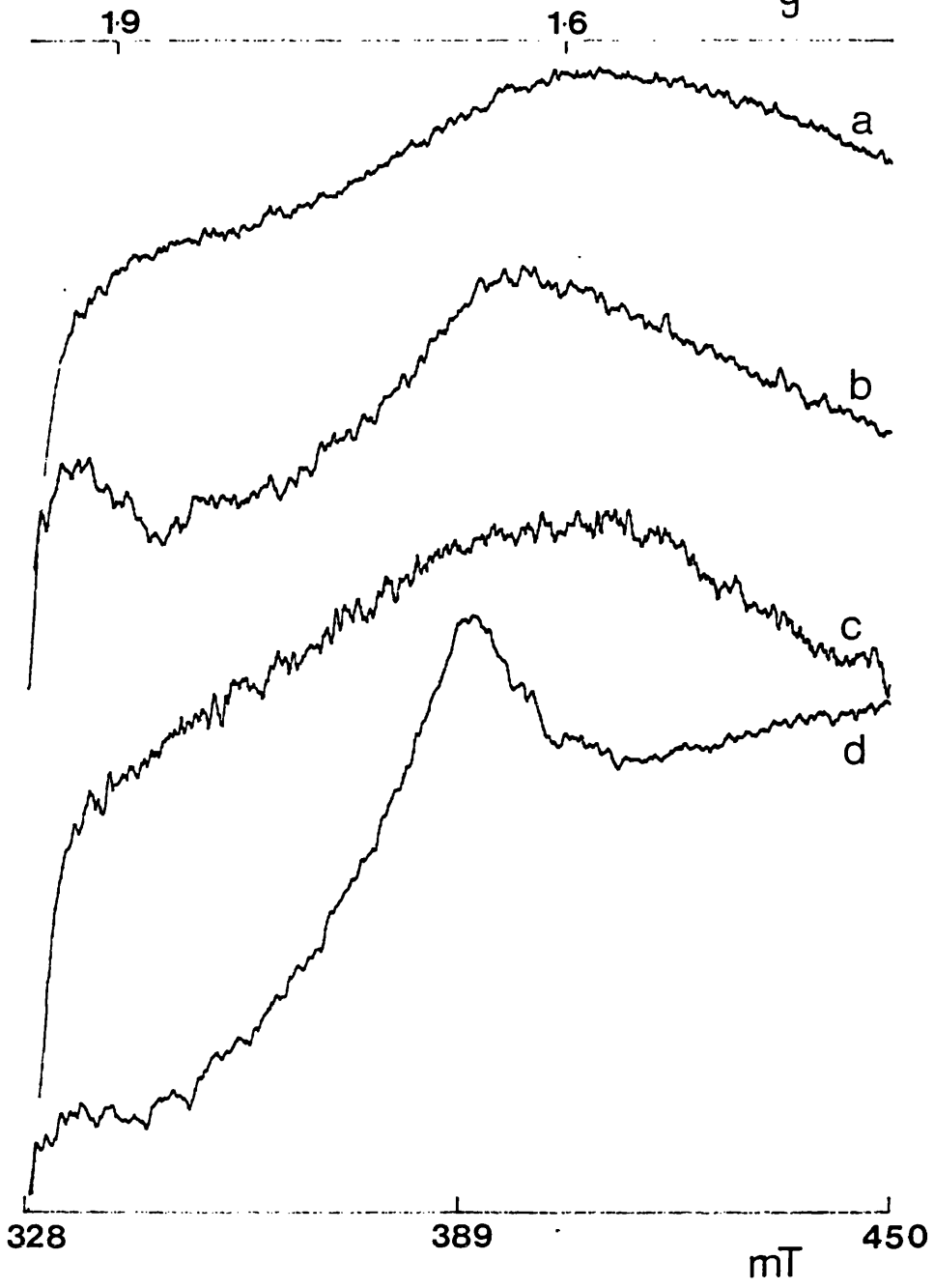

Figure 3.15 Generation of g = 1.66 signal by prior illumination at 293K

(a) shows an epr spectrum from the semiquinone-iron region of PS II from P. laminosum dark adapted for 4h. No signal at g=1.9 is observed but there is perhaps a broad signal in the g=1.6 region. (b) shows the same part of the spectrum following 77K illumination. The g=1.9 Q_a^--Fe^{2+} signal is clearly visible; there is some change in the g=1.6 region, perhaps indicating dark stable Q_b^-. (c) was obtained from a 293K-illuminated sample allowed to relax for 30min. The spectrum is noisier; it shows no g=1.9 signal. Following 77K illumination of the sample in (c), there is a clear yield of the g=1.6 signal. Chlorophyll concentration: 1mg.ml^{-1}. EPR conditions: temperature 5K; microwave power 10mW; modulation width, 1.25mT. Spectra are averages of two recordings.

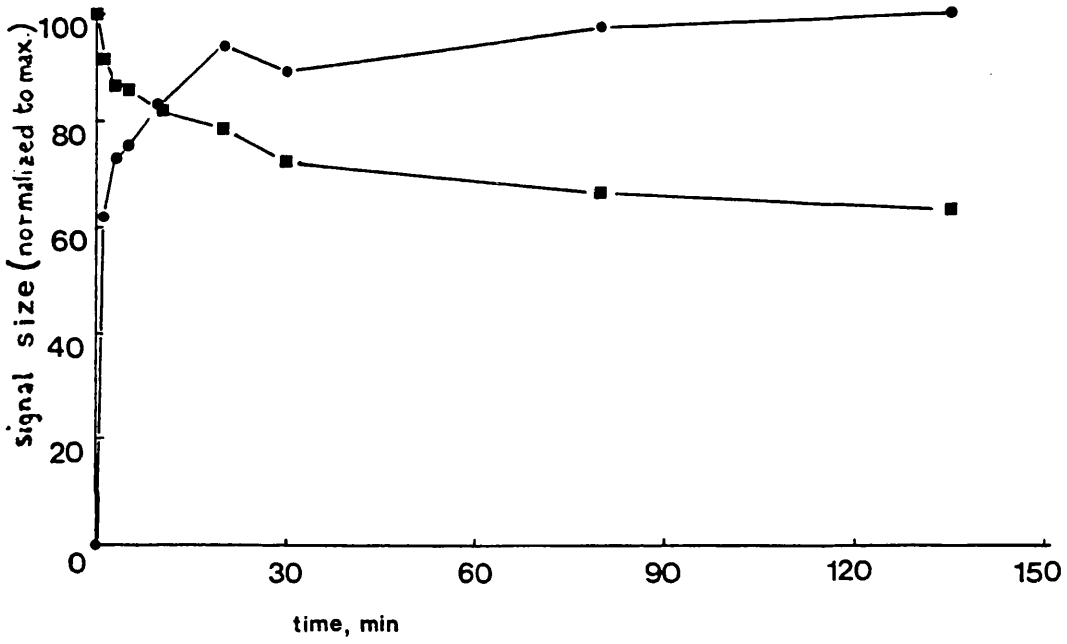

Figure 3.16 Time course for generation of g = 1.66 following room temperature illumination

Circles represent g=1.66 generated by 77K illumination of relaxed samples, except for the point at 0min, taken from 77K-illumination of a sample frozen-under-illumination. Squares indicate Signal II(slow), measured in the dark. Not shown is the effect of 77K-illumination of a dark-adapted sample, where photooxidation of up to 40% of Signal II(slow) is not matched by a corresponding generation of g=1.66.

determine any possible relation between the intensity of the g = 1.66 signal seen after 77K illumination with availability of functional donors at low-temperature.

It was found that in a dark-adapted sample D^+ was present at 60% of the maximal level, which could be induced by freezing under illumination. Following 293K illumination, the level of D^+ is thus initially maximal, and relaxes to the 'dark' level over the 135min course of the experiment, reflecting the re-reduction of this component, Fig. 3.16. However, whilst the amount of D in a dark-adapted sample and in this relaxed sample prior to 77K illumination are almost identical, it is observed that whereas the yield of g = 1.66 signal is maximal in the 135min-relaxed sample it is only 15% maximal in the dark-adapted sample.

Following 77K illumination of PS II, it was seen that the oxidation of D approached maximal levels in all samples. It should be emphasised that this represents a different degree of oxidation of D in each sample since over the course of the dark relaxation following 293K illumination there is a time-dependent restoration of D, and consequently a different amount available for re-oxidation. Nevertheless, in the dark-adapted sample, where oxidation of D at 77K was maximal, there was no corresponding large increase of the g = 1.66 signal. From this, it is concluded that there is no simple relation between the size of the g = 1.66 signal and the presence of reduced D. This result is of great significance: the titration of D described in Section 3.4 suggested that a fraction of this component could be reduced with midpoint at pH 7.8 of $\approx$ +75mV. If it had not been positively shown, as the results in this section do, that the generation of the g = 1.66 is not limited by electron donation, the result from the titration might only have reflected such a limitation.

The epr spectra of high-potential cytochrome b559 at g = 3.05 revealed no differences between dark-adapted, frozen-under-illumination or relaxed samples.

3.5.4 The Generation of the g = 1.6 Signal by Illumination at 200K, Following Pre-illumination at 293K

In the work of McDermott, et al., [120] the ability to generate the g = 1.6 signal was seen to be strongly temperature dependent, with the maximal yields of this form of the primary semiquinone-iron signal being observed following illumination at ≈ 180K. It is feasible that the loss of the g = 1.66, as the temperature of illumination is further increased, is because multiple turnover of P680 may occur. If at these higher temperatures electron transfer from Q_a^- to Q_b^- can occur, which was assumed not to be the case, the second reduction of Q_b would mean that no g = 1.66 signal would be generated.

Having established conditions under which the yield of the g = 1.6 signal following 77K illumination would vary, by pre-illumination at 293K and dark-relaxation, it was decided to alter the protocol, by replacing the illumination at 77K with an illumination at 200K. Again as before, changes in donor side components were monitored in parallel with the changes in acceptor signals.

Figure 3.17 shows spectra from the iron-quinone region of samples following 200K illumination for 10min. A signal similar to the g = 1.66 described above can be seen in 4h dark-adapted and 30 min relaxed samples: the yield is again greater in the relaxed than in the dark-adapted sample. The precise g-value is not easy to determine, owing to the superposition of multiline signal arising from the S2-state of the water oxidising complex.

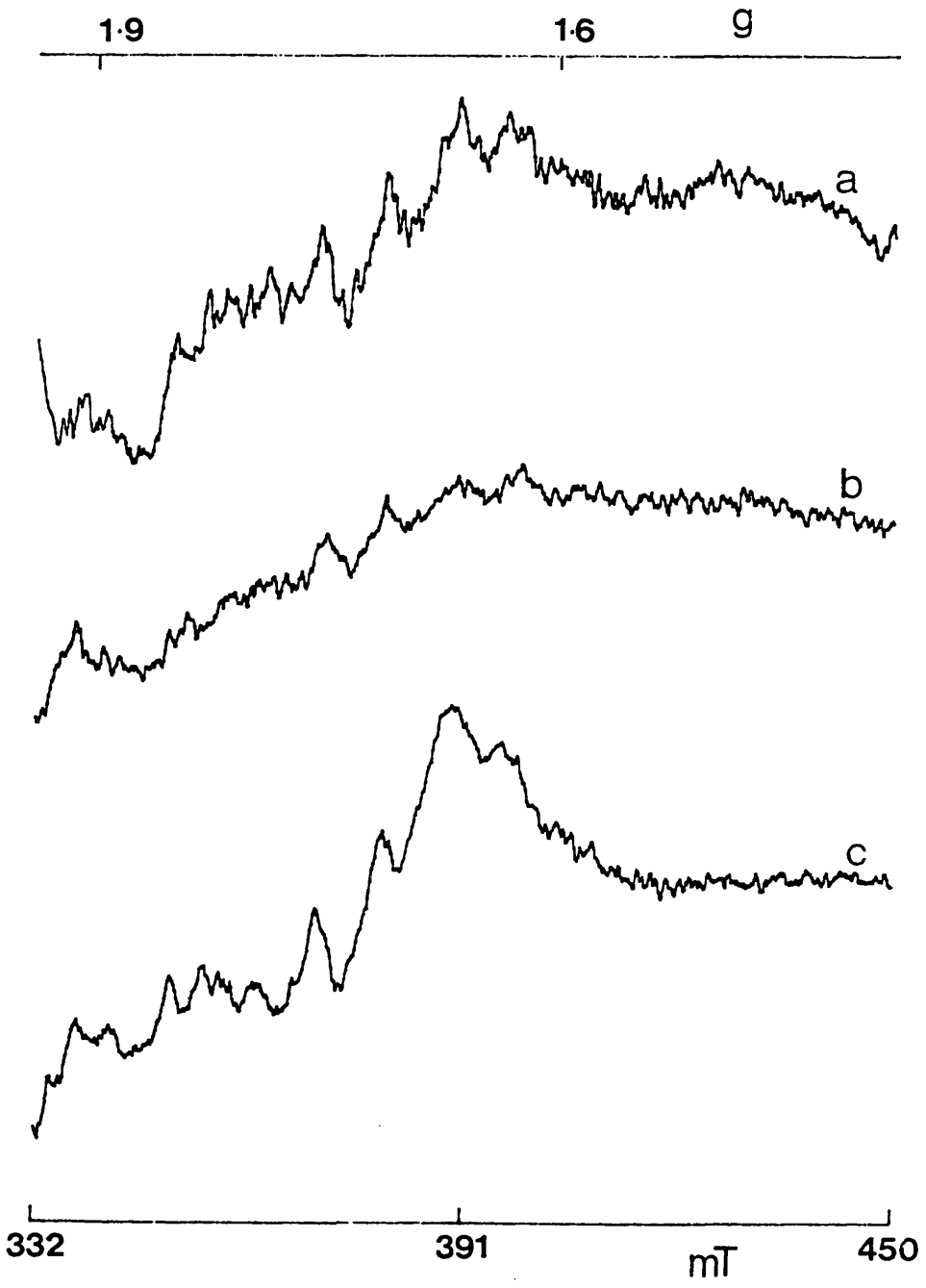

Figure 3.17 Generation of g = 1.66 signal following 200K-illumination

Spectra are shown from the semiquinone-iron region, from 200K-illuminated, untreated samples of PS II following: (a) 4h dark adaption; (b) freezing-under-illumination; and (c) 293K-illumination and 30min dark relaxation. The spectra are complicated by superposition of the multiline signal arising from S_2, but show that a greater yield of g=1.66 is obtained following room temperature illumination. Chlorophyll concentration: 1mg.ml^{-1}. EPR conditions: temperature, 5K; microwave power, 10mW; modulation width 1.25mT. Spectra are averaged from three recordings.

This result is in broad agreement with that obtained following 77K illumination, i.e. that the yield of the g = 1.6 signal is dependent on the time following 293K illumination. The signals seen following 200K illumination, from different preparations of P. laminosum PS II, were never seen to be as intense as those obtained by 77K illumination: however, no direct comparative experiment to show this (using the same preparation and both 77K and 200K illuminations) was performed on untreated samples, but Section 3.5.6 describes such an experiment in samples treated with the Qb-analogue, TBTQ.

The pattern of electron donation was rather complex in these time course experiments. It was observed that following 200K illumination oxidation of D, cytochrome b559 and S1 occurred. The oxidation of D followed a curve identical to that obtained following 77K illumination of 293K-illuminated samples; oxidation of the other two donors appeared uniform in all samples. This raises the possibility of multiple electron transfer, but more accurate quantification of spin poulations would be necessary to confirm this: but with the preparations of PS II used, it was not practicable to use samples of greater than $\approx 3 mg.ml^{-1}$ chlorophyll, and only weak signals could be obtained from cytochromes and from S2, making such a quantification difficult.

3.5.5 Power Saturation and Temperature Dependence of the g = 1.66 Signal

Figures 3.18(a) and 3.18(b) show the power saturation characteristics at 5K of the g = 1.66 and g = 1.9 epr signals from P. laminosum. The determination of $P_{\frac{1}{2}}$ is subject to some error, since the straight line of the saturating limit was fitted by eye, with a greater emphasis given to higher values of log P. However,

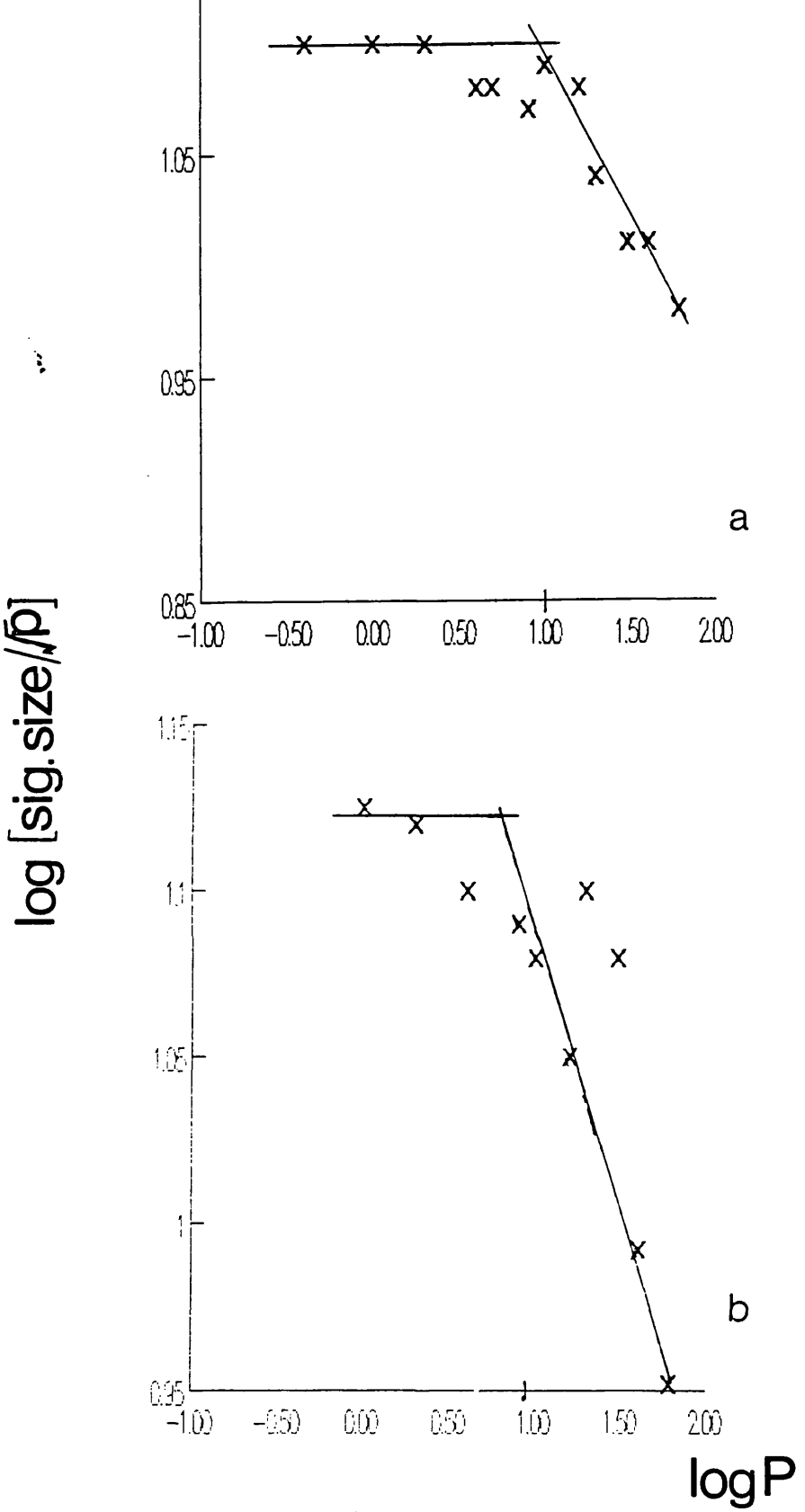

Figure 3.18 Power Saturation Curves for g=1.66 and g=1.9 Signals

Power saturation characteristics of the g=1.66 (a) and g=1.9 (b) epr signals: the data suggest similar $P_{\frac{1}{2}}$s for both signals of approximately 10mW. Spectra from semiquinone-iron components were routinely recorded using 10mW microwave power.

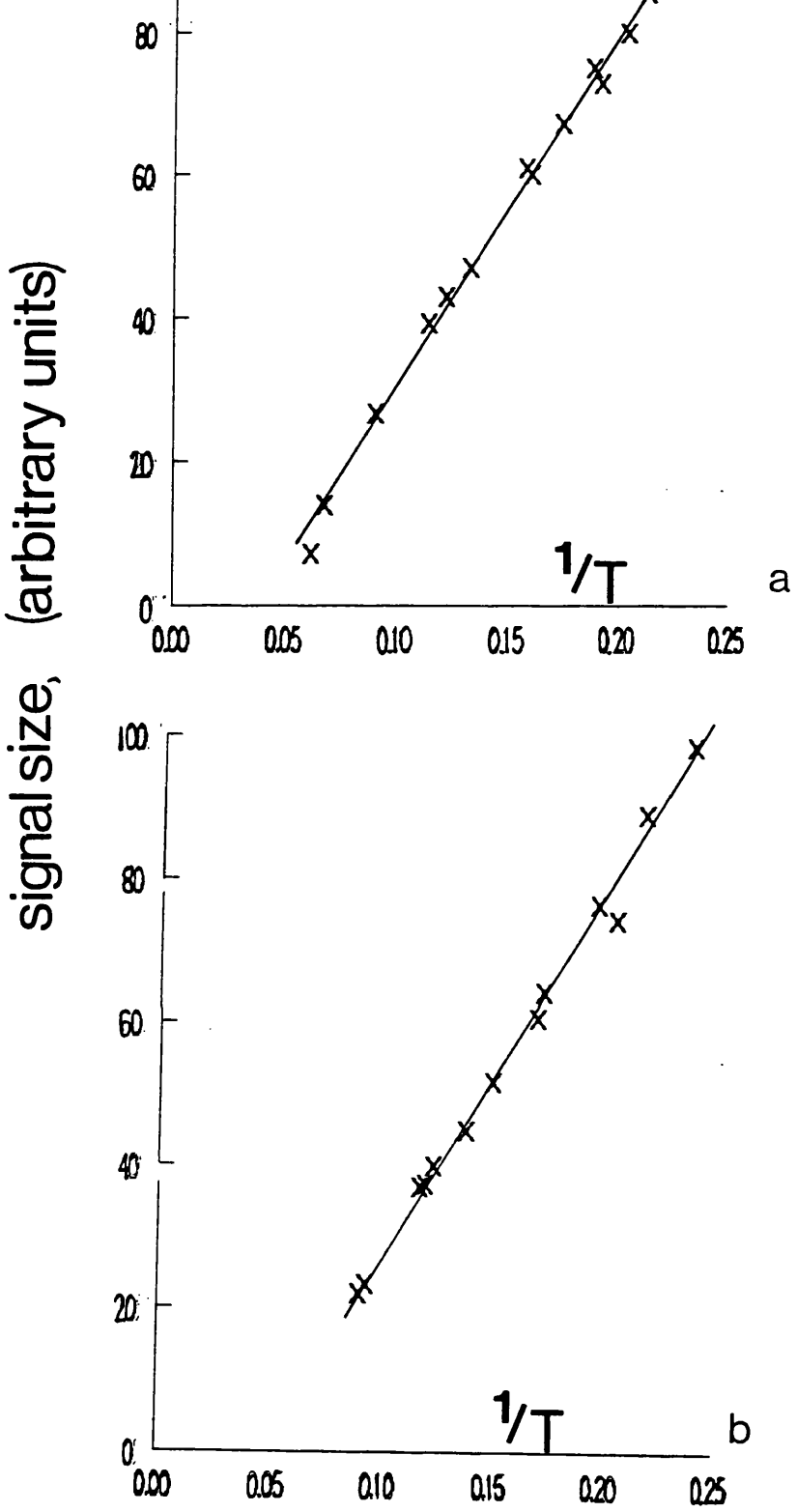

Figure 3.19 Temperature Dependence Curves for g=1.66 and g=1.8 EPR Signals

(a) and (b) are temperature dependence curves from the g=1.66 and g=1.8 curves, respectively. An analogous curve from the g=1.9 was difficult to measure, owing to the presence of the g=1.92 at warmer temperature. Both show simple Curie behaviour (linear with repect to 1/T) in the range 4-20K. Spectra from semiquinone-iron components were routinely recorded at 5K.

values for $P_{\frac{1}{2}}$ for the g = 1.66 and g = 1.9 signals of 9.7mW and 9.0mW are given. Values of $P_{\frac{1}{2}}$ in this range suggest the paramagnetic species giving rise to the epr signals are able to relax efficiently; and the similarity in the values (the difference is probably not outside the error range) suggests the two signals arise from similarly coupled systems.

The temperature dependence of the g = 1.66 signal was determined and is shown in Fig 3.19(a) as a plot of signal size versus 1/T. This can be compared with the temperature dependence of a formate-induced g = 1.8 signal Fig. 3.19(b). Both signals show a linear dependence on 1/T, indicating simple Curie behaviour in the temperature range 4 - 20K.

3.5.6 Investigation of the Effects on PS II of the Halogenated 1,4-Quinone, Tribromotoluquinone (TBTQ)

3.5.6.1 Generation of Signal with g = 1.67 by Treatment of P. laminosum PS II with TBTQ

Renger, et al, [161,162,163], have shown prior to this work that the class of halogenated 1,4-benzoquinones, especially tribromotoluquinone (TBTQ), could function as artificial single-electron acceptors, and furthermore they affected the binding of DCMU to the acceptor side of plant PS II. In particular, preincubation of thylakoids with TBTQ diminishes the blockage of O_2-evolution by DCMU; this effect, however, is strongly dependent upon the order of addition of TBTQ and DCMU to the membrane. A conclusion drawn by these workers was that TBTQ bound at, or close to, the Q_b binding site on the D1 polypeptide, in the form of a semiquinone. In the light of this, an epr study was made of P. laminosum PS II treated with TBTQ, to see whether the g = 1.66 epr signal, attributed to an interaction between Q_a^--Fe^{2+} and Q_b^- on the

evidence,had an analogue in the proposed Q_a^--$Fe2^+$-[TBIQ$^-$] system.

Additions were made in the dark of a 25mM solution of TBIQ (kindly given by Prof. W. Oettmeier) in dimethyl sulphoxide (DMSO) to give a final concentration of 625μM. It is noted that this gives a final concentration of DMSO of 2.5% (v/v).

The effect of 77K illumination on the epr spectrum of dark-adapted P. laminosum PSII treated with 625μM TBIQ is shown in Figure 3.20. Figure 3.20(a) shows the dark spectrum of a TBIQ-treated sample. No features are seen in the g = 1.9 region of the spectrum, perhaps indicating an oxidation by TBIQ of native Q_a. Following 77K illumination, a signal similar to the g = 1.66 signal can be seen, except that the marked peak occurs at g = 1.67, compared with g = 1.66 in 'native' samples, and that the peak-to-trough width of 17mT is narrower.

The pattern of induction of the g = 1.67 after dark-adaption and following 293K illumination is different from that in untreated samples. In particular, a greater fraction of g = 1.67 signal (80%) was seen to be induced following 77K illumination of the dark-adapted samples compared with those that had been illuminated at 293K; whereas in untreated samples this fraction is approximately 15%. However, freezing to 77K under continuous illumination again gives essentially no yield of g = 1.67 signal, but is replaced by the g = 1.9 signal. The implications of these results are discussed later.

It was observed that a signal similar to the g = 1.66 signal that could be detected in native samples could be generated by 77K-illumination of P. laminosum PS II that had been dark-adapted and incubated in the presence of TBIQ. It was shown, too, that the g = 1.66 could be generated in 200K-illuminated samples, although there was the suggestion that the yield of signal was lower at this higher

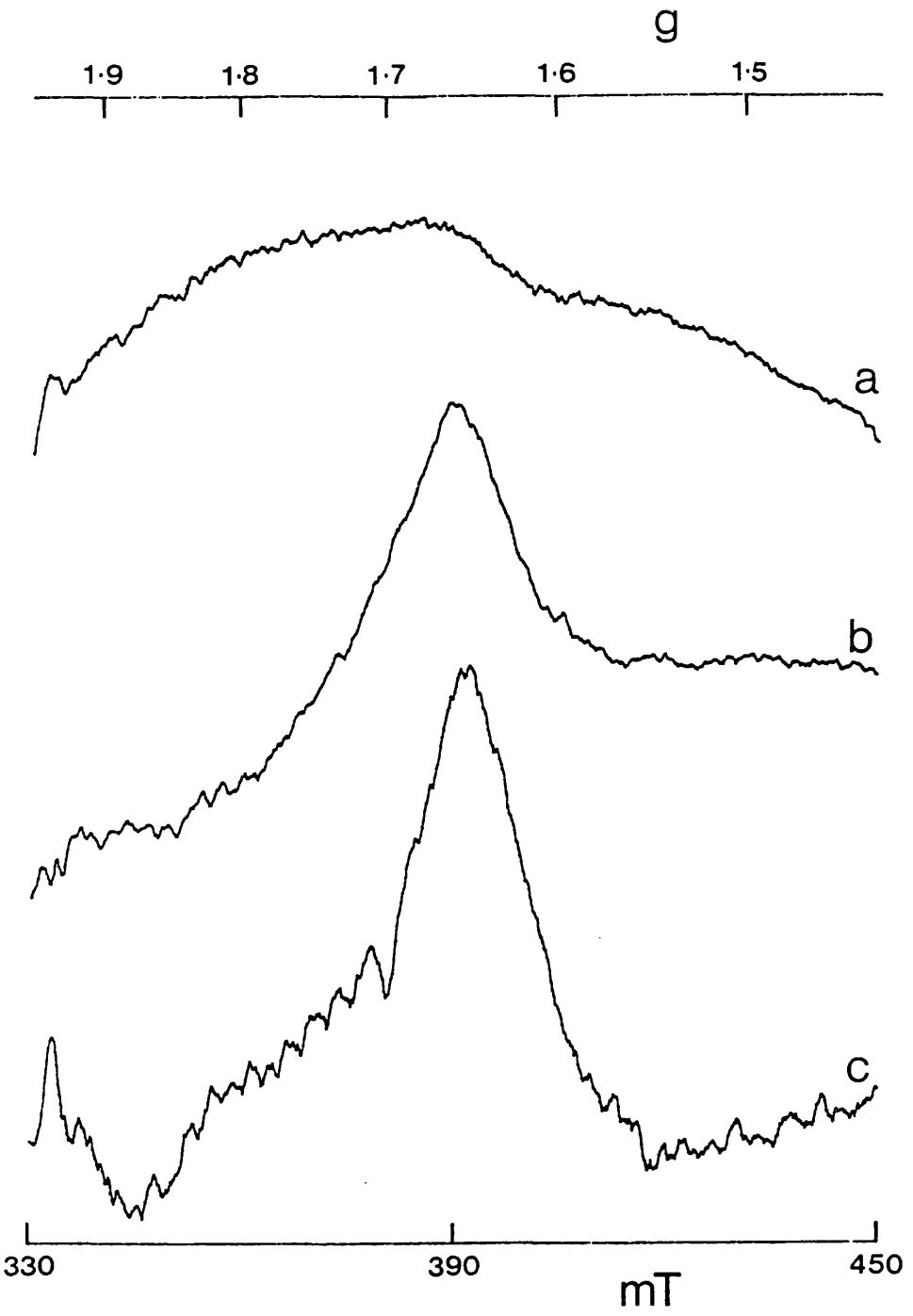

Figure 3.20 Effect of Tribromotoluquinone (TBTQ) on the epr spectrum of semiquinone-iron components from P. laminosum

Epr spectra of P. laminosum PS II treated with 625μM TBTQ. (a) TBTQ-treated sample in darkness; (b), as (a) following 77K illumination, the signal peak is at g=1.67; (c) shows the g=1.66 signal generated in native sample poised at +50mV. Chlorophyll concentration: 1mg.ml^{-1}. EPR conditions: temperature, 5K; microwave power, 10mW; modulation amplitude, 1.25mT.

temperature. The effect on the iron-quinone region of the epr spectrum of 200K-illumination of a 4h dark-adapted sample of P. laminosum PS II treated with TBIQ is shown in Figure 3.21(a), and compared with a sample from the same preparation, again with added TBIQ, illuminated at 77K, Figure 3.21(b). Following 200K-illumination there is little evidence of the g = 1.67 in these samples, contrasting with the high yield obtained following 77K-illumination.

3.5.6.2 The Effect of TBIQ on the EPR Spectrum from D^{+}

The addition of TBIQ almost completely abolishes the dark-stable signal II seen in these samples, Figure 3.22(a), as reported previously in [163]. Instead, we see an asymmetrical, 1.975mT wide signal with g=2.0028, Figure 3.22 (b). This signal can be seen in solutions of 625uM TBIQ in tricine buffer, pH 7.5, and we take it to be due to the semiquinone form of the compound. Addition of $5mg.ml^{-1}$ bovine serum albumen to TBIQ in tricine also increases the intensity of this signal by 5-fold, although its lineshape is not changed. It is proposed, then, that in the presence of protein it is possible, though not necessary, for the proportion of the semiquinone form of TBIQ to be increased, either through reduction of the free molecule by redox active residues in the protein, for example, reduced sulphydryl groups; or by stabilisation of the semiquinone in a redox event coupled to the covalent binding of TBIQ to the protein. There is another mechanism by which the binding of small molecules to macromolecules can bring about an increased intensity in the epr signal: when bound to the protein (for example) dipolar interactions between the paramagnetic species, which may suppress an epr signal, are lessened due to repulsion of the macromolecules. The gain used to record the signal in PSII

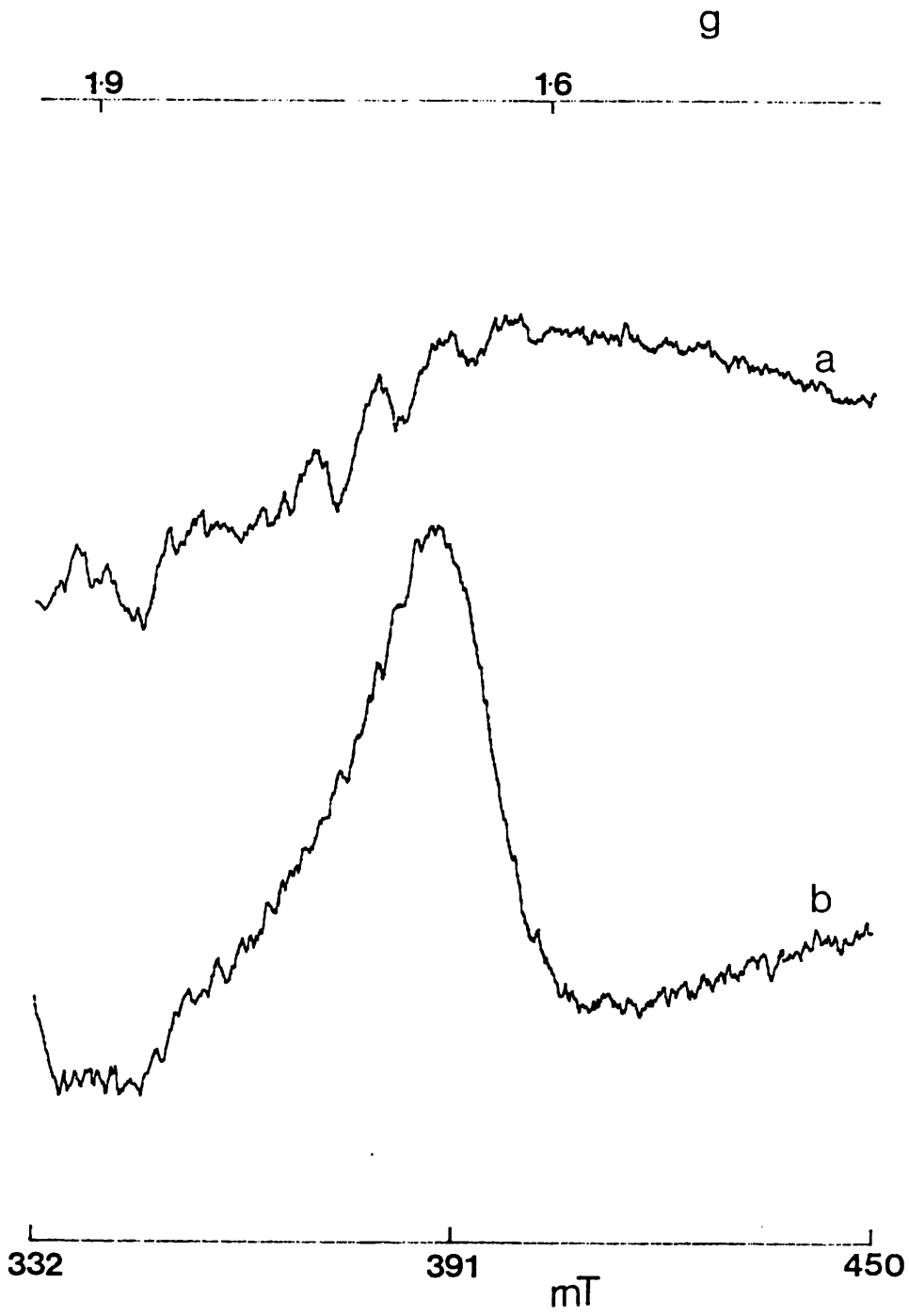

Figure 3.21 200K-illumination of P. laminosum PS II treated with TBTQ

(a) shows the epr spectrum from the semiquinone-iron region of a sample of P. laminosum PS II treated with 625μM TBTQ and illuminated at 200K. In contrast to the pronounced g=1.67 signal generated by 77K illumination, (b), there is little or no signal formed at g=1.67 by illumination at the higher temperature. There is some g=1.9 signal, and formation of the S2-multiline is not impaired. This also contrasts with the result in Fig. 3.15, showing that in native samples it is possible to form the g=1.66 signal by illumination at 200K. Chlorophyll concentration: 1mg.ml^{-1}. EPR conditions: temperature, 5K; microwave power, 10mW; modulation amplitude, 1.25mT.

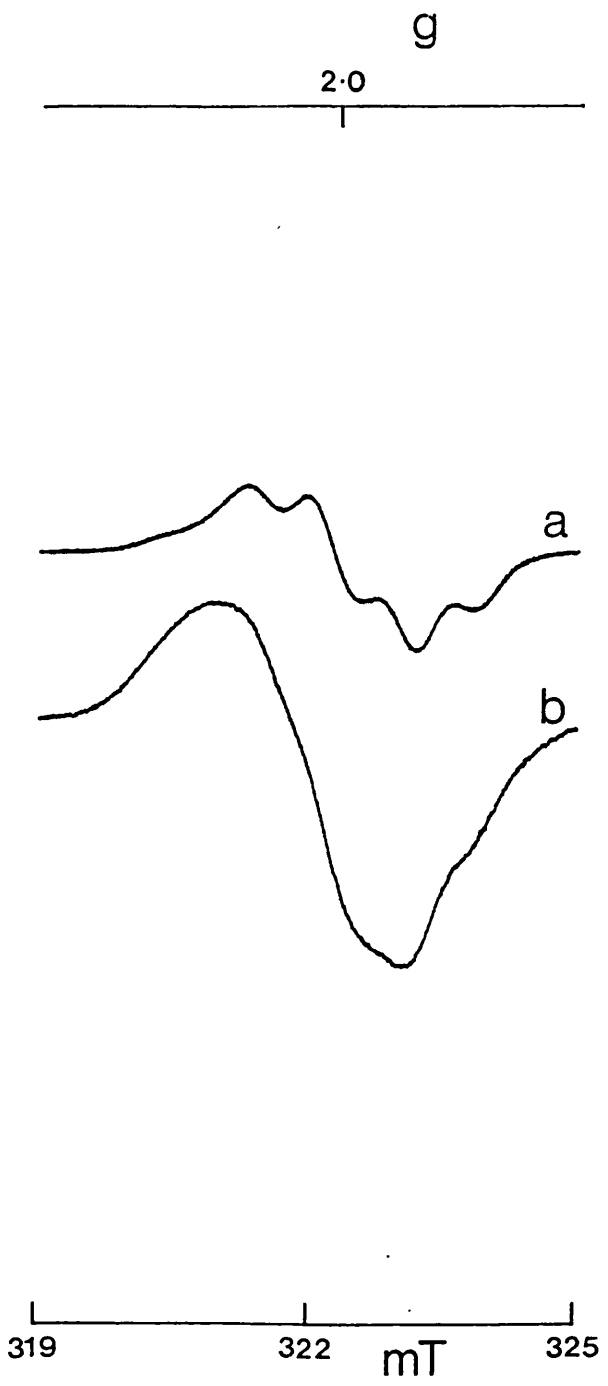

Figure 3.22 Effect of TBTQ on the EPR Spectrum from D^+

Epr spectra of D^+ from P. laminosum, (a) and the effect on this signal of treatment with 625μM TBTQ, (b). Chlorophyll concentration: 1mg.ml^{-1}. Epr conditions: temperature, 14K; microwave power, 100μW; modulation width, 0.2mT.

treated with TBTQ was 5 times greater than that used to record the signal II, and yet there was only a slight indication of a signal II superimposed on the TBTQ signal. Unless an interaction between D^+ and one of the redox forms of TBTQ suppresses signal II, this result may imply a reduction of D^+ by, for example, the quinol form of TBTQ, and the consequent abolition of its epr spectrum. Following illumination at 77K there is some restoration of Signal II superimposed on the TBTQ radical signal (not shown in Figure 3.22).

3.5.6.3 Effect of TBTQ on the EPR Spectra from Cytochrome b559

High- and low- potential forms of cyt b559 have been reported to show different g_z-values: [164] reports g_z = 3.08 (high) and 2.94 (low) in higher plant PS II; [152] cites g_z = 3.1 for the high potential form in P. laminosum.

The effects of addition of 625μM TBTQ on the epr spectrum from 200K-photooxidisable cytochrome b559 is shown in Figures 3.23(c) and 3.23(d); for comparison, spectra from a_{λ}^{native} sample (at identical chlorophyll concentration) are shown in Figures 3.23(a) and (b). The dark spectrum from an untreated sample has a small peak with g = 3.08: since these samples had been poised at +350mV, it would be expected that any low-potential form of the cytochrome would be oxidised (E_m = +80mV [165]), showing a signal with g_z < 3.0. Illumination of the sample gives rise to a signal in this region with g_z = 3.05, which probably represents photooxidation of high-potential cyt b559: it is not known what fraction of total cytochrom was oxidised. The position of the peak differs from that in the dark spectrum. Addition of 625μM TBTQ gives the spectrum shown in 3.23(c): a larger signal with g_z-peak at 3.10 is formed. The size of this signal increases by approximately 100% following 200K-illumination: the position of the peak again appears to shift (or broaden) to g = 3.08.

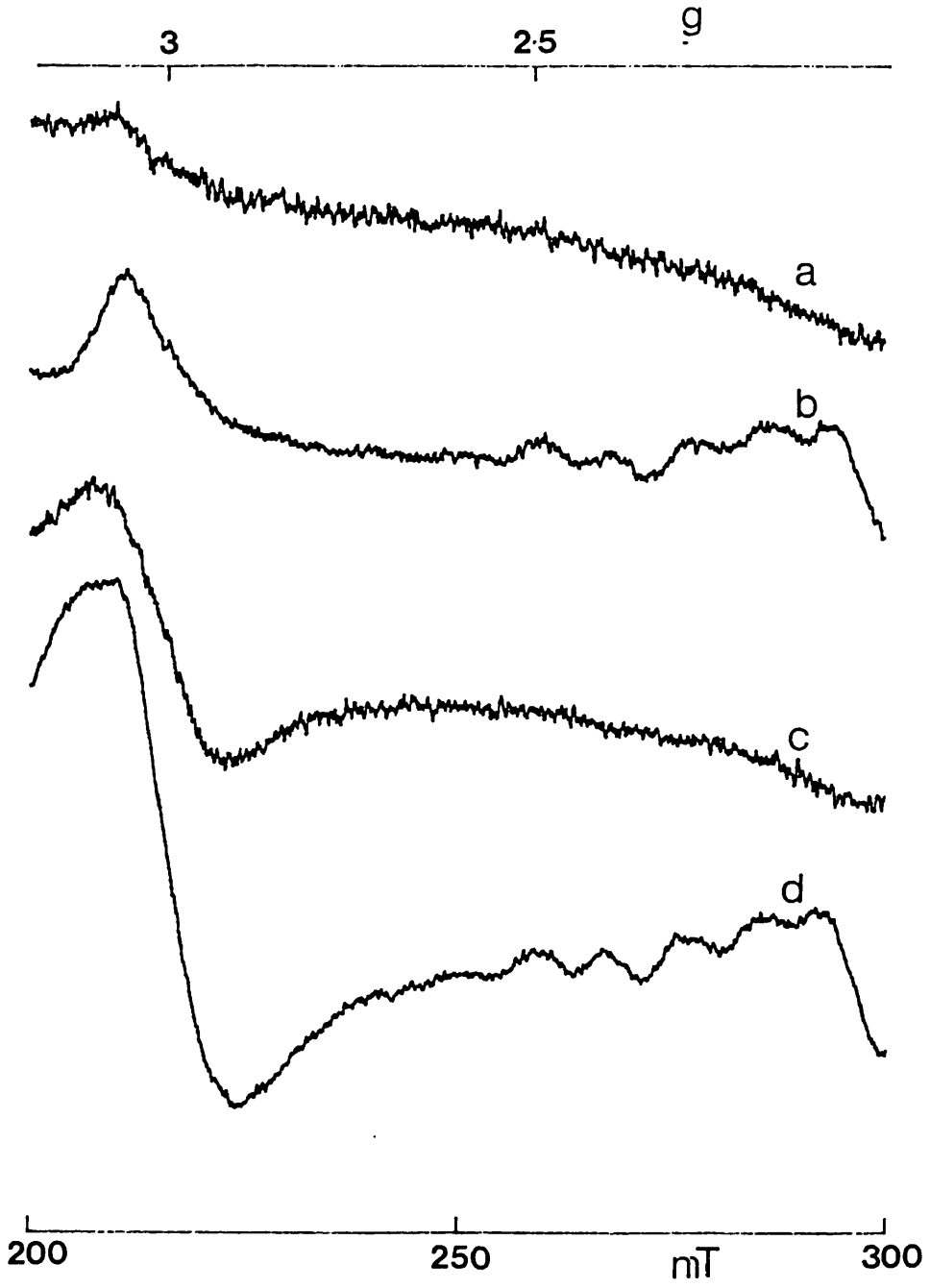

Figure 3.23 Effect of TBTQ on EPR Spectrum of Cytochrome b559

Epr spectra from cytochrome b559 from PS II isolated from P. laminosum. (a) untreated membranes, 4h dark-adapted, showing small peak at g = 3.08; (b) as (a), following 10min 200K-illumination. The position of the peak is different, at g=3.05. Treatment of membranes with 625μM TBTQ is shown in (c) and (d): a large signal with peak shifted to 3.1 is seen in the dark sample (c), which increases by ≈100% after 200K-illumination. Spectra (b) and (d) also show the S2-multiline. Chlorophyll concentration: 1mg.ml^{-1}. Epr conditions: temperature, 12K; microwave power, 5mW; modulation width, 1.25mT.

3.5.6.4 Effect on the EPR Spectrum of Higher Plant PS II Treated with Tribromotoluquinone

Following the detection and optimisation of the g = 1.66 signals from native and TBTQ-treated cyanobacterial PS II, an attempt was made to identify the same signals in PS II from a higher plant source. It had been shown by other workers and by earlier experiments in this thesis that, as judged by their epr properties, the two systems share some but not all properties: for example, both show the g = 1.8 and g = 1.9 forms of epr signals, dependent on broadly conditions. However, it could not necessarily be assumed that the signal would be detected in higher plant preparations.

Samples of PS II from spinach were treated with 625μM TBTQ, and then either dark adapted for 1h prior to freezing in the dark or illuminated at 293K and allowed to relax in the dark for 30min. Spectra from the iron-quinone region were then recorded in the dark and again following 77K illumination.

The epr spectra of the iron-quinone region from these samples are shown in Figure 3.24. The spectrum from an untreated, dark adapted sample, Figure 3.24(a), shows a substantial signal in the g = 1.9 region, indicating dark-stable Q_a^-: no measurement of the ambient potential was made in these samples, neither were there any redox mediators to assist equilibration, but it was assumed that 30min dark-adaption would have been sufficient time for relaxation of Q_a^- to occur. Following 77K illumination an increase in the size of the signal at g = 1.9 is observed, Figure 3.24(b). Addition of 625μM TBTQ causes a change in the semiquinone-iron spectrum in the dark, Figure 3.24(c), where in place of the broader g = 1.9 signal, a sharp signal at g = 1.97 can be seen. It is unclear whether this signal arises from (i) the signal from $Q_a^{\cdot -}$-Fe^{2+}, modified by

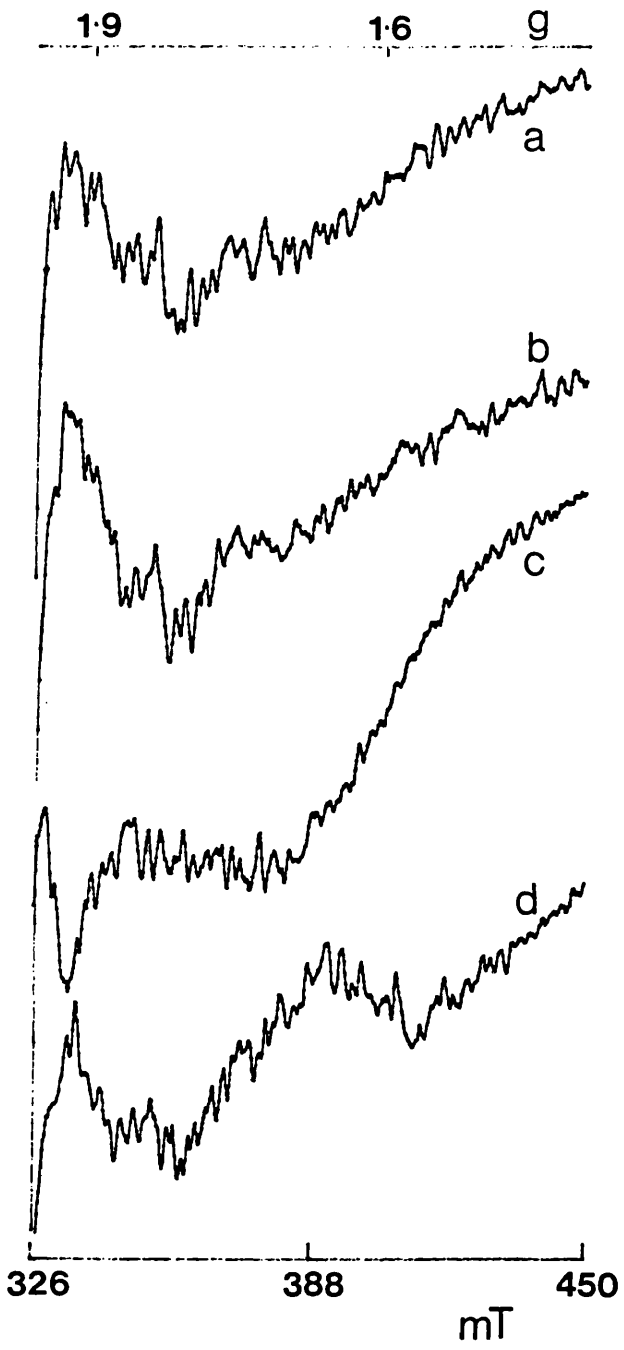

Figure 3.24 Formation of g ≈ 1.6 signal in Spinach PS II by treatment with TBTQ

(a) shows a spectrum from 30min dark-adapted spinach PS II. The spectrum shows a broad g=1.9 signal, probably indicating dark-stable Q_a^-. Following 77K illumination, (b), the size of the g=1.9 has increased, but there is no major change in higher field parts of the spectrum. (c) shows a 30min dark-adapted sample treated with 625μM TBTQ. There is a sharp signal at g=1.97, perhaps due to Fe^{2+}-$TBTQ^-$. After 77K-illumination the spectrum (d) shows a feature at g≈1.6, as well as the g=1.9 signal. Chlorophyll concentration: $5mg.ml^{-1}$. EPR conditions: temperature, 5K; microwave power, 10mW; modulation amplitude, 1.25mT.

binding of the Q_B-analogue; or (ii) a signal arising from, for example, TBTQ$\cdot^-$-Fe^{2+}, where TBTQ has bound at the Q_B-site. The signal resembles a previously-reported signal for the interaction $Q_B\cdot^-$-Fe^{2+} from native PS II [131]. 77K illumination of the TBTQ treated sample gives the spectrum shown in Figure 3.24(d), which has features both at g = 1.9 and in the g = 1.6 region. The precise g-value and linewidth of the peak cannot be determined from these spectra, owing to the background noise. 77K-photoreduction of PS II where TBTQ had not bound would give rise to the g = 1.9 signal; whereas in that fraction of centres where TBTQ had bound as its semiquinone it is suggested that the broad g = 1.6 signal results. This is discussed further in Section 3.5.9.

3.5.7 Oxidation of the Non-Heme Ferrous Iron by Replacement of the Native Secondary Semiquinone by an Artificial High-Potential Semiquinone (PPBQ)

It has previously been shown that certain Q_B analogues are capable of oxidising the non-heme Fe^{2+} to Fe^{3+} [166], [167]. This follows the generation of semiquinones with redox potentials sufficiently positive to oxidise the iron. The epr signal of the non-heme Fe^{3+} has peaks at g=8.1 and g=5.5 [168] in centres with an empty Q_B site [169]. The peaks are removed following illumination in the range 5-200K, indicating reduction of the iron.

In P. laminosum, it is proposed that Q_B^- is present in the dark following the 293K illumination/dark adaption protocol described above, and it was therefore decided to investigate the effect of adding the artificial quinone phenyl-para-benzoquinone (PPBQ) on the epr spectra of both the semiquinone and non-heme iron species.

In a relaxed, untreated sample, at pH 7.5, there is no change

in the epr spectrum arising from the non-heme iron following 77K illumination, Figure 3.25(a). This result indicates that native Q_B^- is not itself capable of oxidising the non-heme iron.

However, addition in the dark of 600μM PPBQ to a 20min dark relaxed sample results in the oxidation of the non-heme iron, giving the spectrum shown in Figure 3.25(b), with signals at g = 8.7, g = 6.9 and g = 5.1. This central peak at g = 6.9 has been attributed to ferric non-heme iron where centres bind oxidised quinone at the Q_B-site [169]. Comparison of the size of the g = 8.7 peak with that derived from ferricyanide-oxidised samples suggest that approximately 50% of the ferricyanide-oxidisable complement of Fe^{2+} is oxidised by this means: of course, it is still uncertain what proportion of the non-heme iron is oxidised by potassium ferricyanide. This result further implies the presence of Q_B^- in the relaxed sample: an exchange can be envisaged at the Q_B-site of the native Q_B^- for PPBQ, which is then able to oxidise the non-heme iron. It is not apparent from this result alone where the oxidation of the Q_B^- by PPBQ takes place. A proposed reaction scheme is shown in Figure 3.26

Illumination of this sample at 77K causes partial photoreduction of the iron (Fe^{3+} ---> Fe^{2+}): this is inferred from the dark-minus-illuminated difference spectrum shown in Figure 3.25(c). The interesting feature of this spectrum is that the peaks at g = 8.7 and 5.1 imply an approximately 50% photoreduction of the iron, whereas the signal at g = 6.9, which is completely absent in the difference spectrum, suggests that no reduction of the iron has occurred.

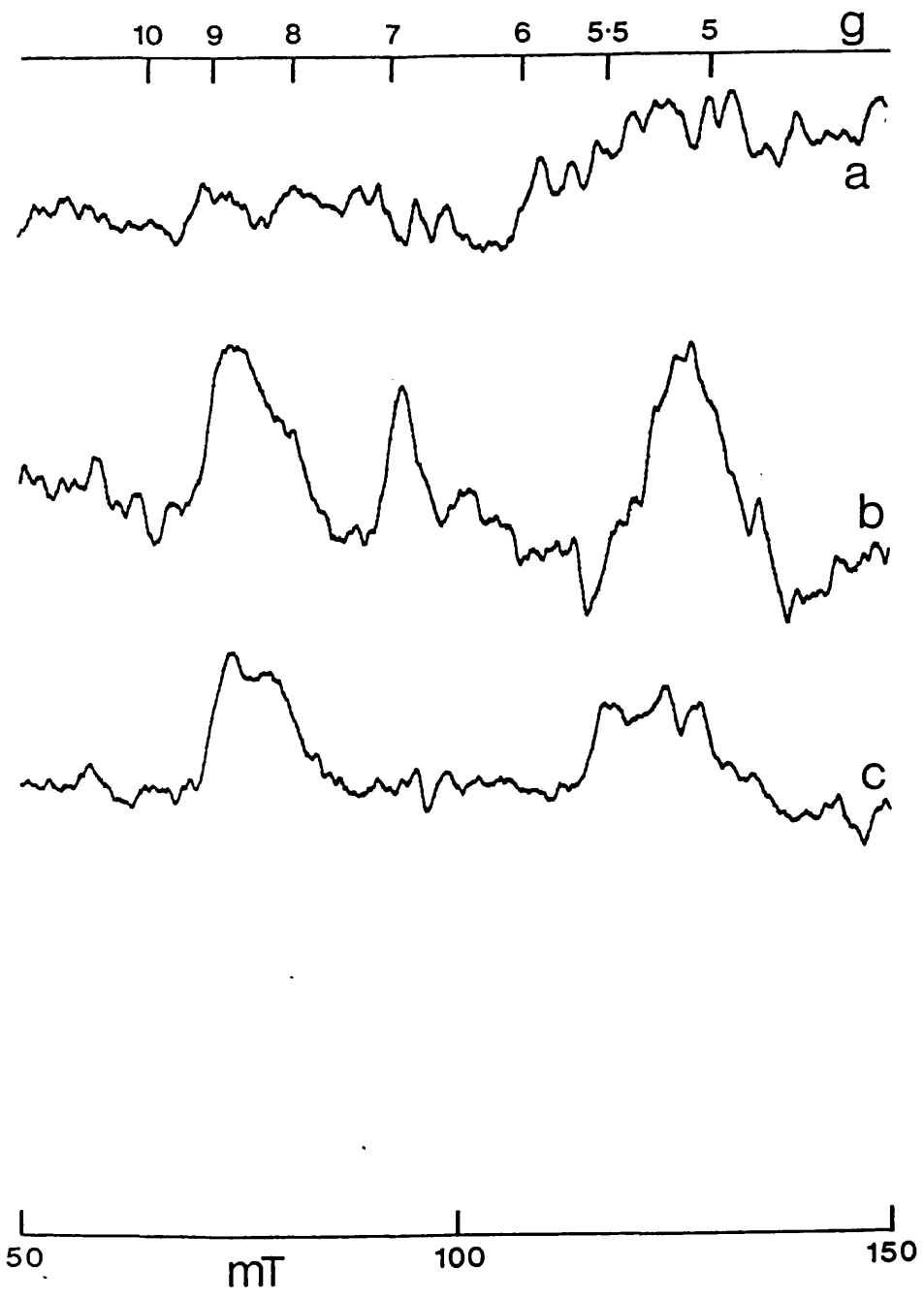

Figure 3.25 Oxidation of non-heme Fe^{2+} by PPBQ in samples illuminated at 293K

Epr spectra of the g=6 non-heme iron region of the spectrum following room temperature illumination and dark relaxation. Chlorophyll concentration: $2mg.ml^{-1}$. (a) 77K illuminated-minus-dark of relaxed sample, with no additions. (b) difference spectrum showing effect of addition of 625μM PPBQ to a relaxed sample. (c) dark-minus-77K illuminated difference spectrum of the PPBQ-treated sample. Epr conditions: temperature, 4.5K; microwave power, 5mW; modulation width, 1.25mT.

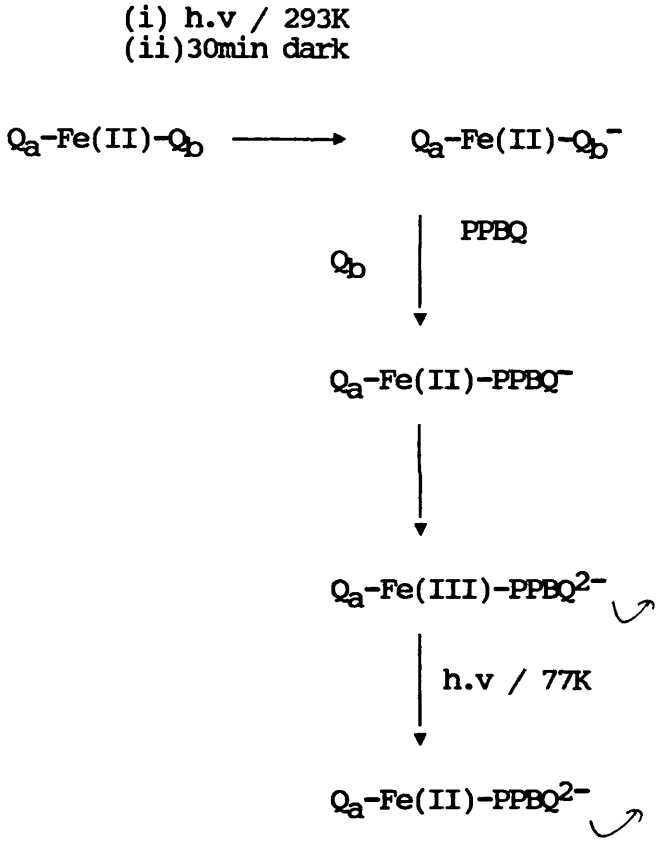

Figure 3.26 Proposed Scheme for Oxidation of Non-Heme Fe^{2+} Following Replacement of Native Q_b-semiquinone by $PPBQ^-$

3.5.8 Detection of an EPR Signal Assigned to an Interaction of Q_b^- with the Non-Heme Iron

In Figure 3.27 are shown changes to the spectra arising from iron-semiquinone components, occurring in parallel with those in the spectra from the non-heme iron. Figure 3.27(a) shows the prominent signal at g = 1.66 obtained after 77K illumination of a 20min relaxed sample. There are no changes in either the g = 1.9 or g = 1.8 regions, suggesting that following low-temperature illumination almost all centres are in the state $Q_a^-Q_b^-$. Therefore, assumimg that at 77K electron transfer from Q_a to Q_b is forbidden, prior to 77K illumination it may be possible to see a signal arising from Q_b^- alone: it is possible to see a weak, broad signal close to g = 1.7, which was removed by incubation with PPBQ. The spectrum shown in Figure 3.27(b) is the difference between the 20min-relaxed sample and the dark, PPBQ-treated sample. This broad signal is different from the signal at g = 1.9 previously ascribed to Q_b^--Fe^{2+} [131]. Finally, 77K illumination of the sample treated with PPBQ does not give rise to changes in the epr spectrum in the iron-semiquinone region, consistent with a removal of Q_b^- and presence of Fe^{3+} as the electron acceptor, Figure 3.27(c).

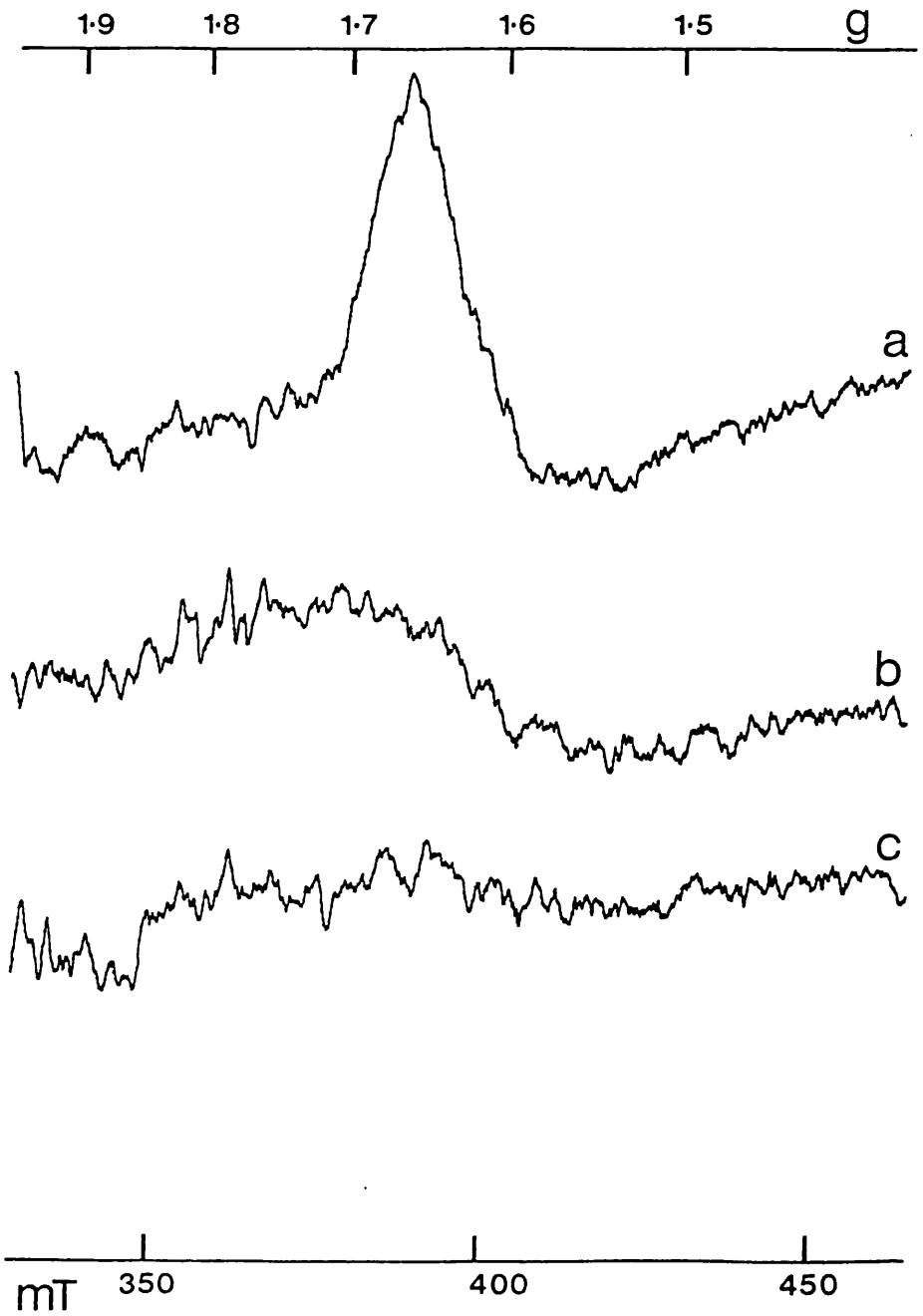

Figure 3.27 EPR signal proposed to arise from the state Q_b^--Fe^{2+} in P. laminosum PS II

Spectra arising from iron-semiquinone components occurring in parallel with those in Fig. 3.25. (a) 77K illumination-minus-dark difference spectrum of a relaxed sample. (b) difference spectrum showing the effect of addition of 625μM PPBQ to a relaxed sample. (c) dark-minus-77K illuminated difference spectrum of the PPBQ-treated sample. Chlorophyll concentration: 2mg.ml^{-1}. Epr conditions: temperature, 5K; microwave power, 10mW; modulation width, 1.25mT.

3.5.9 Discussion of Results from Section 3.5

Titration of the g = 1.66 signal in native samples shows a component which in reducing titrations rises with E_{m8} of ≈+60mV. Accepting the earlier proposal that this signal mirrors the presence of Q_b^- at its site, this figure would represent the first direct determination of a value for the redox couple Q_b/Q_b^- in PS II. An assumption made is that the paramagnetic species, Q_b-semiquinone, will have a greater effect on the spectrum of Fe^{2+}-Q_a^- than the uncharged quinone and quinol forms. In the purple bacterial reaction centre, the effect of this interaction between Q_b-semiquinone and Fe^{2+}-Q_a^- is to attenuate both signals [130]. However, it is proposed here that this state in PSII, if induced at low temperatures, also has a substantially altered epr spectrum, but in a way different from the purple bacteria. There is no reason to suppose that this interaction should be identical in the two analogous systems: since (1) no g = 1.9 signal is observed in the purple bacterial systems concerned and (2) no Fe^{2+}-Q_b^- interaction giving a purple bacterial type g = 1.8 signal has been observed in PSII, it may be that a different balance of interactions can occur.

The pattern of the redox titration curve of the g = 1.66 signal compared with that of the g = 1.9 signal supports this assignment, for the following reason. It is important that the g = 1.66 signal cannot ordinarily be generated at potentials in the region of +350mV: if it is assumed either that the g = 1.66 signal is dependent on an involvement of the fully-oxidised Q_b-quinone, or that it is independent of Q_b altogether, and also that there is a donor functional at 77K, the g = 1.66 signal would be induced at this potential following 77K-photoreduction of Q_a. However, provided dark-adaption has been thorough enough, the g = 1.66 signal is not generated at these potentials. Therefore, a situation is

envisaged at these higher potentials where Q_b is either bound in its fully-oxidised quinone form or not bound at all, and where photoreduction of Q_a at 77K does not give rise to the g = 1.66 signal. Progressive reduction of Q_b to Q_b-semiquinone is then reflected by generation of the g = 1.66 signal after low-temperature illumination.

It is important to show that the rise of the g = 1.66 signal did not merely reflect reduction of a donor component: this is especially important, given the reduction of D^+ (or, at least, a fraction of the D^+ population) with $E_{m7.8}$ of ≈ +75mV. The experiments in which pre-illumination at room temperature, followed by 77K or 200K illumination, favoured formation of the g = 1.66 signal, revealed no limiting dependence on the presence of reduced D. Similarly, the midpoint potential of 'low-potential' cytochrome b559 has been given as + 70-80mV [165]. The samples used in these experiments did not appear to contain a low-potential cytochrome component: the g_z-values of dark-oxidised and (200K) photooxidised cytochrome, at 3.08 and 3.05, are typical of high-potential cytochrome; further, in these samples, poised at +350mV, there was no apparent feature at g ≈ 2.9, suggestive of the low-potential form. It is proposed that, in the potential range used, there are sufficient electron donors: further experiments to quantify donation and would be useful.

The loss of ability to generate the signal with E_{m8} of -10mV, can be explained in one of two ways. (1) as Q_a is chemically reduced, which can be seen by measuring the rise of the g = 1.9 signal in the dark, further photoreduction is not possible. Because the g = 1.66 signal can only be generated by low temperature photoreduction it is not seen. (2) Double reduction of Q_b might also be expected to lead to a loss of the signal. It is reasonable

to suppose that the midpoint potential of the Q_a/Q_a^- couple should be more negative than those of both the Q_b/Q_b^- and Q_b^-/Q_b^{2-} couples, and consequently Q_a should be reduced after the second reduction of Q_b. However, the closeness of the redox potentials means that in titrations there will be substantial mixing of populations. Support for this would come from an observation of the loss of the signal separate from the rise in the dark g = 1.9 signal, but the present results do not allow us completely to distinguish the two. The pH titrations described perhaps indicate the involvement of the second reduction of Q_b, but as already described, the interpretation is of the result is difficult.

In calculating these midpoint values of +63mV and -10mV, another assumption made is that the maximum signal size seen in the experiment is also the true maximum. If this is not so, then the true values will differ from those measured: the value +60mV would be changed to a less positive value. This does not affect the interpretation of the results, though, which depends more on the relative behaviour of the different redox curves than on the absolute values.

The time-dependence of the g=1.66 in samples poised at +350mV on pre-illumination at room temperature, followed by the illumination at 77K is clearly inconsistent with its being due solely to Q_a. Illumination of a dark-adapted sample at 77K does not by itself lead to maximum formation of the signal: under these conditions it is assumed that Q_a will be fully oxidised; or, at least, there should be more oxidised Q_a in the dark-adapted sample than in a sample illuminated 1min before freezing. But the signal is only 15% the size of the same signal generated after the sample has been pre-illuminated at room temperature and allowed to relax in the dark. The explanation for this observation is that

saturating illumination at room temperature will tend to reduce the acceptor side: Q_a^- can be trapped in the g = 1.9 form by freezing under illumination. Accordingly, no g = 1.66 is generated when these samples are further illuminated at 77K. However, after 1min relaxation in the dark, a large yield the g = 1.66 signal can be induced. It is proposed that: as well as (i) an oxidised Qa and (ii) an illumination temperature that allows only single-electron transfer to Q_a, both of which are consistent with the interpretation given in [120] there is a need for (iii) Q_b-semiquinone to be bound at its site.

The electronic state giving rise to the g = 1.82 signal in purple bacteria has been modelled in some detail [109], and attributed to a coupling between the $\underline{S}$=2 state of the Fe^{2+} and the $\underline{S}$=1/2 state of the plastoquinone radical, and an expression for the observed g-value given as:

$$g = g_Q.[1 - 2(J/\Delta E_{1,2})^2]$$

where g is the observed g-value of the coupled system (≈1.82); g_Q is the g-value of the isolated semiquinone (≈2.0); J is the exchange coupling between the iron and the semiquinone (having units of energy); and $\Delta E_{1,2}$ the difference in energy between the two lowest M_S states in the $\underline{S}$=2 manifold of Fe^{2+}. Qualitatively, the equation predicts a deviation in the observed g-values depending on the strength of the exchange coupling, J, or the energy separation, $\Delta E_{1,2}$: the g-value of the 1.6 signal could therefore arise through an increase in J or a decrease in $\Delta E_{1,2}$. More detailed analysis, by Butler et al. [109], suggested that the increase in J would account for the g-value and lineshape changes of the g=1.6 compared with the g=1.8.

From the results presented in this thesis, it has been argued that the g = 1.66 signal (and also the g = 1.67 signal) arise from a system involving two $\underline{S} = \frac{1}{2}$ species, i.e. the two plastosemiquinones of PS II, together with the non-heme iron. Detailed suggestions as to the quantum mechanical origins of this signal are beyond the scope of this work: however, it is suggested that the signal arises through an electrostatic or magnetic interaction of one semiquinone on the semiquinone-iron interaction of the other. If there were substantial mixing of the two semiquinone systems, . electron pairing might demand an $\underline{S} = 0$ system, giving rise (as in purple bacteria) to no epr signal.

The g=1.66 and g=1.67 epr signals, from native and TBIQ-treated P. laminosum PS II, and, to a lesser extent, the broader signal in this region of the epr spectrum detected in TBIQ-treated PS II from higher plants, have sufficiently similar properties (g-value, lineshape, conditions of generation) for them to be assigned to similar states: that is, Q_a^--Fe^{2+}-[Q_b^-] or Q_a^--Fe^{2+}-[$TBIQ^-$].

This assignment of the g = 1.67 signal in P laminosum PS II rests on the following assumptions: (i) that TBIQ in fact binds to the Q_b-site in the form of semiquinone and (ii) that the evidence from previously described experiments is sufficient to show the involvement of Q_b^-. It can easily be argued, if (i) is not true, that the effect of TBIQ is, for example, to bind to PS II in such a way as to affect the epr spectrum (i.e. g = 1.66 ——> g=1.67) that comes from the photoreduction of Q_a at low temperature. This result would then be consistent with the interpretation of McDermott, et.al. described before [120].

However, the evidence put forward in this thesis shows that Q_a alone cannot give rise to this signal. In this case, the result from this experiment is further evidence that TBIQ binds as a

semiquinone at the Q_b-site.

The observation of a broad epr signal in the g = 1.6 region from higher plant PS II may be significant. It is assumed, for this discussion, that the broad signal seen at g = 1.6 in the TBIQ-treated spinach PS II is analogous to the sharper signals seen in native and TBIQ-treated cyanobacterial PS II. This assumption rests on the similarity between the g-values of the peaks observed in the various systems, and on the similar means used to generate the signal (77K illumination). Further experiments could be done to support this idea, for example, power saturation and temperature dependence measurements, and redox titrations.

It was proposed in the work of McDermott et al, that the reason for the lack of a g = 1.6 signal in higher plant PS II was due to the differences in the carboxy-ligation to the iron, and that the binding of formate in cyanobacterial PS II, causing the loss of the g = 1.6 signal, therefore mimicked the normal ligation at the higher plant non-heme iron centre. If it is assumed that the binding of TBIQ does not disturb the ligands to the non-heme iron, the result shown here is not consistent with this view, which ignored the possibility that Qb is involved. However, the g = 1.6 signal from spinach is less sharp than the corresponding signal in P. laminosum, indicating some difference, perhaps in the iron ligation, but the overriding difference is probably that Q_b is not preserved in the preparation of PS II from spinach.

The effect of TBIQ on the epr spectrum from cytochrome b559 was to increase the observed size of the g_z-peak. Since it has been proposed that TBIQ binds as a semiquinone, it may be that TBIQ-quinone can oxidise ferricytochrome b559. However, TBIQ has an effect also on the spectrum seen from D^+, and it can also be suggested that this effect reflected a reduction of D^+ by, for

example, the quinol form of TBTQ· Experiments will be necessary to determine the redox properties of this quinone, in order to establish what fractions of each component are present, and whether these suggestions are tenable. The changes might equally occur through magnetic interaction: this may be indicated by a change in the g_z-value of the high-potential cytochrome.

The epr spectrum from Fe^{3+} (electron configuration: $3d^5$) in the g = 6 region has been explained in terms of a spin Hamiltonian for the high spin state ($\underline{S}$ = 5/2; spin substates, M_S = ±1/2, ±3/2, ±5/2) [169]. The epr for $\underline{S}$ = 5/2 is extremely sensitive to small deviations from octahedral symmetry, characterised by a quotient E/D, where D is the zero field splitting parameter (which is a measure of the differences in energy between the spin substates at zero field) and relates to 'axial' distortions, and E a measure of 'rhombic' distortions, from octahedral symmetry. Appropriate selection of axes (for terms g_x, g_y and g_z) is made to restrict E/D to values between 0 and 0.33. The term features in the Hamiltonian, and predicts variations in g_x, g_y and g_z, within each spin substate, for variations in symmetry.

The Fe^{3+} spectrum from spinach PS II oxidised with ferricyanide showed peaks at 8.15 and 5.64 which were accounted for by Petrouleas and Diner [169] as arising from the M_S = ±1/2 and M_S = ±3/2 doublets, with an E/D of 0.11. Following this assignment, for the spectrum of the oxidised non-heme in P. laminosum the peaks at g = 8.7 and 5.1 may arise from the analogous doublets in the cyanobacterial system, with a more rhombic, i.e. greater than 0.11, value of E/D. Alternatively, the g = 5.1 and g = 6.9, predicted to arise from the M_S = ±1/2 Kramer's doublet with more axial values of E/D, could be assigned, but there would then be a problem in assigning the g = 8.7.

Therefore using the model of [169], it is not possible to fit all three peaks with the assumption of a homogeneous population of centres. Given the similarity in behaviour of the g = 8.7 and g = 5.1 peaks following 77K illumination (i.e. the Fe(III) from which they arise is photoreduced), contrasting with the behaviour of the g = 6.9 peak (which does not decrease in amplitude following 77K illumination), it seems more likely that the g = 8.7 and g = 5.1 arise from centres in one state, and the g = 6.9 from centres in a different one. However, this assignment would have to be confirmed by further quantification.

It has been argued by Petrouleas and Diner that the g = 6.9 signal arises from centres where Q_D is bound. In this case, there is the following suggestion: illumination at 77K causes the loss of the peaks at g = 8.7 and g = 5.1, by photoreduction of Fe_{3+}; it does not, however, also cause the attenuation of the peak at g = 6.9 where the electron is preferentially transferred to another acceptor, or, perhaps, stable electron acceptance cannot occur. It is not at all clear what this acceptor might be, unless double reduction of PPBQ (by oxidation of Fe^{2+}), is followed by replacement at the Q_D-site with fresh quinone.

4. An EXAFS Study of the Manganese Oxygen-Evolving Complex of Photosystem II

4.1 EXAFS Results

EXAFS measurements were made at the manganese K-edge for particles of PS II poised in the S_1 state. The EXAFS measurements were performed at the Synchrotron Radiation Source (SRS) at the SERC Daresbury Laboratory, using station 8.1 with a slitless monochromator and a 13-element solid-state germanium detector. The energy resolution of this type of detector is of the order of 350eV, compared with 500eV of conventional scintillation fluorescence detectors, which enables better resolution of fluorescence and scattered signals, resulting in an improved signal-to-noise in the experimental data. In general, in EXAFS experiments, it is a specific fluorescence, due to the decay of an electron to the inner K-shell from a higher shell, that gives a specific wavelength, and the detector is 'tuned' to this wavelength. In particular, the resolution of the detector should allow one to distinguish between the fluorescent signal of Mn and the adjacent fluorescent signal from Cr (arising from a filter covering the detector) and scattered X-rays. If the resolving power of the detector is too low, there will be contributions from both these sources of error; but the germanium detector used in these studies was able to distinguish the fluorescent signals of Mn and Cr and scattered signals.

The sample was measured at 77K with a beam energy of 2GeV and an average beam current of 180mA. Eight scans were recorded. Figure 4.1(a) shows the X-ray absorption spectrum as measured by averaging data from eight scans from four detector elements. The data from each detector element were examined separately for anomalies and weighted by the edge height before further averaging to give the final absorption spectrum, shown in Figure 4.1(b).

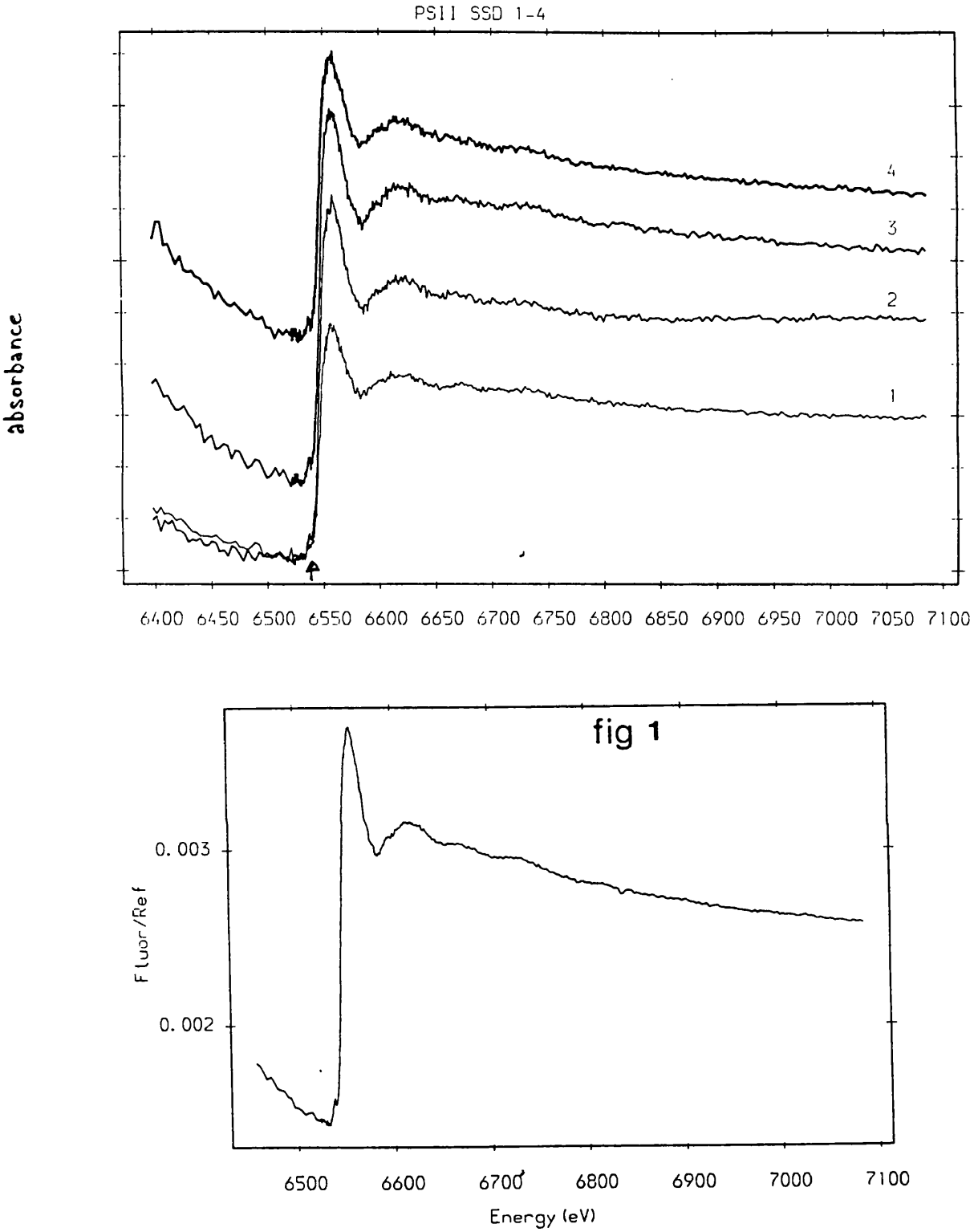

Figure 4.1 X-ray absorption spectrum from spinach PS II particles

(a) shows the data from four of the thirteen detector elements used to measure EXAFS. Each spectrum shown is the average of eight scans. (b) shows the final weighted-average absorption spectrum from all thirteen detectors, prior to background subtraction.

The averaged spectrum was normalised to a unit metal atom and the EXAFS was extracted by removal of the background absorption. The EXAFS was weighted by k^2 and analysed using the non-linear least-squares minimisation program EXCURV88 [170], which calculates the theoretical EXAFS using the fast curved wave approach [171]. The phaseshifts were calculated by *ab initio* methods.

The EXAFS and Fourier transforms of the raw experimental data and the theory are shown in Figure 4.2. The Table 4.1 summarises the atomic types, shell occupancies and distances. The best fit parameters are as follows: two oxygen or nitrogen ligands (O, N) at 1.79Å; two (O, N) at 1.96Å and one Mn at 2.7Å. These results are all in broad agreement with the results of Yachandra, et al, [76]. In addition to these shells of scatterers, the best fit to this experimental data also requires a single (O, N) at 2.15Å.

A fitting procedure was adopted whereby the coordination numbers were varied systematically, while the Debye-Waller factors were refined to obtain the best simulation to the data. The coordination numbers and Debye-Waller factors were also refined together, using different initial values for these parameters. From these calculations the estimated errors associated with the coordination numbers (i.e. the numbers of a particular atom around the average Mn) are: ± 20% for the short Mn-(O,N) shell; ± (30-50)% for the longer Mn-(O,N) shells; and ± 20% for the Mn shell. The estimated error for the shell radii is ± 0.03Å, and for the Debye-Waller factors is ±(30-50)%. The Debye-Waller factor is related to the root-mean-square fluctuation in the position of the scatterer: this last error therefore represents an error in the estimated variation of a particular shell radius.

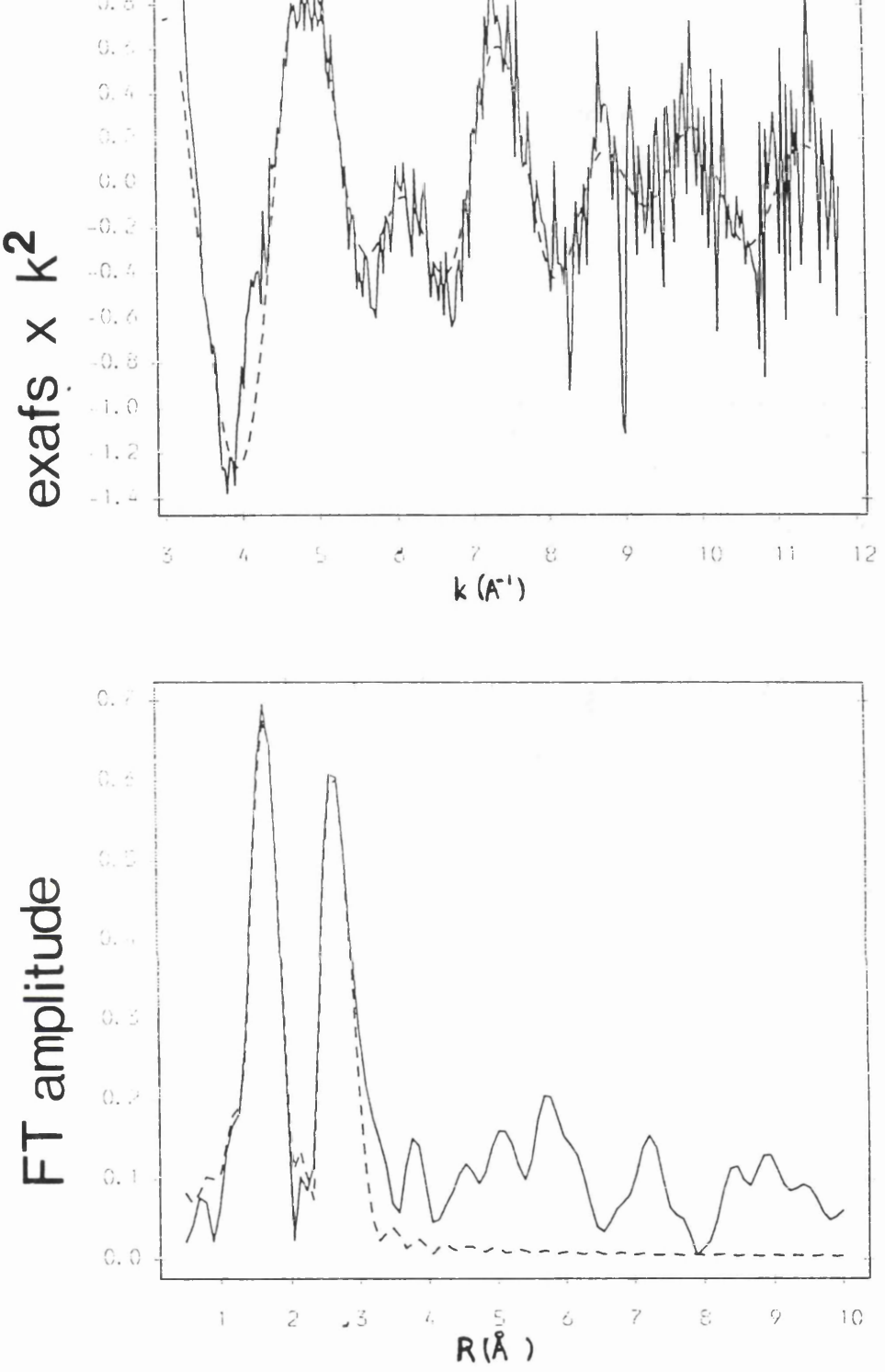

Figure 4.2 Theoretical and experimental EXAFS and Fourier transforms from PS II

(a) shows the experimental (solid line) and best-fit theoretical (broken line) EXAFS, weighted by k^2, for the range k=3-12Å^{-1}. The theoretical EXAFS are back-calculated using the parameters shown in Table 4.1. (b) Fourier transform of experimental (solid line) and theoretical (dotted line) EXAFS. The figure shows a good fit of the theoretical curve to the two peaks of the experiment.

Atom Type[a]	R(Å)	$2\sigma^2(Å^2)$
2O	1.79	0.006
2O	1.96	0.010
1O	2.15	0.013
1Mn	2.70	0.008

Table 4.1 'Best-Fit' Parameters for Modelling the Experimental EXAFS

4.2 Modelling

The deduction of possible structures from the data in Table 4.1 proceeds as follows. It is necessary to remember that the data is averaged to a *single* manganese centre, and manganese was estimated at 5 per reaction centre. Given the potential error (not quantified) in the determination of the amount of manganese in the sample, for the remainder of this discussion it will be assumed there are four manganese (labelled a-d) in the oxygen-evolving complex. For a simple di-μ-oxo bridged Mn(III)-Mn(III) pair, the arrangement of atoms and inter-atomic distances is:

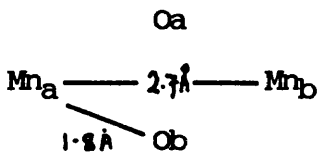

The local environment of Mn_a contains one manganese at 2.7Å and two oxygens at ≈1.8Å; and, by symmetry, the environment of Mn_b is identical. In total, there are <u>two</u> Mn-Mn distances affecting the EXAFS (Mn_a ----> Mn_b and Mn_b ----> Mn_a) and <u>four</u> Mn-O distances (Mna ----> Oa, Ob; Mnb ----> Oa, Ob). When averaged to a single manganese (by dividing by the number of manganese in the complex) the data gives one Mn at 2.7Å and two O at 1.8Å per Mn centre.

<u>Manganese - Manganese</u>

The results in Table 4.1 give a best-fit with one Mn per Mn at 2.7Å, although the shell occupancy has an error of ±50%. Using the assumption that the OEC contains four manganese atoms, this result is consistent with the following two structures:

(1) Mn_a------Mn_b

Mn_c------Mn_d

(2) Mn_a------Mn_b------Mn_c Mn_d

In these representations, manganese connected by dotted lines indicate those that are contributing to the EXAFS, whereas those unconnected do not. Two reasons for the 'invisibility' of certain Mn are: firstly, the scatterer is too distant from the absorber, in which case scattering by intervening atoms attenuates the contribution the more distant centre makes (this can apply to centres that are contained within the same continuous complex, or to unconnected atoms); secondly, in the case of unconnected atoms, the thermal and static disorder of structures decreases the signal-to-noise from these centres. Therefore, although from these results, and the assumptions made, it can be inferred that a longer Mn-Mn distance must exist, there is no suggestion what the value of this is.

It should be emphasised that these structures do not necessarily represent, respectively, a pair of binuclear Mn centres or a trimer-plus-monomer arrangement: both are consistent with distorted tetrahedral complexes, provided that the occupancy of one Mn per Mn is maintained.

The error in the value of 1 Mn per Mn of ±50% allows the possibility of other structures. For the extreme cases, the following structures are allowed:

(3) 0.5 Mn per Mn:

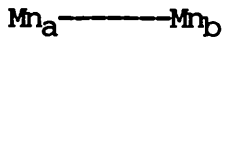

(4) 1.5 Mn per Mn:

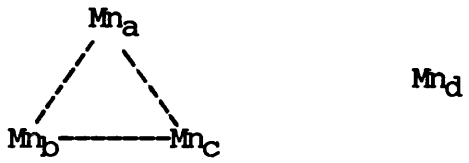

or, 

The short, 2.7Å distance between the manganese centres is typical of more than one bridging ligand connecting the two Mn atoms involved. A bridging ligand can be either monodentate, in which only one atom ligates to two (or more) different metal atoms: examples of this include oxo, hydroxo, water, alkyl- or aryloxides (e.g., serine or tyrosine); or bidentate, where two atoms form the bridge (e.g., carboxylato- or peroxido- bridges). The Mn-Mn separation alone cannot uniquely imply the type of bridging involved: although it has been taken as evidence for di-μ-oxo bridging, the possibility of tri-μ-oxo bridges or di-μ-OH bridges are also permissible.

Manganese - Oxygen (1.79Å)

The best-fit to the data requires a shell of low-Z scatterers at 1.79Å, with an occupancy of 2 ± 0.4. EXAFS spectra cannot distinguish between oxygen and nitrogen ligands, although there is evidence that few, if any, nitrogens bind to the Mn cluster [172], and it will be assumed in this discussion that these ligands are

oxygen ligands.

The distance of 1.79Å is indicative of μ-oxo-bridged Mn(III) or Mn(IV) centres. These could be included into structures (1) and (2) in the following way:

(1) two dimers:

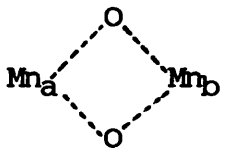

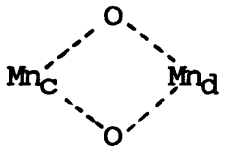

(2) trimer + monomer:

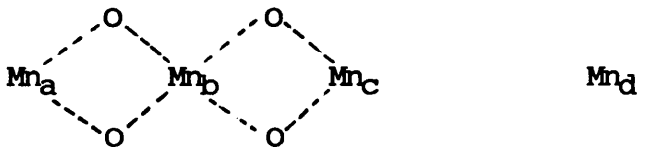

There is an error in the occupancy of this shell of ±40%. Assuming that the total number of μ-oxo bridges is some multiple of four that gives an even value, it is also possible to rule out the occupancies 1.75 and 2.25 O per Mn, also within the error range, which would give a total of 7 or 9 μ-oxo-bridges respectively.

Manganese - Oxygen (1.96Å and 2.15Å)

The longer manganese-oxygen distances, at 1.96Å and 2.15Å, are typical of non-bridging ligands, also called 'terminal' ligands: the shorter distance can be interpreted either as Mn(III)-O or Mn(IV)-O, whilst the more distant shell is only suggestive of

Mn(III)-O. In general, the higher the oxidation state of the metal atom, the shorter the metal-ligand distance, owing to increased electrostatic attraction by the metal.

The results in Table 4.1 indicate a total of 8 (= 4 x 2) terminal ligands at 1.96Å and a further 4 (= 4 x 1) at 2.15Å, giving a total of 12. Complexes of Mn(III) principally have octahedral geometry (i.e., six ligands), although a less important class of square pyramidal (five ligands) is also known; Mn(IV) complexes have octahedral geometry [173]. If it is assumed the metals all have octahedral geometry, and assuming either of the best-fit structures consistent with the arrangement of bridging oxygens, it is probable that there is a total of 16 possible coordination positions to be filled by terminal ligands. Clearly, the best-fit to our data either underestimates this number (which may happen if the complex is substantially distorted) or not all coordination positions are occupied. However, the figure of 16 terminal ligands lies within our error range: obviously, there are numerous ways in which 12 ligands can be arranged into 16 vacant sites.

4.3 Discussion of EXAFS results

As a result of using the solid state detector, with higher resolution, the definition of the EXAFS modulations and the signal-to-noise of the absorption spectrum itself, shown in Fig. 4.2. Although the estimated error for some of the shell occupancies is high, the values obtained for the shell radii are more certain and confirm the presence of short O or N ligands. This, together with the Mn-Mn distance of 2.7Å is consistent with a binuclear Mn-Mn site, as has been previously suggested on the basis of EXAFS studies, or with a linear trinuclear centre, proposed on the basis of EPR studies. The earlier EXAFS measurements found no evidence

for a shell of species of low atomic number at 2.15Å. This may be due to the lesser resolution of the earlier EXAFS measurements, since a subsequent study by the same group, analysing the Mn-complex from PS II from the thermophilic cyanobacterium Synechococcus [120], found evidence for a shell of (O, N) at this distance; but, conversely, in that study there was no report made of the shell at ≈2.0Å. In the later study on Synechococcus, a single-element Ge detector was used, again with a higher resolution than earlier, conventional detectors.

The principal discrepancy over EXAFS measurements in the literature is the absence, in the data of Penner-Hahn and coworkers, of evidence for a shell of low-Z scatterers at 1.75Å. The experimental EXAFS shown in Figure 4.1, as judged by inspection, is in agreement in the energy range corresponding to $k = 3\text{-}8Å^{-1}$ with the data published by Penner-Hahn in [68]. However, the EXAFS modulations in the range k = 8-11Å do not agree.

The difference between these results and those of Penner-Hahn et al may simply reflect the type of preparation used. These experiments were carried out with preparations similar to those used by Yachandra, et al, [76], that is a membrane particle enriched in PS II, but containing a number of polypeptides over and above the minimum required for oxygen evolution. On the other hand, Penner-Hahn's group used a more highly-purified oxygen-evolving 'core' complex, with a chlorophyll:P680 ratio of approximately 50:1, compared with the less purified PS II-enriched membrane sample which has a chlorophyll:P680 ratio of ≈350:1. The preparation of the core complex involves extensive detergent treatment, and it can be envisaged that an alteration of the lipid-protein and detergent-protein interactions that this would entail may affect the environment of the manganese. Nevertheless, both particles are

oxygen-evolving, and therefore both must contain the manganese complex preserved in a functional form. It is reasonable to assume that the range of variations in the structure of the manganese complex that is consistent with the preservation of function is quite narrow; furthermore, the question mark over the short μ-oxo bridges is an important one, since these would maintain the manganese atoms in a firm position, which would be expected, if the assumption of a specific structural were correct.

Klein's group has reassessed the bond length for the short Mn-(low Z) shell in S1, decreasing the quoted value of 1.8Å in earlier reports to a shorter 1.77Å in later results [78]. However, thse values are all within a range consistent with an Mn(III)-O bridge, and they are all still consistent with an Mn-Mn distance of 2.7Å:

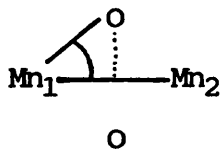

since, by fixing the Mn-Mn separation at 2.7Å, differences in the Mn-O lengths are possible by distortion of the angles away from exact octahedral geometry.

It has recently come to light that the data given in [68] and [69] suffered from contamination with Mn^{2+}: in the first case, from a tape used to secure the sample in the X-ray beam, and in the second, 50% of the manganese in the sample was hexaquo-manganese. This will affect the EXAFS results drastically.

A criticism that can be levelled against the consistency of the data included in this thesis is the relative populations of the S-states in our sample. The context of the experiment was such that these studies were undertaken as a preliminary investigation, with the chief aim of assessing the ability of the 13-element solid-

state germanium detector to provide EXAFS data of sufficient quality at the low concentrations of manganese that could be obtained in these kinds of preparation. The samples were prepared under room light in aluminium sample holders, prior to being wrapped in foil and frozen to liquid nitrogen temperatures. At the concentrations of chlorophyll used in these experiments it seems quite likely that light of such relatively low intensity would not penetrate to the centres much below the surface of the sample, and no turnover of the bulk of centres would occur. However, in the same fashion, the bulk of the measurement will be made on those centres nearest the surface, since the intensity of the X-ray beam will also be attenuated by the sample, through absorption and scattering processes.

5. SUMMARY

The following list summarises the main results from this work:

1) The Q_a^--Fe^{2+} of photosystem II from P.laminosum can give rise to the g=1.9 epr signal, previously identified in higher plant PS II. As in higher plant PS II, the signal converts to the g=1.8 form in the presence of formate. 77K-illumination of P. laminosum PS II can give a third epr signal arising from Q_a^--Fe^{2+}, at g=1.66, shown to reflect the presence of Q_b^-.

2) The midpoint potential ($E_{m7.8}$) of the Q_a/Q_a^- couple in P. laminosum, measured by titration of the g=1.9, g=1.8 and the split signal, was found to be ≈ +25mV. There were no low potential steps in the titrations of the g=1.9 or g=1.8 signals; but the titration of the split signal possibly reflected a low potential acceptor that was not a quinone.

3) A fraction ($\approx$ 60%) of the population of D titrates with $E_{m7.8}$ of ≈ +75mV.

4) The reduction of the component (Q_b) giving rise to the g=1.66 epr signal titrates with $E_{m7.8}$ of ≈ +60mV. Further reduction prevents 77K-photoinduction of the g=1.66 signal, perhaps reflecting double-reduction of Q_b.

5) The g=1.66 epr signal can be 77K-photoinduced in P. laminosum PS II following 293K-illumination and a short period of darkness. This result is inconsistent with the signal arising solely from a low-temperature form of Q_a^-. It is suggested that this protocol generates the state Q_a-$Fe2^+$-Q_b^-. Prior to 77K-illumination, a broad

signal at g≈1.6 can be seen, which is assigned to Q_B^-. The non-heme iron can be oxidised by replacement of the Q_B^-, generated in this way, by PPBQ.

6) An epr signal at g=1.67 can be 77K-photoinduced in P. laminosum PS II treated with TBTQ. A similar signal can also be detected in spinach PS II treated with this reagent.

7) Manganese EXAFS of PS II from spinach suggested that the oxygen-evolving complex contained either a pair of μ-oxo-bridged manganese dimers, or a μ-oxo-bridged trimer plus monomer.

APPENDIX A Derivation of Formulae for Chlorophyll Concentration

In reference [135] the following expressions are given, where A(663) and A(645) are absorbances at 663 and 645nm; and C_a and C_b are concentrations of Chls a and b, given in $mg.ml^{-1}$:

$$A(663) = [82.04 \times C_a] + [9.27 \times C_b] \quad (1)$$

$$A(645) = [16.75 \times C_a] + [45.6 \times C_b] \quad (2)$$

The extinction coefficients, in units of $cm^{-1}.g^{-1}.l$, are from McKinnen, G. (1941) J.Biol.Chem., 140, 315-322. (1) and (2) are treated as simultaneous equations from which the formulae for C_a and C_b are derived, as follows. Multiply equation (1) by (45.6 ÷ 9.27):

$$[4.919 \times A(663)] = [403.6 \times C_a] + [45.6 \times C_b] \quad (3)$$

Subtract (2) from (3):

$$[4.919 \times A(663)] - A(645) = (403.6 - 16.75) \times C_a \quad (4)$$

Given that (403.6 - 16.75) = 386.85, rearranging (4) gives:

$$C_a = [(4.919 \times A(663) \div 386.85] - [A(645) \div 386.85]$$
$$= [\ 0.0127 \times A(663)\ ] - [\ 0.00258 \times A(645)\ ]$$

as given in Materials and Methods.

The procedure is similar to obtain a formula in terms of C_b, beginning by multiplying expression (2) by (82.04 ÷ 16.75).

This derivation is included with this thesis, because there is a difference in the formulae when derived from the extinction

coefficients (as shown) and as cited on p. 63 of a standard text 'Photosynthesis Energy Transduction: a Practical Approach' (eds. Hipkins, M.F and Baker, N.R., 1988, IRL Press Limited). In that text, the formula for C_a is given as:

$$C_a = [\ 0.0127 \times A(663)\ ] - [\ 0.00269 \times A(645)\ ]$$

The difference in the second term of the right-hand side is not accounted for by errors in rounding-up or rounding-down through the various divisions that are done.

REFERENCES

[1] Anderson, J.M. and Andersson, B. (1982) TIBS, 6, 288-292

[2] Marder, J.B. and Barber, J. (1989) Plant Cell and Environment, 12, 595-614

[3] Hill, R. (1966) in Essays in Biochemistry, 121-151

[4] Arnon, D.I. (1971) Proc.Nat.Acad.Sci.USA, 68, 2883-2892

[5] Warburg, O. and Negelein, E. (1922) Z.phys.Chem., 102, 235-266

[6] van Neil, C.B. (1931) Arch.Mikrobiol.Z., 3, 1

[7] van Neil, C.B. (1941) Advan.Enzymol., 1, 263

[8] Hill, R. and Scarisbrick, R. (1940) Nature, 146, 61-62

[9] Ruben, S., Randall, M., Kamen, M., and Hyde, J.L. (1941) J.Amer.Chem.Soc., 63, 877-879

[10] Stemler, A. and Radner, R. (1975) Science, 190, 457-458

[11] Hill, R. and Scarisbrick, R. (1951) New Phytol.,50, 98-111

[12] Hill, R. (1954) Nature, 174, 501-3

[13] Davenport, H.E., Hill, R. and Whatley, F.R. (1952) Proc.Roy.Soc.B, 139, 346-358

[14] Davenport, H.E. (1960) Biochem.J., 77, 471-477

[15] San Pietro, A. and Lang, H.M. (1958) J.Biol.Chem., 231, 211-229

[16] Tagawa, K. and Arnon, D.I. (1962) Nature, 195, 537-543

[17] Frenkel, A. (1954) J.Amer.Chem.Soc., 76, 5568-5569

[18] Arnon, D.I., Whatley, F.R. and Allen, M.B. (1954) J.Amer.Chem.Soc., 76, 6324-6325

[19] Arnon, D.I, Whatley, F.R. and Allen, M.B. (1955) Biochim.Biophys.Acta, 16, 607-608

[20] Bassham, J.A. and Calvin, M. (1957) The Path of Carbon in Photosynthesis, Englewood Cliffs, N.J., Prentice-Hall.

[21] Hill, R. and Bendall, F. (1960) Nature, 186, 136-137.

[22] Duysens, L.N.M., Amesz, J. and Kemp, B.M. (1961) Nature, 190, 510-511.

[23] Emerson, R.L., Chalmers, R.V. and Cederstrand, C. (1957) Proc.Natl.Acad.Sci.USA, 43, 133-143.

[24] Myers, J. and French, C.S. (1960) J.gen.Physiol., 43, 723-736.

[25] Mitchell, P. (1979) Science, 206, 1148-1159.
[26] Jagendorf, A.T. and Uribe, E. (1966) Proc.Natl.Acad.Sci.USA, 55, 170-177.

[27] Schatz, G.H., Brock, H. and Holzwarth, A.R. (1987) Proc.Natl.Acad.Sci.USA, 84,[8414-8418].

[28] Reed, D.W. and Clayton, R.K. (1968) Biochem.Biophys.Res. Commun. 30, 471-475

[29] Deisenhofer, J., Epp, O., Miki, K., Huber, R. and Michel, H. (1984) J.Mol.Biol, 180, 385-398

[30] Deisenhofer, J., Epp, O., Miki, K., Huber, R. and Michel, H. (1985) Nature, 318, 618-624

[31] Allen, J.P., Feher, G., Yeates, T.O., Rees, D.C., Deisenhofer, J., Michel, H. and Huber, R. (1986) Proc.Nat.Acad.Sci.USA, 83, 8589-8593

[32] Chang, C.-H., Tiede, D., Tang, J., Smith, U., Norris J. and Schiffer, M. (1986) FEBS Lett, 205, 82-86

[33] Feher, G., Allen, J.P., Okamura, M.Y. and Rees, D.C. (1989) Nature, 339, 111-116.

[34] Kühlbrandt, W., (1988) Q.Rev.Biophys., 21, 429-477.

[35] Deisenhofer, J. and Michel, H. (1989) Biophys.J., 55, Abstr.1a.

[36] Debus, R.J., Feher, G. and Okamura, M.Y. (1985) Biochemistry, 24, 2488-2500.

[37] Kirmaier, C. and Holten, D. (1987) Photosynth.Res., 13, 225-260.

[38] Holzapfel, W., Finkele, U., Kaiser, W., Oesterhelt, D., Scheer, H., Stilz, H.U., Zinth, W. (1990) Proc.Nat.Acad.Sci.USA., 87, 5168-5170

[39] Bylina, E.J., Jovine, R. and Youvan, D.C. (1988) in 'The Photosynthetic Bacterial Reaction Centre', eds. Breton, J. and Vermeglio, A., 113-118, Plenum, New York.

[40] Marcus, R.A and Sutin, N. (1985) Biochim.Biophys.Acta, 811, 265-322.

[41] Hansson, Ö. and Wydrzynski, T. (1990) Photosynthesis Res.,23, 131-162.

[42] Masojidek, J., Droppa, M. and Horváth, G. (1987) Eur.J.Biochem., 169, 283-288.

[43] Zurawski, G., Bohnert, H., Whitfield, P.R. and Bottomley, W. (1982) Proc.Natl.Acad.Sci.USA, 79 , 7699-7703.

[44] Hearst, J.E. (1986) in Staehlin, L.A. and Arntzen, C.J. eds., Encyclopedia of Plant Physiology New Series, Vol 19, Photosynthesis III, pp. 382-389, Springer Verlag, Berlin.

[45] Youvan, D.C., Bylina, E.J., Alberti, M., Begusch, H. and Hearst, J.E. (1984) Cell, 37, 949-957.

[46] Williams, J.C., Steiner, L.A., Feher, G. and Simon, M.I. (1984) Proc.Natl.Acad.Sci.USA, 81, 7303-7307

[47] Michel, H. and Deisenhofer, J. (1986) in Staehlin, L.A. and Arntzen, C.J. eds., Encyclopedia of Plant Physiology New Series, Vol 19, Photosynthesis III, pp. 371-381, Springer Verlag, Berlin.

[48] Trebst, A. (1986) Z.Naturforsch., 41, 240-245.

[49] Nanba, O. and Satoh, K, (1987) Proc.Natl.Acad.Sci.USA, 84, 109-112.

[50] Barber, J, Chapman, D.J. and Telfer, A. (1987) FEBS Lett., 220, 67-73.

[51] Millner, P.A., Gogel, G. and Barber, J. (1987) Photosynthesis Res., 13, 185-198.

[52] Rolfe, S.A. and Bendall, D.S. (1989) Biochim.Biophys.Acta, 973, 220-226.

[53] Doring, G., Renger, G., Vater, J. and Witt, H.T. (1969) Z.Naturforsch., 24, 1139-1143

[54] Commoner, B., Heise, J.J. and Townsend, J. (1956) Proc.Natl.Acad.Sci.USA, 42, 710.

[55] Norris, J.R., Uphaus, R.A., Crespi, H.L. and Katz, J.J. (1971) Proc.Natl.Acad.Sci.USA, 68, 625-628.

[56] Plato, M., Lubitz, W., Lendzian, W. and Mobius, K. (1988) Isr.J.Chem., 28, 109-119.

[57] Rutherford, A.W. (1986) Biochim.Biophys.Acta, 807, 189-201.

[58] Joliot, P., Barbieri, G. and Chabaud, R. (1969) Photochem.Photobiol, 10, 309-329.

[59] Kok, B., Forbush, B. and McGloin, M. (1970) Photochem.Photobiol, 11, 457-75.

[60] Yocum, C.F., Yerkes, C.T., Blankenship, R.E., Sharp, P.R. and Babcock, G.T. (1981) Proc.Natl.Acad.Sci.USA, 78, 7507-11.

[61] Dismukes, G.C. and Siderer, Y. (1981) Proc.Natl.Acad.Sci.USA, 78, 274-278.

[62] Casey, J.L. and Sauer, K. (1984) Biochim.Biophys.Acta, 767, 21-28.

[63] Zimmermann, J.-L. and Rutherford, A.W. (1984) Biochim.Biophys.Acta, 767, 160-167.

[64] Zimmermann, J.-L. and Rutherford, A.W. (1986) Biochemistry, 25,

[65] de Paula, J.C., Innes, J.B. and Brudvig, G.W. (1985) Biochemistry, 24, 8114-8120

[66] Ono, T., Zimmermann, J.-L., Inoue, Y. and Rutherford, A.W. (1986) Biochim.Biophys.Acta, 851, 193

[67] Sauer, K. (1988) Chemica Scripta, 28A, 87-91.

[68] Penner-Hahn, J.E., Fronko, R.M., Pecoraro, V.L., Yocum, C.F., Betts, S.D. and Bowlby, N.R. (1990) J.Amer.Chem.Soc., 112, 2549-2557.

[69] George, G.N., Prince, R.C. and Cramer, S.P. (1988) Science, 243, 789-791.

[70] Brudvig, G.W. and Crabtree, R.H. (1986) Proc.Natl.Acad.Sci.USA, 83, 4586-4588.

[71] Christou, G. and Vincent, J.B. (1987) Biochim.Biophys.Acta, 895, 259-274.

[72] de Paula, J.C., Beck, W.F. and Brudvig, G.W. (1986) J.Am.Chem.Soc., 108, 4002-4009.

[73] Dismukes, G.C., Ferris, K. and Watnick, P. (1982) Photobiochem.Photobiophys., 3, 243-256.

[74] Hansson, Ö., Aasa,R and Vänngård, T. (1987) Biophys.J., 51, 825-832.

[75] Yachandra, V.K., Guiles, R.D., McDermott, A.E., Britt, R.D., Dexheimer, S.L., Sauer, K. and Klein, M.P. (1986) Biochim.Biophys.Acta, 850, 324-332.

[76] Yachandra, V.K., Guiles, R.D., McDermott, A.E., Cole, J.L., Britt, R.D., Dexheimer, S.L., Sauer, K. and Klein, M.P. (1987) Biochemistry, 26, 5974-5981.

[77] Cole, J., Yachandra, V.K., McDermott, A.E., Britt,R.D., Dexheimer, S.L., Sauer, K. and Klein, M.P. (1987) Biochim.Biophys.Acta, 890, 395-398.

[78] Guiles, R.D., Zimmermann, J.-L., McDermott, A.E., Yachandra, V.K., Cole, J.L., Dexheimer, S.L., Britt, R.D., Wieghardt, K., Bossek, U., Sauer, K. and Klein, M.P. (1990), 29, 471-485.

[79] Boussac, A., Zimmermann, J.-L., Rutherford, A.W. and Lavergne, J. (1990) Nature, 347, 303-306.

[80] Britt, R.D., Zimmermann, J.-L., Sauer, K. and Klein, M.P (1989) J.Amer.Chem.Soc., 111, 3522-3532.

[81] Beck, W.F., de Paula, J.C. and Brudvig, G.W. (1986) J.Amer.Chem.Soc., 108, 4018-4022.

[82] Hansson, Ö., Andréasson, L.-E. and Vänngård, T. (1986) FEBS Lett., 195, 151-154

[83] Plijter, J.J., Aalbers, S.E., Barends, J.P., Vos, M.H. and van Gorkom, H.J. (1988) Biochim.Biophys.Acta, 935, 299-311.

[84] Blankenship, R.E., Babcock, G.T., Warden, J.T. and Sauer, K. (1975) FEBS Lett., 51, 287-293.

[85] Babcock, G.T. and Sauer, K. (1975) Biochim.Biophys.Acta, 376, 315-328.

[86] Babcock, G.T. and Sauer, K. (1973) Biochim.Biopys.Acta, 325, 483-503.

[87] Styring, S. and Rutherford, A.W. (1987) Biochemistry, 26, 2401-2405.

[88] Kohl, D.H. and Wood, P.M. (1969) Plant Physiol., 44, 1439-1445.

[89] Barry, B.A. and Babcock, G.T. (1987) Proc.Natl.Acad.Sci.USA, 84, 7099-7113.

[90] Debus, R.J., Barry, B.A., Babcock, G.T. and McIntosh, L. (1988) Proc.Natl.Acad.Sci.USA, 85, 427-430.

[91] Vermaas, W.F.J., Rutherford, A.W. and Hansson, Ö. (1988) Proc.Natl.Acad.Sci.USA, 85, 8477-8481.

[92] Debus, R.J., Barry, B.A., Sithole, I., Babcock, G.T. and McIntosh, L. (1988) Biochemistry, 27, 9071-9074.

[93] Styring, S. and Rutherford A.W. (1987) Biochim.Biophys.Acta, 890, 179-194.

[94] Babcock, G.T., Widger, W.R., Cramer, W.A., Oertling, W.A. and Metz, J.G. (1985) Biochemistry, 24, 3638-3645.

[95] Klimov, V.V., Klevanik, A.V., Shuvalov, V.A., and Krasnovsky, A.A. (1977) FEBS Lett., 82, 183-186.

[96] Rademaker, M., Hoff, A.J.and Duysens, L.N.M. (1979) Biochim.Biophys.Acta, 546, 248-255.

[97] Klimov, V.V., Dolan, E. and Ke, B. (1980) FEBS Lett., 112, 97-100.

[98] Tiede, D.M., Prince, R.C. and Dutton, P.L. (1976) Biochim.Biophys.Acta, 449, 447-469.

[99] Wasielewski, M.R., Johnson, D.G., Seibert, M. and Govindjee (1989) Proc.Natl.Acad.Sci.USA., 86, 524-528.

[100] Jankowiak, R., Tang, D., Small, G.J. and Seibert, M. (1989) J.Phys.Chem., 93, 1649-1654.

[101] Eckert, H.-J., Wiese, N., Bernarding, J., Eichler, H.-J. and Renger, G. (1988) FEBS Lett., 240, 153-158.

[102] Duysens, L.N.M. and Sweers, H.E. (1963) in Studies on Microalgae and Photosynthetic Bacteria, 353-372, University of Tokyo Press, Tokyo.

[103] Stiehl, H.H. and Witt, H.T. (1969) Z.Naturforsch., 24b, 1588-1598.

[104] van Gorkom, H.J.(1974) Biochim.Biophys.Acta, 347, 439-442.

[105] Knaff, D.B., Malkin, R., Clark, J., Myron, J.C. and Stoller, M. (1977) Biochim.Biophys.Acta, 459, 402-411.

[106] Nugent, J.H.A., Diner, B.A. and Evans, M.C.W. (1981) FEBS Lett., 124, 241-244.

[107] Rutherford, A.W. and Mathis, P. (1983) FEBS Lett., 154, 328-334.

[108] Atkinson, Y.E. and Evans, M.C.W. (1983) FEBS Lett., 159, 141-144.

[109] Butler, W.F., Calvo, R., Fredkin, D.R., Isaacson, R.A., Okamura, M.Y. and Feher, G. (1984) Biophys.J., 45, 947-973.

[110] Rutherford, A.W. and Zimmermann, J.-L. (1984) Biochim.Biophys.Acta, 767, 168-175.

[111] Prince, R.C. and Thornber, J.P. (1977) FEBS Lett., 81, 233-237.

[112] Beijer, C. and Rutherford, A.W. (1987) Biochim.Biophys.Acta, 890, 169-178.

[113] Cramer, W.A. and Butler, W.L. (1969) Biochim.Biophys.Acta, 172, 503-510.

[114] Joliot, P. and Joliot, A. (1979) Biochim.Biophys.Acta, 546, 93-105.

[115] Knaff, D.B. (1975) Biochem.Biophys.Acta, 376, 583-587.

[116] Eckert, H.J. and Renger, G (1980) Photochem.Photobiol., 31, 501-511.

[117] Bowes, J.M., Horton, P and Bendall, D.S. (1983) Arch.Biochem.Biophys., 225, 353-359.

[118] Evans, M.C.W. and Ford, R.C. (1986) FEBS Lett., 195, 290-294.

[119] Evans, M.C.W., Nugent, J.H.A., Tilling, L.A. and Atkinson, Y.E. (1982) FEBS Lett., 145, 176-178.

[120] McDermott, A.E., Yachandra, V.K., Guiles, R.D., Cole, J.L., Dexheimer, S.L., Britt, R.D., Sauer, K and Klein, M.P. (1988) Biochemistry, 27, 4021-4031.

[121] Bouges-Bocquet, B. (1973) Biochim.Biophys.Acta, 314, 250-256.

[122] Velthuys, B.R. and Amesz, J. (1974) Biochim.Biophys.Acta, 333 85-94.

[123] Pulles, M.P.J., van Gorkom, H.J. and Willensen, J.M. (1976) Biochim.Biophys.Acta, 449, 536-540.

[124] Mathis, P. and Haveman, J. (1977) Biochim.Biophys.Acta, 461, 167-181.

[125] Stemler, A. and Govindjee (1973) Plant Physiol., 52, 119-123

[126] Good, N.E. (1963) Plant Physiol., 38, 298-304)

[127] Hideg, E. and Demeter, S. (1985) Z.Naturforsch., 40c, 827-831.

[128] Wraight, C.A. (1977) Biochim.Biophys.Acta, 459, 525-531

[129] Rutherford, A.W. and Evans, M.C.W. (1979) FEBS Lett., 104, 227-230.

[130] Rutherford, A.W. and Evans, M.C.W. (1979) FEBS Lett., 100, 305-308.

[131] Rutherford, A.W., Zimmermann, J.-L. and Mathis, P. in: Advances in Photosynthesis Research (ed. Sybesma, C.) 1, 445-448, Nijhoff/Junk, Dordrecht.

[132] Crofts, A.R. and Wraight, C.A. (1983) Biochim.Biophys.Acta, 726, 149-185.

[133] Stewart, A.C. and Bendall, D.S. (1979) FEBS Lett., 107, 308-312.

[134] Castenholtz, R.W. (1970) Schweiz.Z.Hydrol., 32, 531-538.

[135] Arnon, D.I. (1949) Plant Physiol., 24, 1-15.

[136] Schatz, G.H. and Witt, H.T. (1984) Photobiochem.Photobiophys., 7, 1-14.

[137] Berthold, D.A., Babcock, G.T. and Yocum, C.F. (1981) FEBS Lett., 153, 231-234.

[138] Ford, R.C. and Evans, M.C.W. (1983) FEBS Lett., 160, 159-163.

[139] Chua, N.-H. (1980) Methods in Enzymology, 69, 434

[140] Ford, R.C. and Evans, M.C.W. (1985) Biochim.Biophys.Acta, 807, 1-9.

[141] Mansfield, R.W., Hubbard, J.A.M., Nugent, J.H.A. and Evans, M.C.W. (1987) FEBS Lett., 537, 74-78.

[142] Rupp, H., Rao, K.K., Hall, D. and Cammack, R. (1978) Biochim.Biophys.Acta, 537, 255.

[143] Dutton, P.L. (1971) Biochim.Biophys.Acta, 226, 63-80.

[144] Powers, L. (1982) Biochim.Biophys.Acta, 683, 1-38.

[145] Atkinson, Y.E. and Evans, M.C.W. (1984) in: Advances in Photosynthesis Research (Sybesma, C., ed.) 1, 139-142, Nijhoff/Junk, Dordrecht.

[146] Vermaas, W.F.J. and Rutherford, A.W. (1984) FEBS Lett., 175, 243-248.

[147] Vermaas, W.F.J. and Govindjee (1981) Photobiochem.Photobiophys., 34, 775-793.

[148] Eaton-Rye, J.J. and Govindjee (1988) Biochim.Biophys.Acta, 935, 248-257.

[149] Van Rensen, J.J.S., Tonk, W.J.M. and de Bruijn, S.M. (1988) FEBS Lett., 226, 347-351.

[150] Wraight, C.A. (1978) FEBS Lett., 100, 305-308.

[151] Cammack, R., Ryan, M.D. and Stewart, A.C. (1979) FEBS Lett., 107, 422-426.

[152] Nugent, J.H.A., Stewart, A.C. and Evans, M.C.W. (1983) Biochim.Biophys.Acta, 635, 488-497.

[153] Van Mieghem, F.J.E., Nitschke, W., Mathis, P. and Rutherford, A.W. (1989) Biochim.Biophys.Acta, 977, 207-214.

[154] Evans, M.C.W., Atkinson, Y.E. and Ford, R.C. (1985) Biochim.Biophys.Acta, 806, 247-254.

[156] Nugent, J.H.A., Corrie, A.R., Demetriou, C., Evans, M.C.W. and Lockett, C.J. (1988) FEBS Lett., 235, 71-75.

[157] Evans, M.C.W. (1987) Biochim.Biophys.Acta, 894, 524-533.

[158] Telfer, A., Barber, J. and Evans, M.C.W. (1988) FEBS Lett., 232, 209-213.

[159] Boussac, A. and Etienne, A.-L. (1984) Biochim.Biophys.Acta, 766, 576-581.

[160] Nugent, J.H.A., Demetriou, C. and Lockett, C.J. (1987) Biochim.Biophys.Acta, 894, 534-542.

[161] Oettmeier, W., Masson, K. and Dostatni, R. (1987) Biochim.Biophys.Acta, 890, 260-269.

[162] Renger, G., Kayed, A. and Oettmeier, W. (1987) Z. Naturforsch., 42c, 698-703.

[163] Renger, G., Messinger, J. and Fromme, R. (1989) Z.Naturforsch.,44c, 423-430.

[164] Bergström, J. and Vänngård, T. (1982) Biochim.Biophys.Acta, 682, 452.

[165] Cramer, W.A. and Whitmarsh, J. (1977) Annu.Rev.Plant.Physiol., 28, 133.

[166] Petrouleas, V. and Diner, B.A. (1987) Biochim.Biophys.Acta, 893, 126-137.

[167] Zimmermann, J.-L. and Rutherford, A.W. (1986) Biochim.Biophys.Acta, 851, 416-423.

[168] Petrouleas, V. and Diner, B.A. (1986) Biochim.Biophys.Acta, 849, 264-275.

[169] Diner, B.A. and Petrouleas, V. (1987) Biochim.Biophys.Acta, 895, 107-125.

[170] Binstead, N. Gurman,S.J. and Campbell, J.C. SERC Daresbury Laboratory EXCURV88 Program.

[171] Gurman, S.J., Binstead, N and Ross, I. (1984) J.Phys.c Solid State Physics, 17, 14.

[172] Andréasson, L.-E. (1989) Biochim.Biophys.Acta, 973, 465-467.

[173] Cotton, F.A. and Wilkinson, G. in: Advanced Inorganic Chemistry, 3rd Edition, 1972, Wiley Interscience, New York.